UNIVERSIDADE FEDERAL DE SANTA CATARINA
CAMPUS FLORIANÓPOLIS, CENTRO TECNOLÓGICO
PROGRAMA DE PÓS-GRADUAÇÃO EM CIÊNCIA E ENGENHARIA DE MATERIAIS

Henrique Akira Tajiri

THEORETICAL ANALYSES OF CERAMIC PASTE DIRECT EXTRUSION THROUGH A CIRCULAR DIE BEYOND THE STEADY STATE

Florianópolis
2023

Henrique Akira Tajiri

THEORETICAL ANALYSES OF CERAMIC PASTE DIRECT EXTRUSION THROUGH A CIRCULAR DIE BEYOND THE STEADY STATE

Tese submetida ao Programa de Pós-Graduação em Ciência e Engenharia de Materiais da Universidade Federal de Santa Catarina como requisito parcial para a obtenção do título de Doutor em Engenharia de Materiais.

Orientador: Prof. Emeritus Hazim Ali Al-Qureshi, PhD.
Coorientador: Prof. Dachamir Hotza, Dr.-Ing.

Florianópolis
2023

Ficha de identificação da obra elaborada pelo autor,
através do Programa de Geração Automática da Biblioteca Universitária da UFSC.

Tajiri, Henrique Akira
Theoretical analyses of ceramic paste direct extrusion through a circular die beyond the steady state / Henrique Akira Tajiri ; orientador, Hazim Ali Al-Qureshi, coorientador, Dachamir Hotza, 2023.
129 p.

Tese (doutorado) - Universidade Federal de Santa Catarina, Centro Tecnológico, Programa de Pós-Graduação em Ciência e Engenharia de Materiais, Florianópolis, 2023.

Inclui referências.

1. Ciência e Engenharia de Materiais. 2. Análise Teórica. 3. Extrusão de Cerâmica. 4. Coring Point. 5. Atrito. I. Al-Qureshi, Hazim Ali. II. Hotza, Dachamir. III. Universidade Federal de Santa Catarina. Programa de Pós-Graduação em Ciência e Engenharia de Materiais. IV. Título.

Henrique Akira Tajiri

THEORETICAL ANALYSES OF CERAMIC PASTE DIRECT EXTRUSION THROUGH A CIRCULAR DIE BEYOND THE STEADY STATE

O presente trabalho em nível de Doutorado foi avaliado e aprovado, em 17 de abril de 2023, pela banca examinadora composta pelos seguintes membros:

Prof. João Gustavo Pereira da Silva, Dr.
Instituição Universidade Federal de São Carlos

Prof. Guilherme Mariz de Oliveira Barra, Dr.
Instituição Universidade Federal de Santa Catarina

Prof. Alexandre Mikowski, Dr.
Instituição Universidade Federal de Santa Catarina

Certificamos que esta é a versão original e final do trabalho de conclusão que foi julgado adequado para obtenção do título de Doutor em Ciência e Engenharia de Materiais.

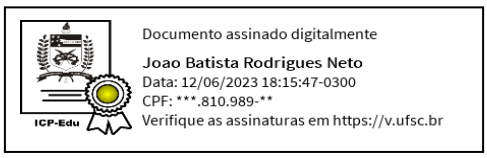

Coordenação do Programa de Pós-Graduação

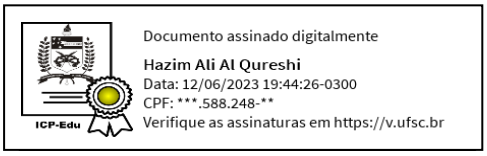

Prof. Emeritus Hazim Ali Al-Qureshi PhD.
Orientador

Florianópolis, 2023.

Dedico este trabalho a Jesus, o Autor e Consumador da minha fé.

ACKNOWLEDGEMENTS

At first, I would like to thank God (the Father, the Son and the Holy Spirit) for His unfailing love, grace and mercy, who sustained me every day during this journey. Second, I thank my wife Gabriela Pires Alves Tajiri, for all her love and comprehension about my physical absence and the time I had to invest on my studies.

I also thank Prof. Emeritus PhD. Hazim Ali Al-Qureshi for accepting to be my supervisor and for always supporting me throughout my doctorate program. I am so thankful for this unique opportunity of being supervised by this great sir. In memoriam I thank, as well, Mrs. Jean Susan, an example of a strong and delicate madam.

I thank Prof. Dr. -Ing. Dachamir Hotza, for accepting to be my co-supervisor and for all insights, revisions, and help in this work.

I thank Prof. Dr. Edson Roberto De Pieri for all support and instant availability to discuss important issues about the topic. I also thank his kindness for offering a place to conduct the theoretical research.

I thank all the administrative staff from the direction of CTC, namely, Prof. Sérgio Peters, Patrícia Fernandes, Jorge Pereira Oda, Marcelo Bittencourt, Stefani de Souza, Ariana Casagrande, Fernanda Selistre da Silva Scheidt, Patrícia Ida Gonçalves Pinheiro, Juliana Blau, and Robson de Carvalho for all relaxing moments and for the great and amazing time we spent together.

I thank Prof. Dr. João Batista Rodrigues Neto and Rogério Antônio Campos for their great zeal and commitment to the Graduate Program in Materials Science and Engineering at the Federal University of Santa Catarina.

I thank the National Council for Scientific and Technological Development (CNPq) for the scholarship, for investing in the future of the Brazilian education and society, and for giving me the opportunity to present part of this work at an International Conference in Japan.

Finally, I thank my family and brethren for always supporting my decisions, for helping me every time I needed them, and for their love and friendship.

“Suppose one of you wants to build a tower. Won’t you first sit down and estimate the cost to see if you have enough money to complete it? For if you lay the foundation and are not able to finish it, everyone who sees it will ridicule you, saying, ‘This person began to build and wasn’t able to finish.’” (Luke, 85)

RESUMO

O principal objetivo da presente tese é propor análises teóricas e equações que descrevam as pressões de extrusão para a extrusão direta de pastas cerâmicas através de uma matriz circular após o regime de estado estacionário, considerando o "coring point". Por exemplo, em uma pasta cerâmica, o "coring point" é evidenciado por um aumento significativo na pressão de extrusão depois do estado estacionário. Esse aumento na pressão de extrusão pode ser atribuído a uma mudança no comportamento da pasta durante o estado não estacionário. Além disso, em relação às variações nas propriedades da matéria-prima, isso pode ser atribuído à perda de água, à densificação da pasta cerâmica e à variação do coeficiente de atrito. Na prática, quando o "coring point" é previsto durante a extrusão, os danos à matriz, problemas de lubrificação, defeitos no produto e aumento do custo de produção podem ser minimizados e até evitados. A presente tese propõe quatro análises teóricas e equações considerando o efeito do "coring point" na pressão de extrusão. Por exemplo, a primeira abordagem associa o aumento da pressão de extrusão após o "coring point" com a variação do atrito em função da densidade do material extrudado; a segunda abordagem relaciona o estado não estacionário com o fenômeno de recuo elástico; a terceira abordagem correlaciona o aumento da pressão de extrusão com a variação do teor de água na pasta cerâmica ao longo do tempo; e, por fim, a quarta abordagem utiliza as principais variáveis encontradas nas três teorias matemáticas anteriores e propõe um novo modelo usando análise dimensional. As quatro abordagens propostas demonstraram uma correlação satisfatória com uma curva experimental. Além disso, entre as quatro análises teóricas, a abordagem da perda de água pareceu ser a mais conservadora e o modelo de análise dimensional produziu a equação mais simples. Também ficou evidente que, durante o estado não estacionário, o perfil de pressão de extrusão era sensível à velocidade de extrusão, ao raio da saída da matriz, à porcentagem de redução de diâmetro da peça extrudada e ao coeficiente de atrito e teor de água da pasta. Em conclusão, é um fato conhecido que, na extrusão direta de cerâmicas, além do estado estacionário, ainda não está totalmente estudado, o que leva a uma falta de informação nessa área. Portanto, a presente tese fornece ao projetista de ferramentas ou ao engenheiro informações importantes que detalham todo o processo de extrusão direta, incluindo o estado não estacionário.

Palavras-chave: Análise Teórica; Extrusão de Cerâmica; Coring Point; Atrito; Spring-Back; Análise Dimensional.

ABSTRACT

The main purpose of the present thesis is to propose theoretical analyses and equations describing the extrusion pressures for direct ceramic paste extrusion through a circular die after the steady state regime, considering the coring point. For instance, in a ceramic paste, the coring point is evidenced by a significant rise in the extrusion pressure beyond the steady state. This increase in the extrusion pressure may be regarded to a change in the paste behavior during the unsteady state. Furthermore, relating to feedstock properties' variations, it may be accounted to water loss, densification of the ceramic paste, and shift of the friction coefficient. In practice, when the coring point is forecast during extrusion, die damages, lubrication problems, product defects, and a raise in the production cost can be minimized and even avoided. The present thesis proposes four theoretical analyses and equations considering the effect of the coring point on the extrusion pressure. For instance, the first approach associates the rise of the extrusion pressure after the coring point with the friction variation as a function of the density of the extruded material; the second approach relates the unsteady state with the spring-back phenomenon; the third approach correlates the increase of the extrusion pressure with the water content change of the ceramic paste over the time; and finally, the fourth approach uses the main variables encountered in the previous three mathematical theories and a new model is proposed using dimensional analysis. The four proposed approaches demonstrated a satisfactory correlation with an experimental curve. In addition, among the four theoretical analyses, the water loss approach seemed to be the most conservative and the dimensional analysis model yielded the simplest equation. Also, it became evident that during the unsteady state, the extrusion pressure profile was sensitive to extrusion velocity, radius of the exit of the die, diameter reduction percentage of the extruded part, and friction coefficient and water content of the paste. In conclusion, it is a known fact, that in the direct extrusion of ceramics, beyond the steady state, still it is not fully studied, leading to a lack of information in this area. Therefore, the present thesis furnishes the tool designer or the engineer with important pieces of information that detail the entire process of direct extrusion, including the unsteady state.

Keywords: Theoretical Analysis; Ceramic Extrusion; Coring Point; Friction, Spring-Back, Dimensional Analysis.

RESUMO EXPANDIDO

Introdução

A extrusão desempenha um papel importante no processamento de materiais. Händle (2007) afirma que a extrusão é uma técnica de conformação amplamente utilizada para produzir produtos de seção transversal constante. Nos materiais cerâmicos, esse processo é usado tanto na indústria tradicional, baseada em argila, por exemplo, quanto na indústria de cerâmica avançada. Por exemplo, tijolos de barro e telhas são exemplos clássicos de cerâmica tradicional citados por Kocserha e Kristály (2010), enquanto Händle (2007) menciona isoladores de alumina e componentes aeroespaciais de zircônia como exemplos de cerâmica avançada. Além disso, Nath Das *et al.* (2002) destacaram a produção de catalisadores em forma colmeia de cordierita na indústria de cerâmica avançada. Além disso, nos últimos anos, a extrusão tem sido citada como sendo fundamental na fabricação aditiva, popularmente referida como impressão 3D. É importante destacar que a extrusão é empregada não apenas na indústria cerâmica, mas também amplamente encontrada nas indústrias metalúrgicas, de plásticos, de alimentos e de fármacos entre outras.

O processo de extrusão consiste em empurrar o material através de uma abertura, conhecida como matriz. Portanto, pressão é necessária para o processo ocorrer. Na extrusão de materiais cerâmicos, o tipo de extrusor pode ser classificado de acordo com o mecanismo em que a pressão é produzida e, posteriormente, transferida para a massa. Existem três maneiras mais frequentes em que a pressão pode ser gerada. Por exemplo, Benbow e Bridgwater (1993) identificaram três tipos diferentes de extrusão. Se a pressão é alcançada forçando duas superfícies rolantes, este processo é conhecido como extrusão rotativa; se a pressão é produzida por meio de parafusos ou helicoides rotativos, é denominado extrusão de rosca; e se a pressão é gerada depositando a pasta dentro de um cilindro, sendo ela posteriormente pressionada por um êmbolo ou pistão, é chamado de extrusão direta.

De acordo com Vitorino *et al.* (2014), na extrusão cerâmica, a plasticidade da massa contribui significativamente durante todo o processo. Reed (1995) definiu a plasticidade em cerâmica como um modo particular de comportamento mecânico quando um material plástico apresenta deformação permanente sem fratura sob tensão de cisalhamento maior que a resistência do material. Além disso, um problema é encontrado na literatura sobre extrusão cerâmica: os pesquisadores não têm um consenso comum sobre qual método deve ser utilizado para avaliar a plasticidade da massa. Por exemplo, Andrade *et al.* (2011) revisaram os principais métodos para avaliar a plasticidade da massa cerâmica, dentre elas: análise reológica; índice de plasticidade de Pferfferkorn; índice de plasticidade de Atterberg; curvas de tensão/deformação e indentação. Dondi (2006) sugere que há uma variedade de métodos para avaliar a plasticidade da massa cerâmica; no entanto, eles podem não produzir resultados semelhantes.

Ainda assim, Burbidge e Bridgwater (1995) afirmaram que a extrusão cerâmica tem sido compreendida e explorada de forma restrita em comparação com a extrusão polimérica. Além disso, há poucos trabalhos que investigam o comportamento da massa extrudada além do estado estacionário. O motivo para isso é que, historicamente, a extrusão de massas cerâmicas foi limitada à produção de bens de baixo custo, como a indústria baseada em argila, que, de acordo com Macedo *et al.* (2008), não exigia um controle dimensional e de qualidade meticuloso. Além disso, testes que tentam prever o comportamento da massa cerâmica durante

a extrusão, bem como a modelagem matemática de algumas propriedades, especialmente a plasticidade, são difíceis devido a muitos parâmetros envolvidos no processo.

No processamento de metais, Johnson (1956; 1959), investigando a extrusão em estado plano de alumínio e chumbo, observou uma queda na carga de extrusão enquanto o êmbolo se movia para o metal ser extrudado. No entanto, o punção se aproximou de uma posição antes de atingir o estado instável, que Johnson chamou de "*coring point*". Mais tarde, isso também foi identificado e relatado por Avitzur (1967) e Hoffmanner *et al.* (1971). Graficamente, nesse ponto específico, Johnson (1956) e Dodeja e Johnson (1957) identificaram uma notável aceleração da taxa de diminuição da pressão de extrusão. Além disso, Johnson (1956) chamou de "*coring point*" o ponto em que o pistão, ou o final do cilindro, a montante do material, entra na zona plástica. Nos metais, o fenômeno do aumento de pressão, próximo ao final do processo de extrusão (encontrado tanto na extrusão direta quanto na indireta) pode gerar defeitos, como formação de tubo ou orifício no lingote. Portanto, uma perturbação é iniciada, o que leva ao fim da fase estável o fluxo de material.

Outros autores, como Sturgess e Dean (1979), observaram um comportamento diferente para o "*coring point*", como afirmado por Johnson (1956) e por Dodeja e Johson (1957). Em vez de uma queda na pressão de extrusão, foi observado um aumento nesta pressão. Portanto, Sturgess e Dean (1979) sugeriram que o "*coring point*" está localizado na pressão mínima de carga de extrusão no regime de estado estacionário. Esse fenômeno também é encontrado na extrusão de pastas cerâmicas, conforme demonstrado anteriormente por Janney (1995) e Benbow e Bridgwater (1993); no entanto, até o momento ainda não é bem explicado ou estudado.

A modelagem matemática aplicada à extrusão é atraente. Ela é uma ferramenta poderosa que ajuda a otimizar o processo de extrusão e a obter uma melhor compreensão das variáveis dentro do processo. De acordo com Reed (1995), um corpo ou pasta plástica cerâmica compreende de uma fase líquida e uma fase sólida, dentro dos limites plásticos e líquidos. Surge uma divergência ao lidar com a modelagem matemática de cerâmicas submetidas à extrusão. Por exemplo, Horrobin e Nedderman (1998) propuseram um modelo que assume a pasta cerâmica como uma formulação plástico-elástica; por outro lado, Benbow e Bridgwater (1993) propuseram um modelo amplamente utilizado e citado na literatura, onde conjecturaram a pasta cerâmica como uma mistura de fluxo plástico perfeito e viscoso na região de entrada.

De acordo com o modelo de extrusão de Benbow e Bridgwater (1993), a pressão de extrusão depende das propriedades do fluxo, taxa de extrusão e detalhes físicos e geométricos da extrusora. Além disso, dez variáveis estão envolvidas em sua equação. Vitorino *et al.* (2014) agruparam essas variáveis em quatro grupos: parâmetros geométricos conhecidos (D_0, D e L), parâmetros de processamento (v_d), parâmetros físicos desconhecidos (α, β, σ_0 e τ_0) e ajuste matemático (n e m). Apesar de este modelo ser amplamente citado e utilizado na literatura, variação de pressão é válida apenas no estado estacionário.

Andrade (2009) propôs um modelo utilizando a abordagem de equilíbrio de corpo livre para modelar o comportamento da pressão durante a extrusão. O autor considerou a pasta cerâmica como um sólido plástico ideal, sendo que o comportamento da pasta foi modelado utilizando diferentes suposições de fluxo. No entanto, não há um consenso entre os pesquisadores sobre qual abordagem

apresenta uma descrição mais precisa do comportamento da pasta cerâmica durante o processo de extrusão.

Como mostram os resultados experimentais de pesquisadores como Benbow e Bridgwater (1993), Liu *et al.* (2013), Rough *et al.* (2002), entre outros, a pressão de extrusão não permanece constante durante todo o processo de extrusão e há uma falta de estudos e de investigações detalhadas nesse tópico. Além disso, é possível observar um aumento significativo na pressão de extrusão, destacando a transição de um estado estacionário para um estado não estacionário. É importante lembrar que quando a transição do estado estacionário para o estado não estacionário é negligenciada, pode levar a problemas vulneráveis que vão desde a qualidade comprometida do produto final até danos ao equipamento de extrusão.

Portanto, a fim de preencher essa lacuna no campo científico e industrial e incrementar e modificar a teoria proposta por Andrade (2009), serão realizadas novas análises teóricas e quatro equações serão propostas. A primeira abordagem associa o aumento da pressão de extrusão após o *"coring point"* com a variação de atrito como função da densidade do material extrudado; a segunda abordagem relaciona o estado não estacionário com o fenômeno de *"spring-back"*, termo mais comumente utilizado em materiais metálicos; a terceira abordagem correlaciona o aumento da pressão de extrusão com a mudança da quantidade de água na pasta cerâmica ao longo do tempo; e finalmente, a quarta abordagem utiliza as principais variáveis encontradas nas três teorias matemáticas citadas anteriormente e propõe um novo modelo usando a análise dimensional.

Objetivos

O objetivo deste trabalho é desenvolver análises teóricas, propondo equações que considerem algumas variáveis que levam ao aumento da pressão de extrusão no regime de estado não estacionário (após o "*coring point*") no processo de extrusão direta de cerâmica.

Objetivos específicos:

• Revisão da literatura sobre extrusão direta de material cerâmico, plasticidade cerâmica, teste de compressão em cerâmica como um meio de determinar a plasticidade da pasta cerâmica, equação publicada relacionada à extrusão de cerâmica e análise dimensional.

• Desenvolvimento e análise de quatro diferentes análises teóricas acompanhadas pela proposta de quatro equações distintas que consideram o *"coring point*" e o aumento posterior da pressão de extrusão.

Metodologia

Nesta seção, é apresentada uma descrição detalhada de oito tipo de materiais diferentes (variando desde alumina até diferentes tipos de argilas). Além disso, todos esses materiais listados foram citados na literatura como o material inicial para a extrusão direta. Esses materiais foram utilizados para construir e complementar as análises teóricas e, posteriormente, os modelos produzidos foram testados e aplicados neles.

Em seguida, quatro novas análises teóricas são introduzidas, seguidas por quatro equações distintas. A primeira abordagem associa o aumento da pressão de extrusão após o *"coring point"* com a variação do atrito como uma função da densidade do material extrudado; a segunda abordagem relaciona o estado não-

estacionário com o fenômeno de "*spring-back*"; a terceira abordagem correlaciona o aumento da pressão de extrusão com a variação da quantidade de água na pasta cerâmica ao longo do tempo; e, por fim, a quarta abordagem utiliza as principais variáveis encontradas nas três análises teóricas anteriormente citadas e um novo modelo é proposto usando a análise dimensional.

Resultados e Discussão

Para fins de comparação, validação e avaliação das quatro novas equações propostas, foi utilizado e reproduzido um trabalho previamente publicado por Andrade (2009). Três fases podem ser reconhecidas na extrusão direta de material cerâmico, conforme já relatado por Andrade (2009): uma fase de compactação, marcada pela compressão da pasta cerâmica; uma fase estacionária, onde a pressão é estabilizada e a extrusão continua de forma constante; e uma fase não estacionária, além do "coring point", mostrando um aumento evidente na pressão de extrusão. Como pode ser observado, para o modelo de Andrade, é possível notar apenas duas fases durante o processo de extrusão: a fase de compactação e a fase estacionária, uma vez que em sua modelagem matemática, ele não levou em consideração as implicações além do ponto de empilhamento.

Agora, focando nas quatro análises teóricas propostas, exibidas com maior amplificação, é perceptível que, entre as quatro equações propostas, o modelo que considera a perda de água durante a extrusão parece ser a abordagem mais conservadora, uma vez que forneceu a maior pressão de extrusão. Por outro lado, a abordagem que relatou a influência do atrito na extrusão, forneceu a menor pressão de extrusão. Da mesma forma, embora a equação de variação de atrito apresente um bom ajuste com a curva experimental, como já foi mencionado, é mais provável que a resistência à compressão tenha um impacto maior na pressão de extrusão quando comparada ao coeficiente de atrito. A equação que considerou a migração de água apresentou os resultados mais próximos quando comparada com os pontos experimentais; no entanto, é mais difícil reconhecer todas as variáveis dentro da equação com precisão. Finalmente, a abordagem de análise dimensional apresentou resultados promissores, com uma equação simples e direta.

A partir dos resultados das teorias matemáticas propostas, foi possível observar que o raio da saída do dado, o ângulo de saída, o coeficiente de atrito, a porcentagem de redução de diâmetro, a velocidade do pistão e a migração de água influenciam consideravelmente o perfil da pressão de extrusão. O aumento dessas variáveis levou a um aumento na pressão de extrusão e, em alguns casos, a uma antecipação do ponto de obstrução.

Em conclusão, essas teorias ajudarão o projetista do produto a conceber projetos evitando defeitos devido a gradientes de material e pressão, garantindo a integridade de suas propriedades projetadas. Por exemplo, para minimizar o efeito da migração de água (ou solvente) implicando na alteração da qualidade do produto e na pressão de extrusão, sugere-se o uso de sensores de umidade e uma ferramenta acoplada à extrusão, seria possível rastrear o teor de água na pasta cerâmica e água (solvente) poderia ser adicionada à pasta quando necessário

Considerações Finais

No presente trabalho, foi possível realizar uma breve revisão bibliográfica sobre: conceitos básicos de extrusão cerâmica; plasticidade cerâmica; teste de

compressão como um meio de avaliar a plasticidade da pasta cerâmica; análise dimensional; e recapitular uma equação do processo de extrusão considerando atrito e variação angular. Portanto, como conclusão deste trabalho, pode-se observar que: em primeiro lugar, a extrusão é uma técnica de processamento amplamente empregada desde a indústria tradicional até a indústria cerâmica avançada; em segundo lugar, a plasticidade desempenha um papel muito importante na extrusão cerâmica, além disso, existem, pelo menos, cinco maneiras diferentes de avaliar a plasticidade da pasta cerâmica, citadas na literatura; em terceiro lugar, o teste de compressão parece ser uma técnica adequada para avaliar a plasticidade da pasta cerâmica; em quarto lugar, a análise dimensional é uma ferramenta poderosa que permite modelar dimensões físicas em equações simples e diretas; finalmente, há uma lacuna evidente na literatura em relação à modelagem matemática e à pressão de extrusão além do estado estacionário. Portanto, foi possível desenvolver quatro equações matemáticas para a extrusão de pasta cerâmica para analisar o aumento de pressão além da fase de estado estacionário.

Com relação às análises teóricas propostas, uma equação propôs um coeficiente de atrito como função da densidade do material cerâmico extrudado, outra abordagem considerou o efeito do fenômeno de “spring-back” sobre a pressão de extrusão, o terceiro modelo introduziu a relação matemática entre o a pressão efetiva de compressão e o teor de água do material e, finalmente, o último modelo matemático empregou as principais variáveis encontradas nas outras três abordagens e propôs uma nova análise teórica usando a técnica de análise dimensional.

Em conclusão, todas as novas equações propostas apresentaram boa concordância com os dados experimentais e novas variáveis dentro do processo de extrusão foram introduzidas e relacionadas matematicamente a uma equação já publicada. As análises teóricas pareceram ser muito úteis em termos de auxiliar a construção de novas equações. Assim, foi possível preencher uma lacuna na extrusão direta de cerâmica, onde publicações sobre o regime de estado não estacionário e equações que o reconhecem são muito escassas.

Como sugestão para trabalhos futuros, propõe-se a construção de uma extrusora adaptada com um cilindro dividido. Além disso, esse aparato é proposto para avaliar o comportamento do material além do estado estacionário. Será possível avaliar a relação entre a pressão de extrusão e as propriedades químicas e físicas do material, como a densidade e o teor de água ao longo do processo de extrusão. Com esse cilindro dividido, também será viável investigar possíveis variações das propriedades da pasta ao longo do cilindro.

Também é sugerido para trabalhos futuros um estudo minucioso na reologia das pastas cerâmicas para avaliar a influência dos aglomerados (e também do potencial zeta da pasta) sobre a pressão de extrusão. Seria de grande valor refinar a equação proposta usando análise dimensional, introduzindo novas variáveis que possam ser importantes durante a extrusão direta de pistão.

Palavras-chave: Análise Teórica; Extrusão de Cerâmica; *Coring Point*; Atrito; *Spring-Back*; Análise Dimensional

LIST OF FIGURES

LIST OF CHARTS

LIST OF TABLES

LIST OF ABBREVIATIONS AND SYMBOLS

A: LIQUID AND PLASTIC LIMIT AVERAGE

a: ANGULAR COEFFICIENT OF THE LINEAR EQUATION

b: COEFFICIENT OF THE LINEAR EQUATION

D: DIAMETER OF THE EXTRUDATE SPECIMEN IN THE DIE OUTLET

D_d: EXIT DIE´S DIAMETER

D_0: INITIAL DIAMETER (BARREL'S DIAMETER)

dw/dt: WATER CONTENT VARIATION OVER TIME

F: INSTANTANEOUS AXIAL FORCE

h: FINAL HEIGHT OF THE SAMPLE

L: LENGTH OF THE DIE LAND

L_C: CRITICAL LENGTH (CORING POINT)

P_{AVE}: AVERAGE EXTRUSION PRESSURE

R: RADIUS OF THE OUTLET DIE

R_0: INITIAL RADIUS (BARREL'S DIAMETER)

R_F: FINAL RADIUS (DIE'S DIAMETER)

r_F: FINAL RADIUS OF THE SPECIMEN

t: TIME

v: PASTE VELOCITY IN THE BARREL

w: WATER CONTENT

w_0: INITIAL WATER CONTENT

w_A: WATER CONTENT IN POINT A

w_{PL}: WATER CONTENT IN THE PLASTIC LIMIT

x: POSITION OF THE RAM

z: PUNCH TRAVEL

α: SEMI CONE OF THE DIE

ε_r: RADIAL STRAIN

ε_z: AXIAL STRAIN

$\bar{\varepsilon}$: FLOW STRAIN

μ: COEFFICIENT OF FRICTION BETWEEN THE COMPRESSION MACHINE AND THE CLAY

μ_{CIL}: COEFFICIENT OF FRICTION BETWEEN PUNCH AND CLAY PASTE

μ_W: COEFFICIENT OF FRICTION BETWEEN WALL AND CLAY PASTE

ν: POISSON'S RATIO

ρ: DENSITY OF THE CERAMIC PASTE

θ: SEMICONE ANGLE OF THE DIE

σ_A: COMPRESSIVE STRENGTH AT THE POINT A

σ_{AVE}: AVERAGE EXTRUSION PRESSURE

σ_{PL}: COMPRESSIVE STRENGTH IN THE PLASTIC LIMIT

σ_R: RADIAL STRESS

σ_Z: AXIAL STRESS

$\bar{\sigma}$: FLOW STRESS

$\bar{\sigma}_{COMP}$: COMPRESSIVE EFFECTIVE STRESS

SUMMARY

1 INTRODUCTION

Extrusion plays an important role in material processing. Händle (2007) states that extrusion is a shaping technique widely employed to produce constant cross-sectional area products. In ceramics, this process is used either in the traditional clay-based industry as well as in the advanced ceramic industry. For instance, clay bricks and roof-tiles are classic examples of traditional ceramics cited by Kocserha and Kristály (2010), while Händle (2007) mentioned high-alumina insulators and zirconia aerospace components as examples of advanced ceramics. In addition, Nath Das *et al.* (2002) highlighted the cordierite honeycomb catalyst production in the advanced ceramic industry. Also, in the past few years, extrusion has been cited as being pivotal in additive manufacturing, popularly known as 3D printing (CHEN; LI; LI; LIU *et al.*, 2019; HALL; REGIS; RENTERIA; CHAVEZ *et al.*, 2021; HU; MIKOLAJCZYK; PIMENOV; GUPTA, 2021; ORDOÑEZ; GALLEGO; COLORADO, 2019; ROMANCZUK-RUSZUK; SZTORCH; PAKUŁA; GABRIEL *et al.*, 2023; RUSCITTI; TAPIA; RENDTORFF, 2020) Importantly, extrusion is employed not only in the ceramic industry, but also widely found in the metallic, polymeric, and food industry (HARPER, 2019; JOHNSON; KUDŌ, 1962; LAFLEUR; VERGNES, 2014).

The extrusion process consists of pushing material through an orifice, known as a die (CARLEY; STRUB, 1953; CHEVALIER; HAMMOND; POITOU, 1997). Therefore, pressure is required in the process. In ceramic extrusion, the type of extruders can be classified according to the mechanism in which pressure is produced and further it is transferred to the paste. There are three more frequent ways in which pressure can be generated. For example, Benbow and Bridgwater (1993) identified three different types of extrusion. For instance, if the pressure is achieved by forcing two rolling surfaces, it is known as a rotary extruder; if the pressure is produced by means of rotating screws or augers, it is termed a screw extruder; and if the pressure is generated by casting the paste inside a cylinder pressed with a ram or piston, it is named as a ram or direct extruder.

According to Vitorino *et al.* (2014), in ceramic extrusion, the plasticity of the paste contributes significantly throughout the process. Reed (1995) defined plasticity in ceramics as a particular mode of mechanical behavior when a plastic material

features a permanent deformation without fracture under shear stress greater than the yield strength of the material. Furthermore, an issue is found in the literature regarding ceramic extrusion: the researchers do not have a universal consensus concerning which method should be used to evaluate the plasticity of the paste. For example, Andrade *et al.* (2011) reviewed the main methods to assess the ceramic paste's plasticity: rheological analysis; Pferfferkorn's plasticity index; Atterberg's plasticity index; stress/strain curves and indentation. Dondi (2006) suggested that there are a variety of methods to evaluate the plasticity of the ceramic paste; nevertheless, they may not yield similar outcomes.

Still, Burbidge and Bridgwater (1995) affirmed that ceramic extrusion has been understood and explored in a restricted way when compared to polymeric extrusion. Moreover, there are scarce works that investigate the behavior of the extruded paste beyond the steady state. The reason for that is that, historically, the extrusion of ceramic pastes was restrained to the production of goods of low cost, such as the clay-based industry, which according to Macedo *et al.* (2008) did not demand a meticulous dimensional and quality control. Besides that, tests trying to predict the behavior of the ceramic paste during extrusion, as well as mathematical modeling of some properties, especially plasticity, are difficult due to many parameters involved in the process.

In metal processing, Johnson (1956; 1959), investigating the plane-strain extrusion of aluminum and lead, noticed a decline in the extrusion load while the ram moved forward. Nevertheless, the punch approached a position before reaching the unsteady state, which Johnson coined as the "coring point". Later on, it was also identified and reported by Avitzur (1967) and Hoffmanner *et al.* (1971). Graphically, at this specific point, Johnson (1956) and Dodeja and Johnson (1957) identified a remarkable acceleration of the extrusion pressure decrease rate. Moreover, Johnson (1956) named as "coring point" the point at which the piston, or the end of the cylinder, upstream from the die, enters the plastic zone in front of the die. In metals, the phenomenon of pressure increase, close to the end of the extrusion process (encountered either in direct and also in indirect extrusion) can generate defects such as pipe or hole formation in the billet. Therefore, a disturbance is initiated, which leads to the end of the steady phase of the flow pattern.

Other authors, such as Sturgess and Dean (1979), observed a different behavior for the coring point as stated by Johnson (1956) and by Dodeja and Johson (1957). Rather than a decline in the extrusion load, a raise in this load was observed. Therefore, Sturgess and Dean (1979) suggested that the coring point is located at the minimum extrusion load pressure in the steady state regime. This phenomenon is also found in the extrusion of ceramic pastes as early displayed by Janney (1995) and Benbow and Bridgwater (1993); however, it is still not well explained or studied.

Mathematical modeling applied to extrusion is appealing. It is a powerful tool that helps to optimize the extrusion process and get a better understanding of the variables within the process. According to Reed (1995) a ceramic plastic body or paste comprises a liquid and a solid phase, within the plastic and the liquid limits. A divergence emerges when dealing with the mathematical modeling of ceramics submitted to extrusion. For example, Horrobin and Nedderman (1998), proposed a model assuming the ceramic paste as a plastic-elastic formulation; on the other hand, Benbow and Bridgwater (1993) proposed a model, broadly used and cited in the literature, where they conjectured the ceramic paste as a mixture of perfect plastic and viscous flow in the die entry region and as a rigid plug flow, as stated by Horrobin and Nedderman (1998) (velocity of the fluid is considered constant along the cross-section) in the die land region.

According to Benbow and Bridgwater's (1993) extrusion model, the extrusion pressure depends on flow properties, extrusion rate, and physical and geometrical details of the extruder. Moreover, ten variables are involved in their equation. Vitorino *et al.* (2014) aggrouped these variables into four groups: known geometrical parameters (D_0, D, and L), processing parameters (v_d), unknown physical parameters (α, β, σ_0, and τ_0), and mathematical fitting (n and m). Even though this model is widely cited and used in the literature, the calculated overall pressure drop is only valid in the steady state.

Andrade (2009) in an attempt to model the pressure behavior during extrusion, the author used the free-body equilibrium approach. Therefore, he considered the ceramic paste as an ideal plastic solid. Thus, the paste behavior has been modeled

using different flow assumptions. Furthermore, there is no consensus among the researchers concerning which approach presents a more accurate description of the ceramic paste behavior during the extrusion process.

As shown through experimental results by some researchers such as Benbow and Bridgwater (1993), Liu *et al.* (2013), Rough *et al.*(2002), and others (AZZOLINI; SGLAVO; DOWNS, 2014; JIANG; YANG; GAO, 2009; LIU; LEU, 2009) the extrusion pressure does not remain constant throughout the entire extrusion process, and there is a lack of studies and thorough investigation in this topic. Moreover, it is possible to observe a significant rise in the extrusion pressure, highlighting the shift from a steady state to an unsteady state behavior. It is also important to bear in mind that when the transition from the steady state to the unsteady state is neglected it can lead to vulnerable issues ranging from the compromised quality of the final product to damage to the extrusion equipment.

Therefore, in order to fill this gap in the scientific and industrial realm and increment and modify the theory proposed by Andrade (2009), novel theoretical analyses will be performed and four equations will be introduced. The first approach associates the rise of the extrusion pressure after the coring point with the friction variation as a function of the density of the extruded material; the second approach relates the unsteady state with the spring-back phenomenon; the third approach correlates the increase of the extrusion pressure with the water content change of the ceramic paste over the time; and finally, the fourth approach uses the main variables encountered in the previous three mathematical theories and new model is proposed using *Dimensional Analysi*s.

1.1 GENERAL OBJECTIVES

The aim of this work is to develop theoretical analyses, proposing equations that consider some variables leading to the extrusion pressures raise in the unsteady state regime (after the coring point) in the ceramic direct extrusion process.

1.2 SPECIFIC OBJECTIVES

- Literature review on ceramic direct ram extrusion, ceramic plasticity, compression test in ceramics as a mean to determine the plasticity of the ceramic paste, published equations related to extrusion of ceramic, and dimensional analysis.
- Development and further analysis of four different theoretical models accompanied by a proposal of four distinct equations that consider the coring point and further rise of the extrusion pressure.

2 THEORETICAL BACKGROUND

2.1 EXTRUSION

In summary, the extrusion process consists of pushing a material through an orifice, known as a die (CARLEY; STRUB, 1953; CHEVALIER; HAMMOND; POITOU, 1997). Therefore, pressure is required in the process. In ceramic extrusion, the type of the extruders can be classified according to the method in which pressure is produced to be transferred to the paste. There are three more frequent ways where the pressure is applied. For example, if the pressure is generated by the forcing of two rolling surfaces, it is called rotary extrusion (W. NELSON; P. BARRINGTON; J. STRAUB; D. BRUHN, 1983; YU; ZHANG; WANG; HAO *et al.*, 2018); if the pressure is produced by the use of rotating screws or augers, it is named screw's extruder (BURBIDGE; BRIDGWATER, 1995; POTENTE; HANHART; RESKI, 1994); and, finally, if the pressure is achieved by casting the paste inside a cylinder pressed with a ram, it is termed ram extruder (BENBOW; BRIDGWATER, 1993; HÄNDLE, 2007). These three types of extruders are displayed in Figure 1.

Figure 1 - Typical types of extruders: a) rotary b) screw extruder c) and ram extruder

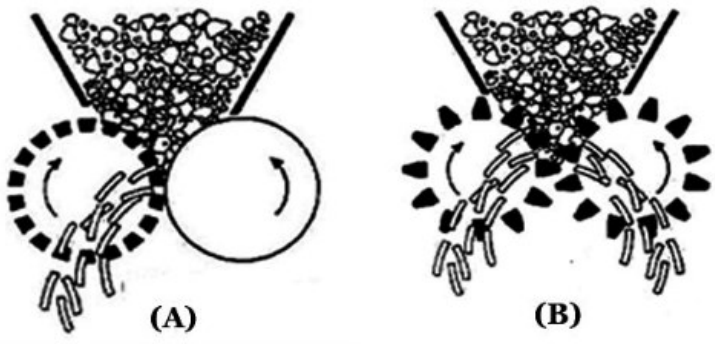

a) Rotary extruder [(A) rotary cylinder extruder, (B) rotary gear extruder]

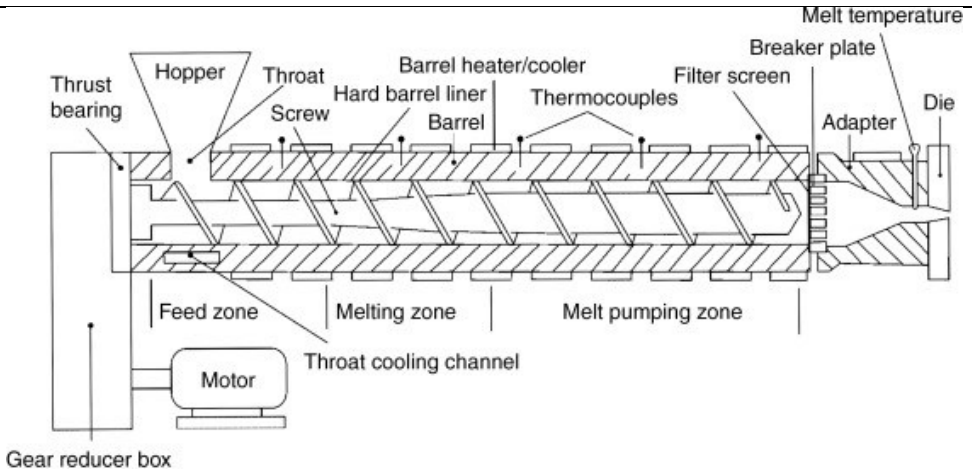

b) Screw extruder

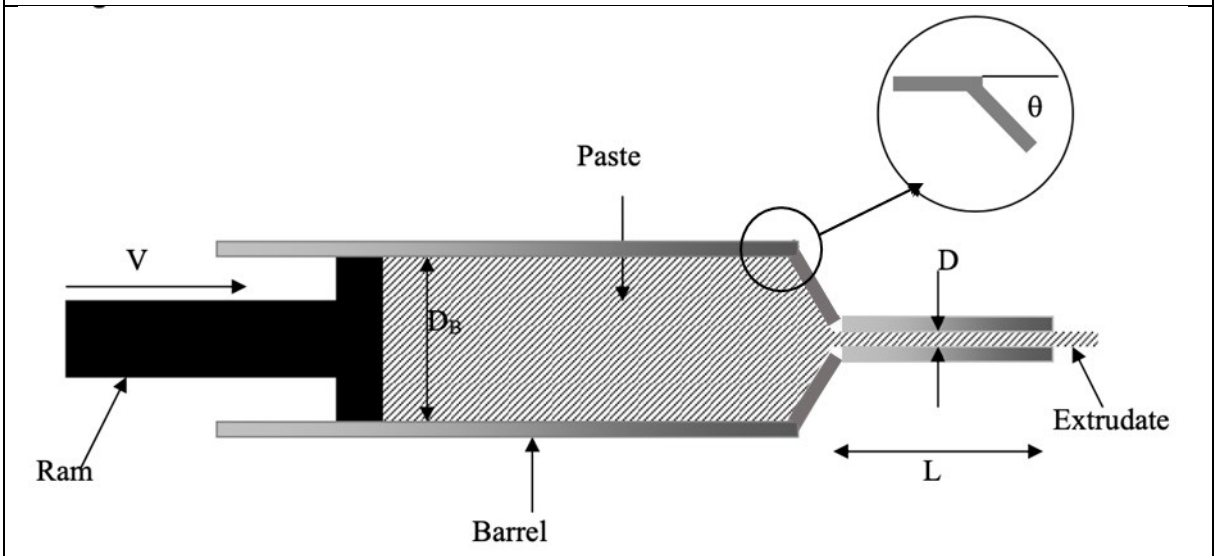

c) Ram extruder (D, L, and V are the diameter and the length of the die, and the ram's speed, respectively)

Source: Adapted from Altinkaynak (2010), Bhairy *et al.* (2015) and Russel *et al.* (2002)

Focusing on direct extrusion, in terms of extrusion pressure and extrusion ram displacement, as shown in Figure 2, initially the ram extrusion is marked by a steep extrusion pressure raise while the paste is flattened by the ram. Afterwards, the paste reaches a steady state, where it is noticeable a modest and gradual decrease of the extrusion pressure until it approaches a minimum. Finally, it is noticeable a sharp increase in the extrusion pressure, entering an unsteady state (BENBOW; BRIDGWATER, 1993). This point, which occurs the shift from steady to unsteady state is also known as the coring point. Moreover, Alfani *et al.* (2007) state that how and where the pressure measurement is made has a considerable effect on the calculated extrusion pressure.

Figure 2 - Extrusion pressure of an alumina paste as a function of the ram's displacement

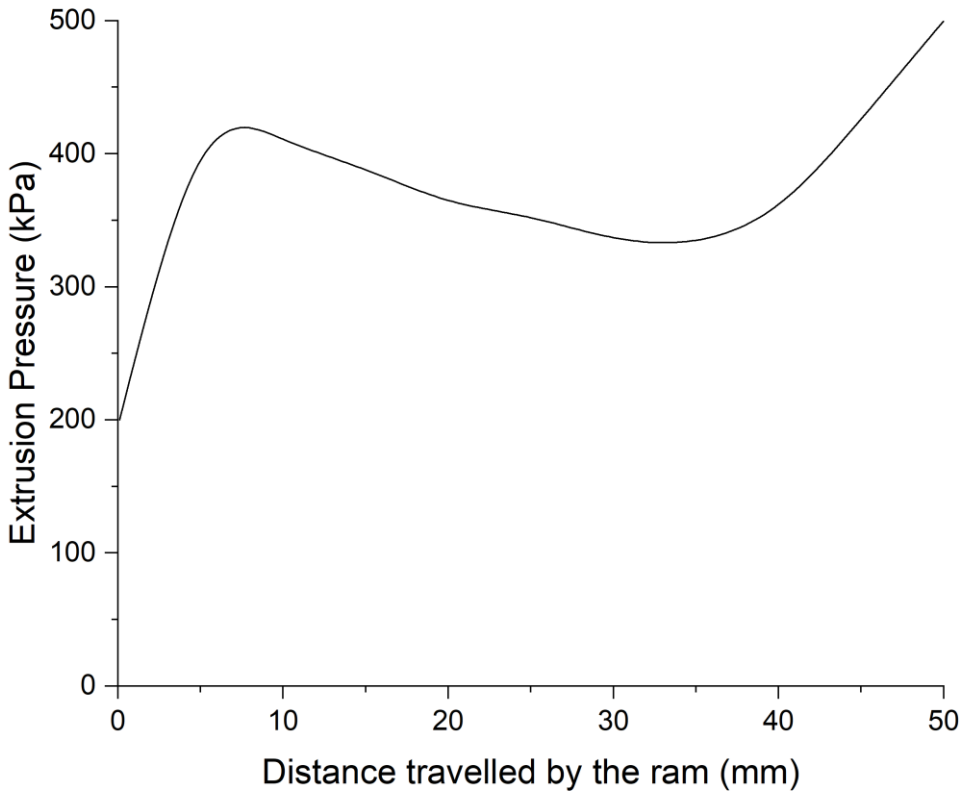

Source: Adapted from Benbow and Bridgwater (1993)

2.2 PLASTICITY

In ceramic extrusion, the

In ceramic extrusion, the plasticity of the ceramic paste contributes significantly throughout the process (VITORINO; FREITAS; RIBEIRO; ABRANTES *et al.*, 2014). Reed (1995) defined plasticity in ceramics as a particular mode of mechanical behavior when a plastic material features a permanent deformation without fracture under shear stress greater than the yield strength of the material. Furthermore, an issue is found in the literature regarding ceramic extrusion: the researchers do not have a universal consensus concerning which method should be used to evaluate the plasticity of the paste. For instance, Andrade *et al.* (2011) listed five main methods trying to assess the plasticity of a ceramic paste: Pferfferkorn's plasticity index; Atterberg's plasticity index; indentation; stress/strain curves; and rheological analysis. Even though there is a variety of methods suggested to evaluate the plasticity of the paste, Dondi (2006) stated that these different methods may not yield equivalent outcomes.

In addition, according to Händle (2007) and Ribeiro *et al.* (2003), the plasticity depends on intrinsic factors of the ceramic paste such as: deairing degree; water content and properties (viscosity and surface tension); particle size and particle size distribution; additives; and mineralogical components. However, not only the intrinsic properties of the paste have an effect on the plasticity, but also the process factors. For example, the temperature in which extrusion occurs as well as the pressures applied may alter the plasticity (ANDRADE, 2009). Thus, it is interesting to consider these intrinsic and process factors in order to optimize the extrusion process.

2.3 COMPRESSION TEST AS A MEANS TO ASSESS THE PLASTICITY

For the sake of defining some parameters, which are very important in the extrusion process, Flores *et al.* (2006) proposed a mathematical equation that seemed very promising. The authors considered the hypothesis that the cylindrical clay body, under compression stress, presents an axial and symmetrical deformation. Moreover, they stated that as the compression force is applied, the height of the specimen decreased while its instantaneous radius increased. Using the equations from Levy-Mises for the plastic zone (AVITZUR; FUEYO; THOMPSON, 1967) and the equation from von Mises for the effective stress, they proposed the following mathematical equation (Equation 1) (ANDRADE, 2009; FLORES; MENDES; OLIVEIRA; FREDEL *et al.*, 2006):

$$F = -2\pi\bar{\sigma}\left[-\frac{h}{2\mu}\left(r_f + \frac{h}{2\mu}\right) + \frac{h^2}{4\mu^2}exp\left(\frac{2\mu r_f}{h}\right)\right] \quad (1)$$

where F is the instantaneous axial force, $\bar{\sigma}$ the flow stress, h the final height of the sample, μ the friction coefficient between the surface of the compression machine and the clay, and r_f the final radius of the specimen.

Equation 1 is used to assess the plasticity of the clay during the axial compression test. Additionally, using Equation 1 it is possible to determine the effective stress ($\bar{\sigma}$) and the friction coefficient (μ) between the clay and the punch by an iterative method. The flow stress was measured using different uniaxial compressive loadings as shown in Figure 3. It can be easily seen that barreling has occurred, and this is due to the friction between the ends of the specimen and the deforming tools/punch. As a result, the coefficient of friction was included as one of the mathematical parameters to analyze the forces that act on a cylindrical clay compact and was also assumed to be constant according to Andrade *et al.* (2013).

Figure 3 - Sectioned clay paste sample showing strain lines representing the stress distribution

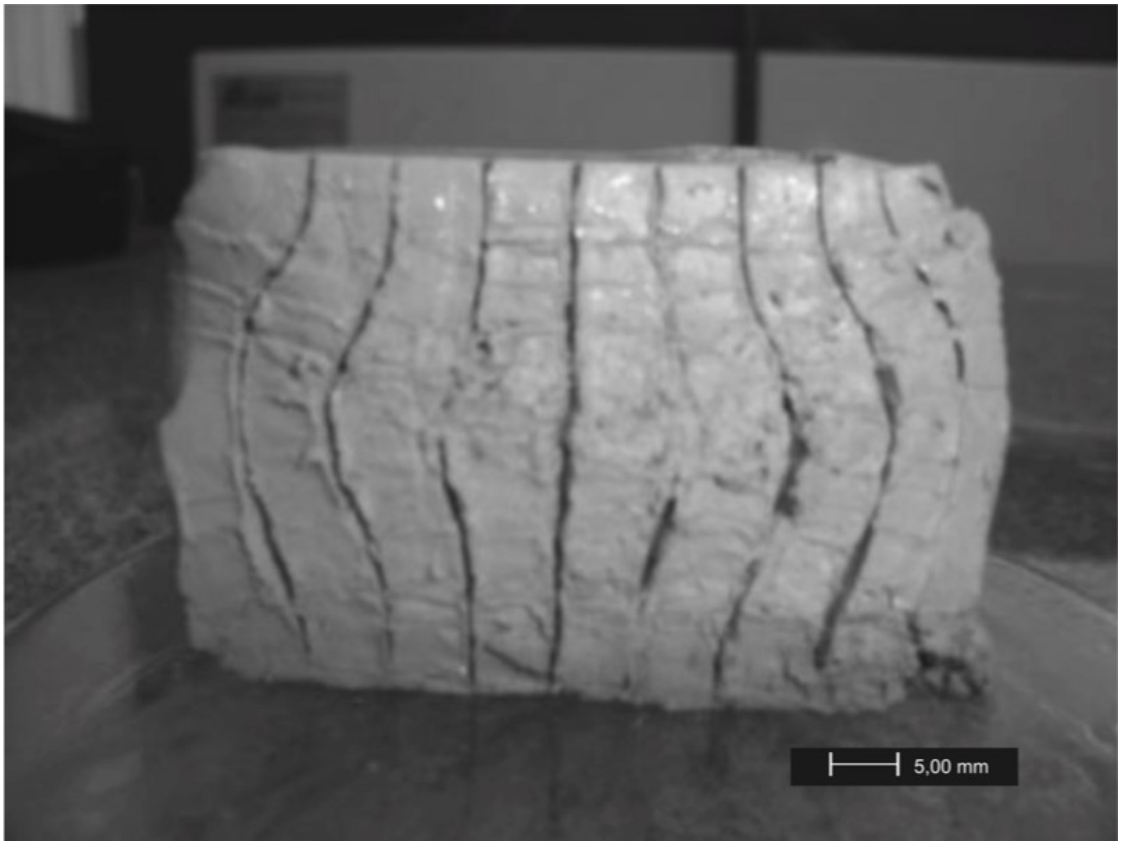

Source: adapted from: Andrade *et al.* (2013)

2.4 EQUATION IN THE EXTRUSION PROCESS TAKING INTO ACCOUNT THE FRICTION AND THE ANGULAR VARIATION

The extrusion molding process consists of compelling a paste through a die with a desired final cross section. Moreover, it shortens its cross-sectional area from initial (A_0) to final (A_f) and expands its length. At first, in order to simplify the extrusion molding process, it will be assumed the behavior of the ceramic past until the coring point (only the steady state regime). As it has already been published by Andrade (2009) and considering the second law of Newton (the acceleration of an object is dependent upon two variables: the net force acting upon the object and the mass of the object), the ideal average extrusion pressure (considering no friction during the process $\mu_{comp}=\mu_w=0$) for uniform deformation can be expressed as shown in Equation 2:

$$\sigma_{ave}\Big|_{\mu=0} = 1.5\int_0^{\bar{\varepsilon}} \bar{\sigma} d\bar{\varepsilon} \tag{2}$$

where σ_{ave} is the average extrusion pressure, μ is the coefficient of friction between the cylinder wall and the clay paste, 1.5 is the shear factor which is used to compensate the energy loss, mainly due to the friction and redundant work that is not included in equation, $\bar{\sigma}$ is the flow stress, and $\bar{\varepsilon}$ is the flow strain. Moreover, there are three different types of deformations that can be described in the extrusion: homogenous deformation, frictional deformation, and redundant deformation. For instance, the homogeneous deformation is related only to the geometric change (variation between the final and initial dimensions); the frictional deformation is associated with the strains which are generated where there is a relative movement between the two surfaces; finally, the redundant deformation is akin to deformation which does not lead to any dimensional modification (shear stress in cross-section reduction).

In Equation 2, it is possible to observe that it does not consider the friction in the cylinder wall (μ=0); therefore, in Equation 3, it is proposed a new approach, which

takes into account the cylinder wall friction (μ_w) in the extrusion direction (Figure 4) as it happens during the process.

$$d\sigma_z = \frac{4\mu_w \sigma_r}{D_0} dz \quad (3)$$

where σ_z is the axial stress, μ_w the coefficient of friction between the wall and the clay paste, σ_r the radial stress, *z* the punch travel and D_0 the initial diameter.

Figure 4 - Diagrammatic sketch of extrusion of clay paste through a circular die with angular variation

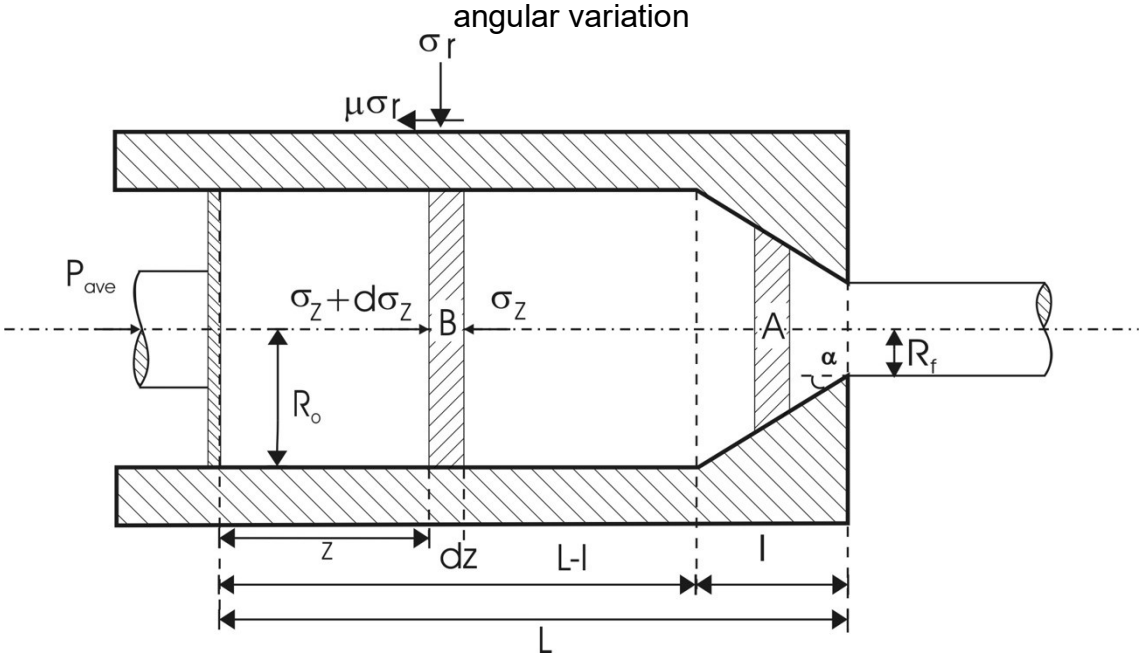

Source: Adapted from Andrade (2009)

Observing, Figure 4, one can note that the diameter of the cylinder is constant, until reaching the conical part of the extruder (L-l). Moreover, considering the Levy-Mises relationships (HOFFMAN; SACHS, 1953), which states that σ_r=σ_z, Equation 4 is reached:

$$\ln \sigma_z = \frac{4\mu_w z}{D_0} + C \quad (4)$$

Taking into account the boundary condition where $\sigma_{ave}(\mu_w=0)$ at $z=L_c$, considering that the total pressure can be written as $(\sigma_z)_{total} = (\sigma_z)_{\mu\neq 0} + (\sigma_z)_{\mu=0}$, and the funneling effect (ANDRADE; AL-QURESHI; HOTZA, 2013), Equation 5 and Equation 6 can be derived:

$$P_{total} = (\sigma_z)_{total} = \left\{1 + exp\left[\frac{4\mu_w}{D_0}(z - L_c)\right]\right\} 1.5 \int_0^{\bar{\varepsilon}} \bar{\sigma} d\bar{\varepsilon} \tag{5}$$

$$\bar{\sigma} = \sigma_z = -\bar{\sigma}_{comp} exp\left[\frac{2\mu}{h}(R_f - R_0)\right] \tag{6}$$

where $\bar{\sigma}_{comp}$ stands for the effective stress of compression, R_f the final radius and R_0 the initial radius.

Combining Equation 5 and Equation 6, yields Equation 7:

$$P_{total} = 0.75 \frac{\bar{\sigma}_{comp} z}{(R_f - R_0)\mu_{cil}} \left\{1 + exp\left[\frac{2\mu_w}{R_0}(z - L_c)\right]\right\} \left\{1 - exp\left[\frac{2\mu_{cil}}{z}(R_f - R_0)\right]\right\} \tag{7}$$

Equation 7 does not consider a circular die with angular variation, it is only the expression for total extrusion pressure, when the semi cone angle of the die (α) is equal to 90°. However, taking into account the angular variation of the die and making the pressure balance in the A and B regions of the die, as can be seen in Figure 4, the average extrusion pressure can be determined in Equation 8, as published by Andrade (2009):

$$\frac{P_{ave}}{\bar{\sigma}_{comp}} = \frac{1}{(R_f - R_0)} \frac{z}{2\mu_{cil}} \Bigg\{ 1 - exp\left[\frac{2\mu_{cil}}{z}(R_f - R_0)\right] \Bigg\} \Bigg\{ \Bigg\{ 1 + \frac{(1 + \mu_w \cot\alpha)}{\mu_w \cot\alpha} \left[\left(\frac{R_0}{R_f}\right)^{2\mu_w \cot\alpha} - 1 \right] \Bigg\} exp\left\{ 2\mu_w \cot\alpha \left[-\frac{L_c}{R_0} \tan\alpha + \left(1 - \frac{R_f}{R_0}\right) \right] \right\} - 1 \Bigg\} \tag{8}$$

Therefore, with Equation 8, developed by Andrade (2009), it was possible to evaluate the extrusion pressure as a function of the distance traveled by the ram. His mathematical model seemed to be robust since he considered important variables within the process such as the barrel and die's geometry and the coefficient of friction. Additionally, there was a good fit between his proposed equation and the experimental data up to the unsteady state regime, as it is displayed in Figure 5.

Figure 5 - Plot of experimental data (squares) and an extrusion pressure equation (solid line) proposed by Andrade (2009)

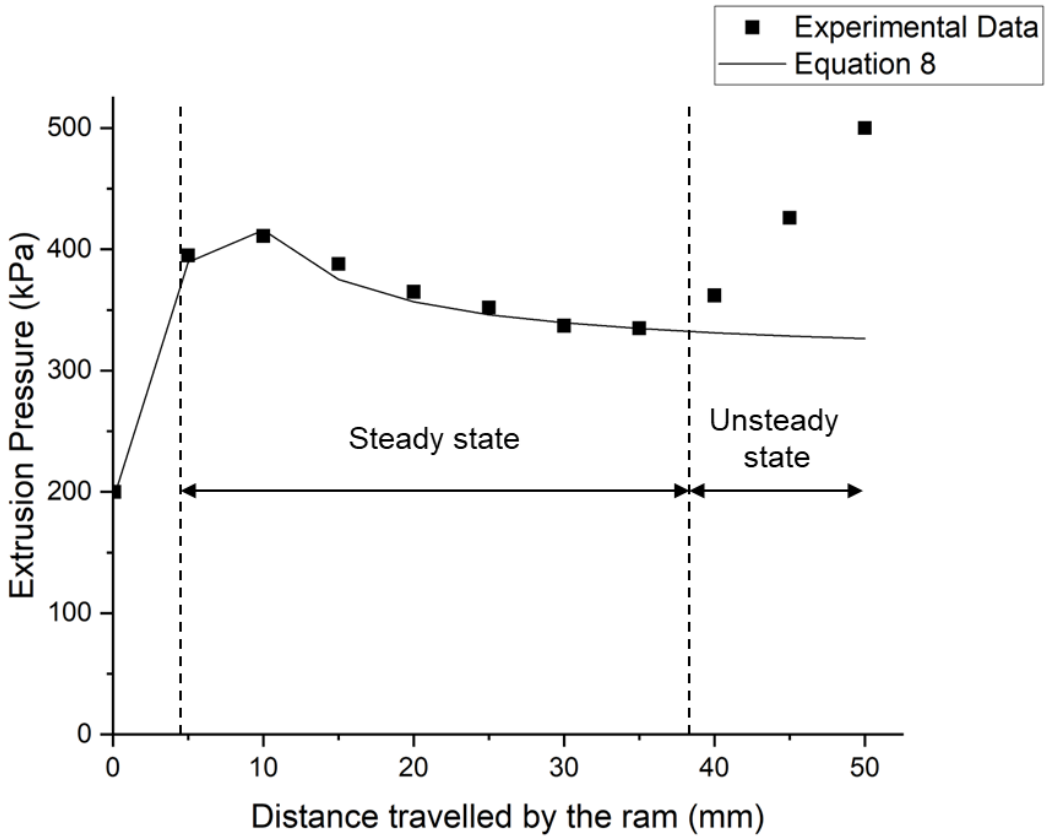

Source: Adapted from: Andrade (2009)

For the sake of further analyses, modifications, and simplifications of Equation 8, this will be partitioned into four parts (Part 1; Part 2; Part 3; and Part 4) as it is shown in Chart 1. A detailed analysis of such parts can also be found in Andrade (2009).

Chart 1 - Partition of Equation 8 into 4 parts, for better visualization and further analyses

$\frac{\bar{\sigma}_{comp}}{(R_f - R_0)} \frac{z}{2\mu_{cil}}$	$1 - exp\left[\frac{2\mu_{cil}}{z}(R_f - R_0)\right]$	$1 + \frac{(1+\mu_w \cot\alpha)}{\mu_w \cot\alpha}\left[\left(\frac{R_0}{R_f}\right)^{2\mu_w \cot\alpha} - 1\right]$	$exp\left\{2\mu_w \cot\alpha\left[-\frac{L_c}{R_0}\tan\alpha + \left(1 - \frac{R_f}{R_0}\right)\right]\right\} - 1$
Part 1	***Part 2***	***Part 3***	***Part 4***

Source: Author

2.5 DIMENSIONAL ANALYSIS

The fundamental principle behind dimensional analysis, according to Barenblatt (1987; 1996), is that physical laws are not dependent on randomly selected basic units of measurement. As a result, the functions that express physical laws must handle particular mathematical property, which is also known in the literature as the generalized homogeneity (BRIDGMAN, 1922; GIBBINGS, 2011). Moreover, it means that each of the additive terms in the function will have the same dimensions or units (CHENG; CHENG, 2004; TRANCANELLI, 2016).

Before advancing in this topic, it is fundamental to emphasize the difference between the terms “dimensions” and “units”. Trancanelli (2016) defines “dimensions” as the intrinsic properties of the physical quantity, while “units” as a conventional unit of measure that are employed to describe the dimensions of a quantity. For example, *meter* is a unit used to measure the length L, but it is not the length itself.

The physical quantities can be classified into two different categories: *fundamental* (sometimes called as *base* units as well) or *derived* units. There are seven well-defined units which by convention are reputed as dimensionally independent. For instance: the meter, the kilogram, the second, the ampere, the kelvin, the mole, and the candela are these seven dimensionally independent units (CHENG; CHENG, 2004; MEASURES; TAYLOR; THOMPSON, 2001). Moreover, these seven base units are listed and described in Chart 2.

On the other hand, the second class of SI units is that of derived units. These units are originated as products of powers of the fundamental units according to the algebraic relations linking the quantities concerned. In addition, it is possible to form new units from the fundamental ones, and these new units might have other special names and symbols, which can themselves be used to form expressions and symbols for other derived units (MEASURES; TAYLOR; THOMPSON, 2001).

Chart 2 - Fundamental units (or base units) according to the International System of Units (SI)

Base Unit	Name	Symbol	Dimension
Length	meter	m	L
Mass	kilogram	kg	M
Time	second	s	T
Electric Current	ampere	A	I
Temperature	kelvin	K	θ
Luminous intensity	candela	Cd	I_0
Amount of substance	mole	mol	N

Source: Adapted from International Bureau of Weights and Measures (2001)

The dimension of any physical quantity is invariant concerning the chosen units. In other words, dimension is an objective quantity. For example, in the length/time/mass system, the dimensions for length, time, and mass are designated by *L*, *T*, and *M*, respectively, as shown in Chart 2. As an illustration, *pressure* with the unit of mass/(length*time) has the dimension $ML^{-1}T^{-2}$ (CHENG; CHENG, 2004).

It can be demonstrated meticulously that the dimension of any physical quantity is always a power-law monomial (BARENBLATT; ISAAKOVICH, 1996; CHENG; CHENG, 2004). Specifically, the dimension [*z*] of any physical quantity *z* in the length/time/mass system is a function of *L*, *T*, and *M* in the following form:

$$[z] = L^{\alpha}T^{\beta}M^{\gamma}$$

In this case, the exponents are real numbers associated with z. The previous equation is a consequence of that all systems within a given class of units are equivalent. In the specific example of length/time/mass, the cm-min-g and m-h-kg systems are equivalent. Moreover, a quantity is dimensionless if all α, β, and γ are zero in a given system of units (BARENBLATT; ISAAKOVICH, 1996).

To use the dimensional analysis technique, two steps are fundamental. The first step comprises of acquiring a complete set of dimensionless products. This set of dimensionless products are represented below by the π_n terms:

$$\varphi(\pi_1, \pi_2, \pi_3, \dots, \pi_{m-n}) = 0$$

Two definitions are crucial for the first step in dimensional analysis. The first one is the definition of a complete set of dimensionless products. Additionally, the set is complete if and only if all possible dimensionless products of the dimensional variables and constants can be expressed as a product of powers of members of this set. The second one is the definition of the independence of the members of the set. Moreover, it means that the members of this set are independent if and only if none of them can be expressed as a product of powers of the other members (LEMONS, 2017).

Now the second step consists of utilizing those dimensional products to obtain an equation to model the desired process. The equation bellow demonstrates that for the desired process the dimensionless π groups can be manipulated, once keeping them dimensionless (ALMEIDA; AL-QURESHI; TUSHTEV; REZWAN, 2018). Also, it is important to mention that multivariable function approximations are necessary if the number of dimensional products found is greater than one.

$$\varphi\left(exp(\pi_1), ln(\pi_2), (\pi_3)^i, \dots, \pi_{m-n}\right) = 0$$

With those definitions clarified, the Buckingham π theorem can now be introduced. The Buckingham π theorem affirms that the number of complete and independent dimensionless products (Np) is equal to the number of dimensional variables and constants (Nv) minus the number of dimensions (Nd) needed to express their dimensional formulae (BUCKINGHAM, 1914):

$$N_p = N_v - N_d$$

In the common case of multiple independent dimensionless products, in order to solve the values of the products, first, it is necessary to establish the repeating or the fundamental variables. The only requisite for the repeating variables is that they must be independent as defined previously (BUCKINGHAM, 1914). One way to

assure that the chosen repeating variables are adequate for the system is calculating the determinant of those candidates' repeating variables. For instance, if the determinant is different than zero, it means that the selected repeating variable can be used as the repeated variables. Now, with the repeating variables selected the remaining dimensionless products can be found by forming individual linear systems with each of the remaining dimensionless products and the repeating variables (ALMEIDA; AL-QURESHI; TUSHTEV; REZWAN, 2018; LEMONS, 2017).

In conclusion, dimensional analysis is a very effective tool for indicating relevant data and how they are related. This analysis consists of mathematically expressing a relationship between the variables involved in a physical situation. The resulting expression can then be used to effectively obtain any unknown factor from experimental results (ALMEIDA; AL-QURESHI; TUSHTEV; REZWAN, 2018; TRANCANELLI, 2016).

3 MATERIALS AND PROPOSED THEORETICAL ANALYSES

Within this section, a detailed description on eight distinct materials (ranging from alumina to different types of clays) is listed. Moreover, all these listed materials were cited in the literature as the starting material for direct ram extrusion. These materials were used to build and supplement the theoretical analyses and later the produced models were tested and applied using them.

Next, four novel theoretical analyses, followed by four equations are introduced. The first theoretical analysis associates the rise of the extrusion pressure after the coring point with the friction variation as a function of the density of the extruded material; the second approach relates the unsteady state with the spring-back phenomenon; the third theoretical analysis correlates the increase of the extrusion pressure with the water content variation of the ceramic paste over the time; and lastly, the fourth approach uses the main variables encountered in the previous three theoretical analyses and a new model is proposed using *dimensional analysi*s.

3.1 MATERIALS

The materials that were used in the present work as the reference materials are listed in Chart 3. These materials were selected since either they were processed using a direct ram extruder or they were assessed using certain techniques that yielded results that supported the theoretical analyses. As it can be noted in Chart 3, the materials varied from alumina to different kinds of clay.

Chart 3 - List of materials employed in the present work

Material	**Chemical Composition**	**Description**	**Reference**
Alumina	Al_2O_3	α-alumina	Benbow, Oxley and Bridgwater (1987)
Clay	SiO_2, Al_2O_3, Fe_2O_3, CaO, Na_2O, K_2O, MnO, TiO_2, MgO, P_2O_5	Caulinite, quartz	Andrade (2009)
Bentonite	$(Na,Ca)_{0.33}(Al,Mg)_2(Si_4O_{10})(OH)_2nH_2O$	Montmorillonite	De Wit and Arens (1950)
Earthenware	N/A	Ball clay, kaolin, quartz, feldspar, calcite, talc	Ribeiro, Ferreira and Labrincha (2005)
Grey clay – carbonate clay	N/A	Quartz, illite, muscovite, smectite, albite, goethite, kaolinite, calcite, dolomite, microcline, chabazite, amorphous content	Hamza *et al.* (2019)
Yellow clay – carbonate clay	N/A	Quartz, illite, muscovite, smectite, albite, goethite, kaolinite, calcite, dolomite, microcline, chabazite	Hamza *et al.* (2019)
Carbonate free clay	N/A	Quartz, illite, muscovite, smectite, albite, goethite, kaolinite, microcline, chabazite, amorphous content	Hamza *et al.* (2019)
Red mud	N/A	Quartz, gibbsite, calcite, hematite, cancrinite, goethite, kimezeyite	Hamza *et al.* (2019)

Source: Author

3.2 PROPOSED THEORETICAL ANALYSES

Extrusion pressure beyond the steady state

As shown through experimental results by some researchers such as Benbow and Bridgwater (1993), Liu *et al.* (2013), Rough *et al.* (2002), and others, the extrusion pressure does not remain constant throughout the entire extrusion process. Moreover, it is possible to observe a significant rise in the extrusion pressure, highlighting the shift from a steady state to a unsteady state behavior. This transition, also known as “point of coring”, can be associated with significant changes in the chemical and physical properties of the ceramic paste.

The mathematical model proposed by Andrade (2009), described previously in Equation 8, seems to be a very promising and accurate equation to evaluate the extrusion pressure profile along the ram displacement. Nevertheless, his equation does not take into account the point of coring. Thus, the transition from the steady state to the unsteady state is neglected which can lead to vulnerable issues ranging from the compromised quality of the final product to damage to the equipment.

In order to fill this gap in the scientific and industrial realm, theoretical analyses will be performed and four equations will be proposed modifying the Andrade (2009) equation (Equation 8) and proposing new theories as well. The first approach associates the rise of the extrusion pressure after the coring point with the friction variation as a function of the density of the extruded material; the second approach relates the unsteady state with the spring-back phenomenon; the third approach correlates the increase of the extrusion pressure with the water content change of the ceramic paste over the time; and finally, the fourth approach uses the main variables encountered in the previous three mathematical theories and new a model is proposed using *dimensional analysi*s. For instance, Figure 6 presents a simple scheme of the whole work.

Figure 6 - Summary of the broad diagram for the proposed theoretical analyses

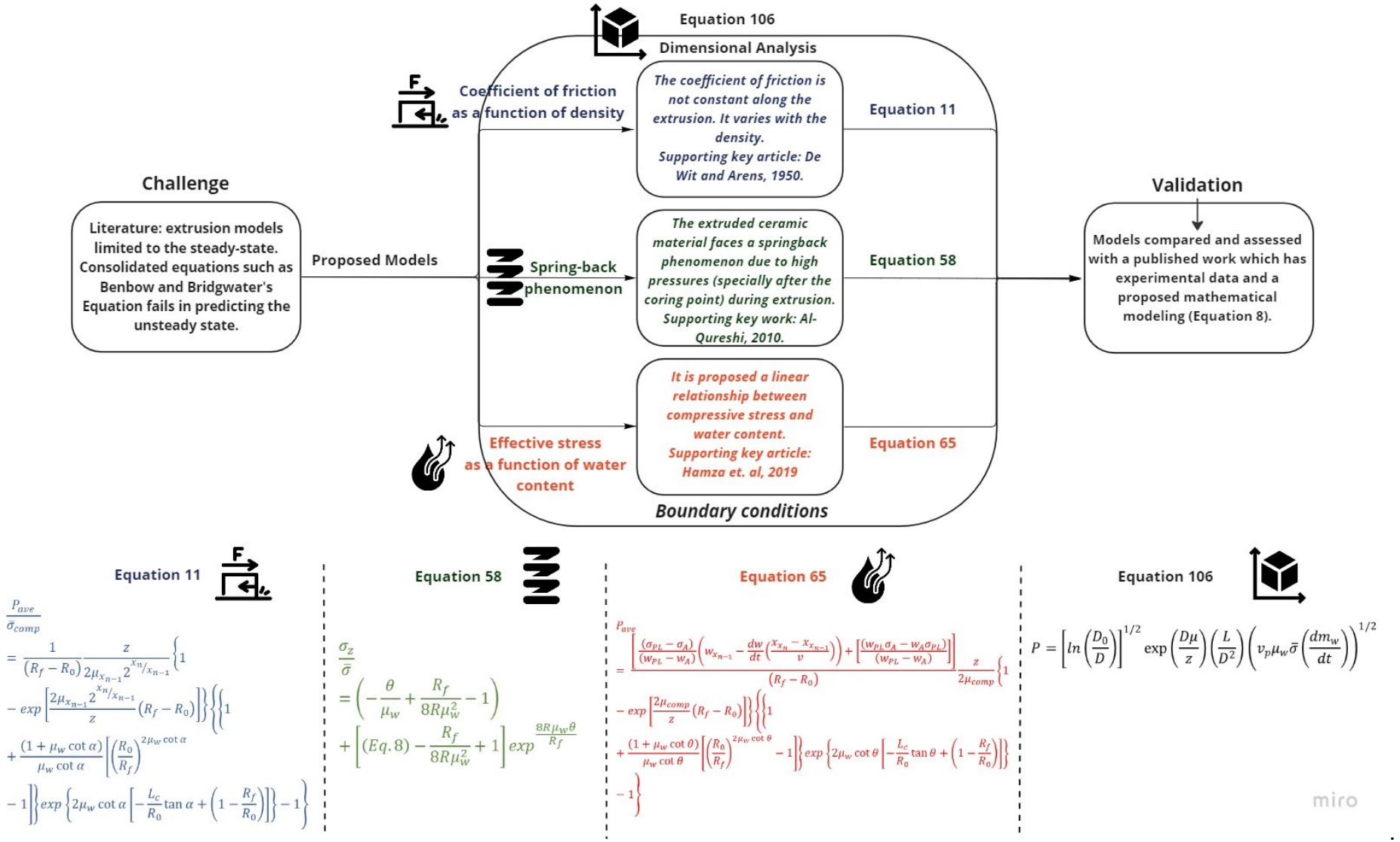

Source: Author

4 RESULTS AND DISCUSSION

For a better organization of the results, this section is divided into two categories: specific and general results and discussion.

4.1 SPECIFIC RESULTS AND DISCUSSION

4.1.1 Coefficient of friction as a function of the density

This approach considers that the friction coefficient (μ) during the extrusion is not constant during the entire process; on contrary, it is proposed that it is a function of the density of the extruded material. As the punch proceeds to move forward, to the end of the barrel, some operational parameters may change. As a result, it is assumed that the friction changes along the punch and the cylinder wall. In addition, it is considered that the extrudate composition and the pressure are not anymore at a steady state as in the previous stage. It is observed that it becomes unsteady and it varies according to the punch movement. This action might cause loss of water content (water migration) and densification of the clay, and there might also be changes in the viscosity of the clay paste. It is well known that friction dominates the flow of the clay paste throughout the die. Hence it influences greatly the extrusion pressure along the extruded part after the coring point.

It is very difficult to derive these variations of the parameters mathematically. However, the initial trial is to assess the varieties of the experimental entries, considering, for instance, the Arrhenius relation. In this work it is suggested that the relationship among ram displacement, coefficient of friction, and density can be given by the following equation:

$$\mu_{x_n} = \mu_{x_{n-1}} \left[\frac{\rho_{x_n}}{\rho_{x_{n-1}}} \right]^{x_n / x_{n-1}} \tag{9}$$

where μ_{x_n} , $\mu_{x_{n-1}}$ are the coefficient of friction at the x_n and x_{n-1} positions of the ram. Similarly, ρ_{x_n} and $\rho_{x_{n-1}}$, are the densities of the ceramic paste at the position, respectively.

De Wit and Arens (1950) demonstrated in a conference held in Amsterdam that the density of some clay minerals, can have their densities doubled depending on the moisture content of the material (DE WIT; ARENS, 1950). Moreover, Figure 7 shows their experimental results.

Figure 7 - Density as a function of moisture (water) content for three types of clay-based raw material

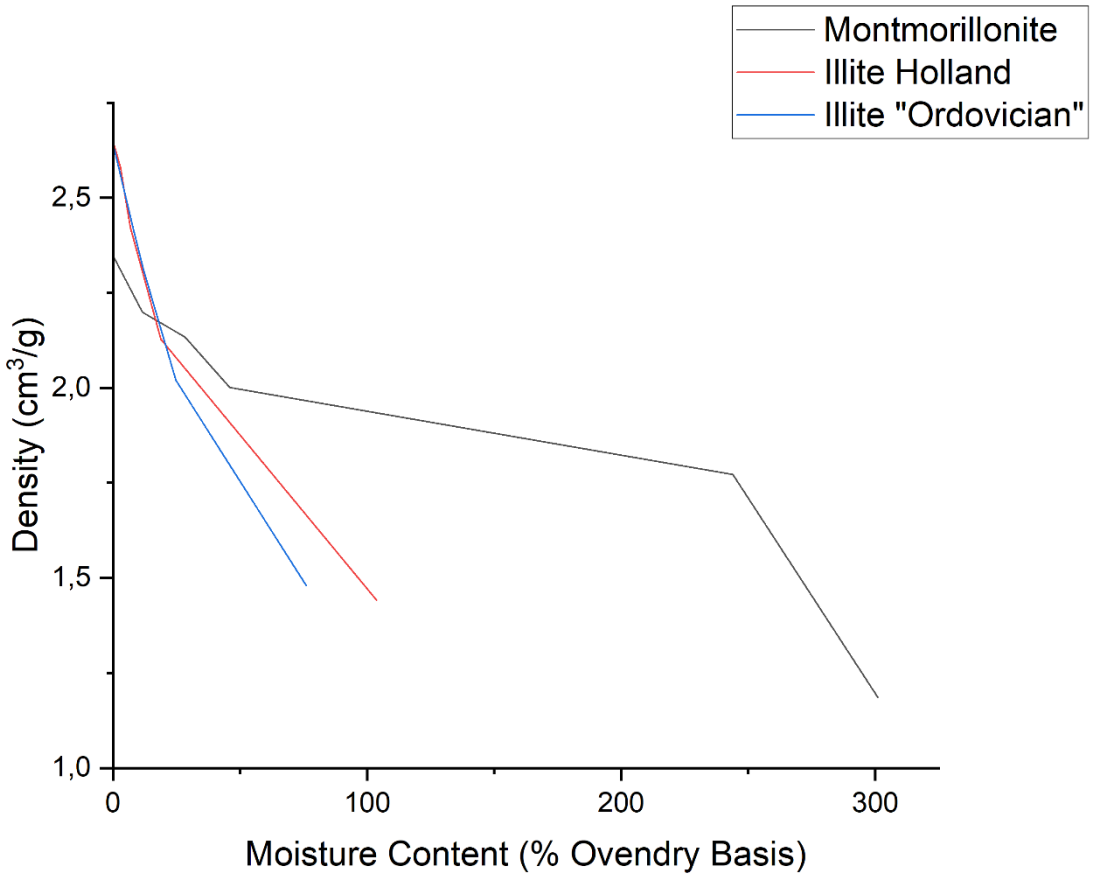

Source: Adapted from De Wit and Arens (1950)

In fact, the plot of ρ_{x_n} against $\rho_{x_{n-1}}$ can be considered linear and $\rho_{x_{n-1}}$ have their approximate relationship, expressed in Equation 10:

$$\rho_{x_n} = 2\rho_{x_{n-1}} \quad (10)$$

The above equation makes the solution of Equation 9 easier and enhances the extrusion pressure, given in Equation 8 at any ram position, which would predict the final extrusion pressure as expressed in Equation 11:

$$\frac{P_{ave}}{\bar{\sigma}_{comp}} = \frac{1}{(R_f - R_0)} \frac{z}{2\mu_{x_{n-1}} 2^{x_n/x_{n-1}}} \Bigg\{ 1 - exp\left[\frac{2\mu_{x_{n-1}} 2^{x_n/x_{n-1}}}{z} (R_f - R_0) \right] \Bigg\} \Bigg\{ \Bigg\{ \Bigg(1 + \frac{(1 + \mu_w \cot\alpha)}{\mu_w \cot\alpha} \left[\left(\frac{R_0}{R_f} \right)^{2\mu_w \cot\alpha} - 1 \right] \Bigg\} exp\left\{ 2\mu_w \cot\alpha \left[-\frac{L_c}{R_0} \tan\alpha + \left(1 - \frac{R_f}{R_0} \right) \right] \right\} - 1 \Bigg\} \tag{11}$$

Thus, analyzing Equation 11 and comparing it with Equation 8, it is possible to notice that the Part 1 and Part 2 (displayed in Chart 1) of Equation 8 are different, since the μ_{cil}, in Equation 8, was replaced by $\mu_{x_{n-1}} 2^{x_n/x_{n-1}}$, in Equation 11. Additionally, this variable (μ_{cil}) is present only in Part 1 and Part 2; whereas Part 3 and Part 4 of Equation 8 remained the same. Moreover, the plots of the comparison between Equation 8 and Equation 11, in Part 1 and Part 2, are shown respectively in Figure 8 and Figure 9. They will be discussed later on.

Figure 8 - Part 1 plot of Equation 8. In Equation 11, the term μ_{cil} is substituted by $\mu_{x_{n-1}} 2^{x_n / x_{n-1}}$

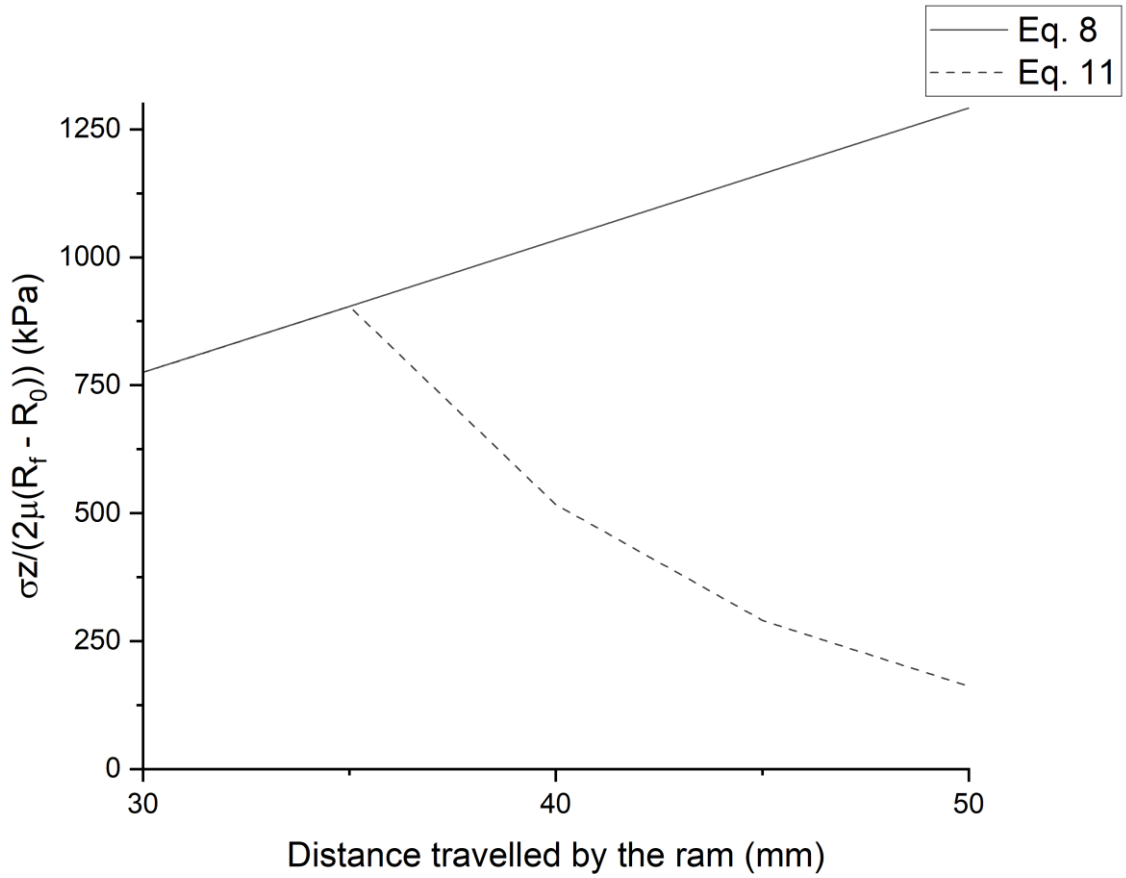

Source: Author

Figure 9 - Part 2 plot of Equation 8. In Equation 11, the term μ_{cil} is substituted by $\mu_{x_{n-1}} 2^{x_n / x_{n-1}}$

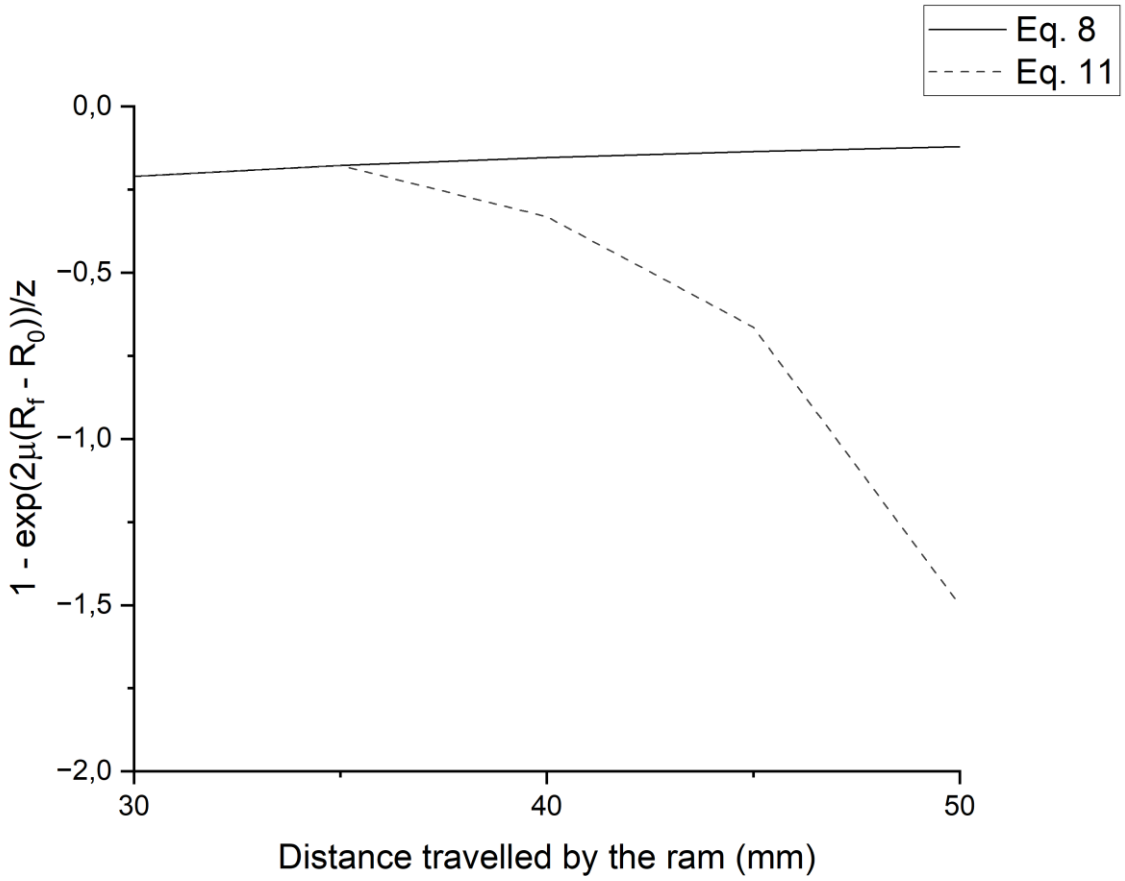

Source: Author

Analyzing Figure 8 and Figure 9, one can recognize that after reaching the coring point (approximately after 35 mm of ram displacement), both, Part 1 (Figure 8) and Part 2 (Figure 9) display a decrease in their values as the ram moves forward. It is also possible to discern that evaluating the parts individually would lead to contradictory results. Once the values are diminishing after reaching the coring point, instead of increasing, as it is expected.

Taking close attention to the results of Equation 11, it is evident that the value becomes more negative as the piston advances in the barrel. Moreover, Equation 8 is a product of Part 1, Part 2, Part 3, and Part 4, as already stated previously (Chart 1). Part 3 also has a negative value; therefore, the product of Part 2 and Part 3 always leads to a positive value.

Even though the value of Part 1 of Equation 11 is decreasing as extrusion proceeds, the product of Part 2 and Part 3 is increasing. Additionally, the values of Part 3 and Part 4 in Equation 8 and Equation 11 are the same during the whole extrusion process. Still, after the coring point, there is a net extrusion pressure raise, because the increase rate in Part 2 (≈0.56 1/mm) is superior to the decrease rate in Part 1 (≈0.37 kPa/mm).

4.1.2 Spring-back phenomenon

As mentioned previously, the point of coring can be marked by a sudden increase in the extrusion pressure (DODEJA; JOHNSON, 1957; JOHNSON, 1956). Moreover, another theoretical explanation for it could be reached by analyzing the effect of the elastic recovery of the material after being extruded.

This theory considers the influence of the material spring-back. The spring-back phenomenon is widely referred to and studied mainly in the field of metal forming (AL-QURESHI, 1974; 1999; AL-QURESHI; RUSSO, 2002). In metallurgy, according to Chongthairungruang *et al.* (2013), spring-back phenomenon can be inferred as a physical phenomenon that is associated with elastic strain recovery after reloading deformation loads. In addition, the authors state that it is a mechanism that is governed basically by stress (CHONGTHAIRUNGRUANG; UTHAISANGSUK; SURANUNTCHAI; JIRATHEARANAT, 2013).

In summary, when the material is extruded, it is under compressive stresses duo to the barrel and die constraint. After the material exits the die, there is no longer any constraint in the radial direction and the material is free for elastic recovery. Furthermore, the greater the compressive stress, the greater the strain of the material. Regarding the strain of the material, it is deeply linked to the Poisson's ratio. The Poisson's ratio is the negative of the ratio of transverse strain to axial or lateral strain. In this case, $\upsilon = -{}^{\varepsilon_R}/_{\varepsilon_z}$, where v is the Poisson's ratio and ε_R and ε_z are the strains in the radial and axial direction (z direction). Therefore, when the material is relieved from the radial stress (after exiting the die's outlet) and it causes a counter axial stress, opposite to the extrusion direction, rising the extrusion pressure. The combination of the radial stress release and the effect of the counter axial stress causes the spring-back phenomenon.

So far, in the literature (regarding direct extrusion of ceramic), it is not possible to find any published work which considers this phenomenon and expresses it mathematically. Thus, it becomes evident that all the previous responses that the material undergoes during extrusion, in special the spring-back phenomenon is the

main objective of this approach; however, once again it is worth to mentioning that this kind of behavior has, yet not been published previously. Hence, the proposed spring-back phenomenon can be incorporated in the extrusion equation as it follows.

Figure 10a clearly shows that on the exit side of the die, the material recovers elastically after being processed. For further analyses, the circled area on the die (Figure 10a) is amplified to show the acting stresses in that section (Figure 10b). Now, considering a simple element in equilibrium, represented by the shaded area displayed in Figure 10a, the balance of forces can be calculated ($\sum F_z = 0$), which leads to the following equation:

Figure 10 - Illustration of the spring-back phenomenon during the extrusion of ceramic paste after the coring point

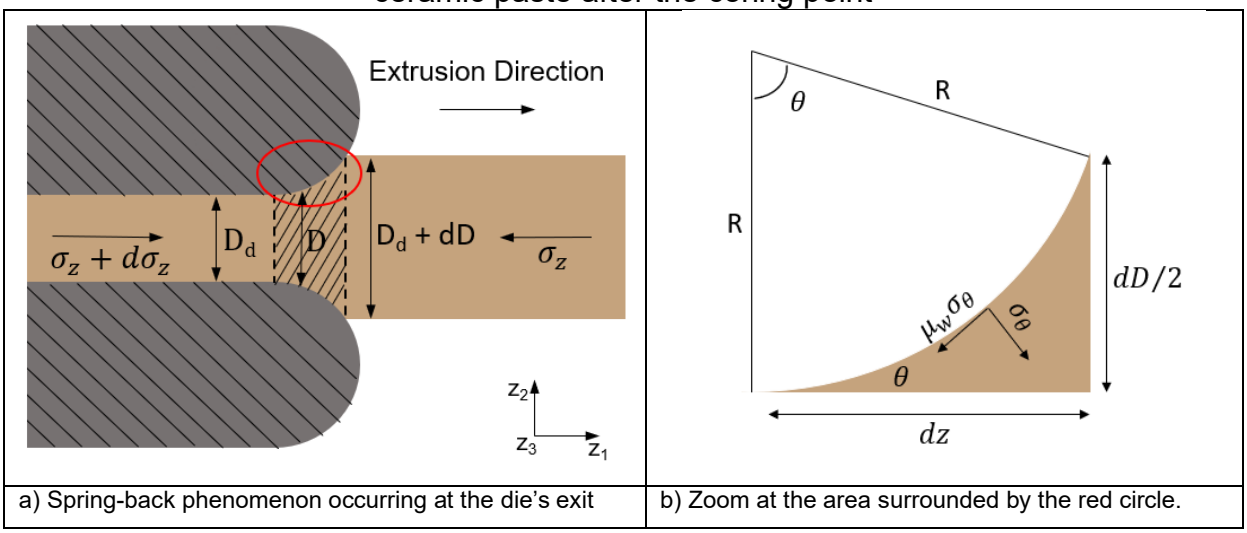

a) Spring-back phenomenon occurring at the die's exit

b) Zoom at the area surrounded by the red circle.

Source: Author

$$(\sigma_z + d\sigma_z)\frac{\pi {D_d}^2}{4} - \sigma_z\pi\frac{(D_d + dD)^2}{4} - \mu_w\sigma_R\cos\theta\frac{dz}{\cos\theta}\pi D_d + \sigma_R\sin\theta\frac{dz}{\cos\theta}\pi D_d = 0 \quad (12)$$

where σ_z is the axial stress, μ_w the coefficient of friction between the wall and the clay paste, σ_R the radial stress, *z* the punch travel, D_d the diameter of the die, and *D* is the diameter of the extrudate within the shaded area (Figure 10a). This is the typical behavior after the steady state. Furthermore, the above equation can be simplified:

$$\frac{\sigma_z D_d^2}{4} + \frac{d\sigma_z D_d^2}{4} - \frac{\sigma_z D_d^2}{4} - \frac{\sigma_z D_d dD}{2} - \frac{\sigma_z d^2 D}{4} - \mu_w \sigma_R D_d dz + \sigma_R D_d \tan\theta \, dz = 0 \quad (13)$$

Once again, Equation 13 can be modified, ignoring the second derivative of the equation since it is a very small quantity, hence d^2D is approximately 0 and it yields:

$$D_d d\sigma_z - 2\sigma_z dD - 4\mu_w \sigma_R dz + 4\sigma_R \tan\theta \, dz = 0 \quad (14)$$

Yet, analyzing the geometry displayed in Figure 10b, the following equation can be achieved:

$$dz = \frac{dD}{2\tan\theta} \quad (15)$$

Considering the equations above (Equation 14 and Equation 15), it becomes fundamental to find a relation*,* in order to eliminate *D,* in Equation 14. Simply, the equation, itself, is difficult to be solved in a simplified way. For this reason, the present work simplifies the calculations by replacing the circle of radius *R*, exhibited in Figure 10b, with a second-order parabola, using the principles of an osculating circle. In addition, the osculating circle of a curve can be defined as the circle which presents the same tangent and the same curvature at a point (GRAY, 1996). An example of the osculating circle of a second-order parabola is displayed in Figure 11.

Figure 11 - Example of an osculating circle of a second-order parabola

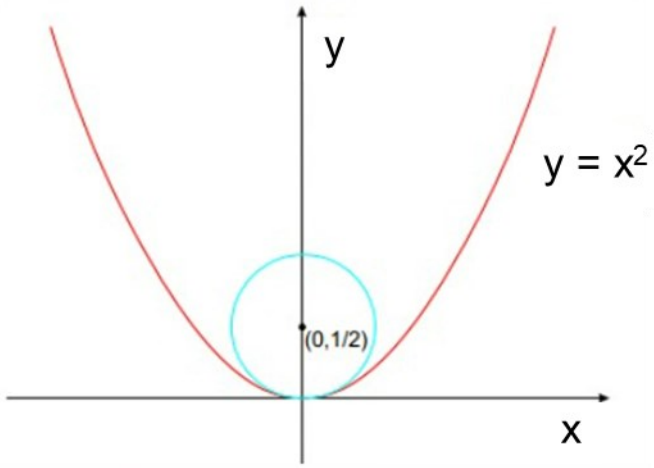

Source: Adapted from Simoni (2005)

Still related to osculating circle, it is known that it can be mathematically described as:

$$\kappa(x) = \frac{|f''(x)|}{\left(1+(f'(x))^2\right)^{3/2}} \text{ and } \rho(x) = \frac{1}{\kappa(x)}$$

where $\kappa(x)$ is the curvature of the curve; $f'(x)$ and $f''(x)$ are, respectively, the first and second derivative of the equation of the curve; and $\rho(x)$ is the radius of the curve. Thus, as stated previously, for the sake of eliminating D, the osculating circle concept was adopted, and a second-order parabolic equation was used to simplify the calculus. This proposed equation is described as follows:

$$D = D_d + \frac{z^2}{R} \tag{16}$$

Once Equation 16 describes this simplified equation and differentiating it, the following equation is achieved:

$$dD = \frac{2zdz}{R} \tag{17}$$

Now combining Equation 15 and Equation 17, it is possible to eliminate the *D* term, as expected:

$$dz = \frac{2zdz}{2R\tan\theta} \tag{18}$$

Simplifying the terms in Equation 18, a new equation is proposed:

$$z = R\tan\theta \tag{19}$$

Substituting z in Equation 16, with the expression obtained in Equation 19 leads to:

$$D = D_d + \frac{R^2\tan^2\theta}{R} \tag{20}$$

Simplifying Equation 20, one can reach the following:

$$D = D_d + R\tan^2\theta \tag{21}$$

Now differentiating Equation 19:

$$\frac{dz}{d\theta} = R\sec^2\theta \tag{22}$$

And also differentiating Equation 21 yields:

$$\frac{dD}{d\theta} = 2R\tan\theta\sec^2\theta \tag{23}$$

As mentioned before, it is possible to eliminate *D* and *dD,* leading Equation 14 in a simpler way in terms of θ and σ, by combining and arranging Equation 14, Equation 22, and Equation 23:

$$\begin{aligned} D_d d\sigma_z - 2\sigma_z 2R\tan\theta\sec^2\theta\, d\theta - 4\mu_w\sigma_\theta R\sec^2\theta\, d\theta \\ + 4\sigma_\theta\tan\theta\, R\sec^2\theta\, d\theta = 0 \end{aligned} \tag{24}$$

Arranging the terms in Equation 24:

$$D_d d\sigma_z - 4\sigma_z R \tan\theta \sec^2\theta \, d\theta - 4\mu_w \sigma_\theta R \sec^2\theta \, d\theta + 4\sigma_\theta R \tan\theta \sec^2\theta \, d\theta = 0 \quad (25)$$

Now using the relation from von Misses:

$$\bar{\sigma} = \pm(\sigma_R - \sigma_z) \quad (26)$$

And considering: $\sigma_\theta = \sigma_R$, it is achieved:

$$\bar{\sigma} = \sigma_\theta - \sigma_z \quad (27)$$

Replacing Equation 27 in Equation 25:

$$RD_d d\sigma_z - 4\sigma_z R \tan\theta \sec^2\theta \, d\theta - 4(\bar{\sigma} + \sigma_z)\mu_w R \sec^2\theta \, d\theta + 4(\bar{\sigma} + \sigma_z) R \tan\theta \sec^2\theta \, d\theta = 0 \quad (28)$$

Simplifying the terms in Equation 28:

$$D_d d\sigma_z - 4(\bar{\sigma} + \sigma_z)\mu_w R \sec^2\theta \, d\theta + 4\bar{\sigma} R \tan\theta \sec^2\theta \, d\theta = 0 \quad (29)$$

It is possible to simplify Equation 29, considering θ so small, so that it is a reasonable approximation that $\sec\theta = 1$ and $\tan\theta = \theta$. Applying this consideration into Equation 29:

$$D_d d\sigma_z - 4(\bar{\sigma} + \sigma_z)\mu_w R d\theta + 4\bar{\sigma} R\theta d\theta = 0 \quad (30)$$

Rearranging the terms in Equation 30:

$$D_d d\sigma_z - 4\sigma_z \mu_w R d\theta - 4\bar{\sigma} R d\theta(\mu_w - \theta) = 0 \quad (31)$$

Dividing Equation 31 by D_d and dθ:

$$\frac{d\sigma_z}{d\theta} - \frac{4\sigma_z\mu_w R}{D_d} - \frac{4\bar{\sigma}R}{D_d}(\mu_w - \theta) = 0 \quad (32)$$

Now considering $B = 4R/D_d$ and rearranging Equation 32:

$$\frac{d\sigma_z}{d\theta} - \sigma_z B\mu_w = \bar{\sigma}B(\mu_w - \theta) \quad (33)$$

The solution for the previous differential equation (Equation 33) can be achieved by the method of integrating factor. In addition, Equation 33 presents the following pattern:

$$y' + p(x)y = q(x) \quad (34)$$

where $p(x) = -B\mu_w$. The integrating factor (I_f) can be determined by:

$$I_f = exp^{\int -B\mu_w d\theta} \quad (35)$$

Integrating Equation 35:

$$I_f = exp^{-B\mu_w\theta} \quad (36)$$

Multiplying Equation 33 by the integrating factor (I_f):

$$\frac{d\sigma_z}{d\theta}exp^{-B\mu_m\theta} + \sigma_z exp^{-B\mu_w\theta}(-B\mu_w) = \bar{\sigma}B(\mu_w - \theta)exp^{-B\mu_w\theta} \quad (37)$$

Analyzing Equation 37, it has the following structure: $f'g + fg'$, where $f' = \frac{\sigma_z}{d\theta}, g = exp^{-B\mu_w\theta}$, $f = \sigma_z$ and $g' = exp^{B\mu_w\theta}(-B\mu_w)$, which in calculus it is known as product rule or Leibniz product rule. Rearranging the terms considering the Leibniz product rule:

$$d\left(\sigma_z exp^{-B\mu_w\theta}\right) = \left(\bar{\sigma}B(\mu_w - \theta)exp^{-B\mu_w\theta}\right)d\theta \quad (38)$$

Now integrating the first term in Equation 38, it leads to:

$$\sigma_z exp^{-B\mu_w\theta} = \bar{\sigma}B(\mu_w - \theta)exp^{-B\mu_w\theta}d\theta \quad (39)$$

Integrating the second term in Equation 39 yields:

$$\sigma_z exp^{-B\mu_w\theta} = -\bar{\sigma}B\int(\theta - \mu_w)exp^{-B\mu_w\theta}d\theta \quad (40)$$

Distributing and repositioning the terms, it leads to:

$$\frac{\sigma_z}{\bar{\sigma}}exp^{-B\mu_w\theta} = -B\int\theta exp^{-B\mu_w\theta}d\theta + B\int\mu_w exp^{-B\mu_w\theta}d\theta \quad (41)$$

Making the following consideration:

$$t = -B\mu_w\theta \quad (42)$$

Differentiating Equation 42:

$$\frac{dt}{d\theta} = -B\mu_w \quad (43)$$

Replacing Equation 43 in the second term of the Equation 41 ($B\int\theta exp^{-B\mu_w\theta}d\theta$):

$$-\frac{1}{\mu_w}\int t\, exp^t\frac{dt}{B\mu_w} \quad (44)$$

Organizing the terms of Equation 44:

$$-\frac{1}{B\mu_w^2}\int t\, exp^t dt \quad (45)$$

Now, it is possible to integrate Equation 45 in an easy way:

$$-\frac{1}{B\mu_w^2}(texp^t + exp^t) + E \quad (46)$$

Now replacing Equation 43 in the third term of the Equation 41 ($B\int \mu_w exp^{-B\mu_w\theta} d\theta$):

$$-B\mu_w \int exp^t \frac{dt}{B\mu_w} \quad (47)$$

Simplifying the terms of the Equation 47 gives:

$$-\int exp^t dt \quad (48)$$

The indefinite integral of Equation 48 is:

$$-exp^t + F \quad (49)$$

Finally, substituting the second and third terms of Equation 41 by, respectively, Equation 46 and Equation 49 (E and F are constants, therefore C = E + F, C is another constant):

$$\frac{\sigma_z}{\bar{\sigma}} exp^t = \frac{1}{B\mu_w^2}(texp^t + exp^t) - exp^t + C \quad (50)$$

Regrouping the terms in Equation 50:

$$\frac{\sigma_z}{\bar{\sigma}} exp^t = \frac{exp^t}{B\mu_w^2}(t + 1 - B\mu_w^2) + C \quad (51)$$

Replacing t, in Equation 51, by -$B\mu_w\theta$ (Equation 42):

$$\frac{\sigma_z}{\bar{\sigma}} exp^{-B\mu_w\theta} = \frac{exp^{-B\mu_e\theta}}{B\mu_w^2}(-B\mu_w\theta + 1 - B\mu_w^2) + C \quad (52)$$

Reordering the terms in Equation 52:

$$\frac{\sigma_z}{\bar{\sigma}} exp^{-B\mu_w\theta} = exp^{-B\mu_w\theta}\left(-\frac{\theta}{\mu_w} + \frac{1}{B\mu_w^2} - 1\right) + C_1 \quad (53)$$

As stated before, $B = 4R/D_d$ and simplifying Equation 53, therefore:

$$\frac{\sigma_z}{\bar{\sigma}} = \left(-\frac{\theta}{\mu_w} + \frac{D_d}{4R\mu_w^2} - 1\right) + C_1 exp^{\frac{4R\mu_w\theta}{D_d}} \quad (54)$$

Setting the boundary conditions:

In the threshold of the die outlet, before the ceramic paste is extruded: $\theta = 0$ and $\frac{\sigma_z}{\bar{\sigma}} = \left(\frac{\sigma_z}{\bar{\sigma}}\right)|stead - state$. Moreover, considering the Equation 8 from (ANDRADE, 2009) as a suitable model for the extrusion of ceramics within the steady-state. The following approach was adopted:

$\left(\frac{\sigma_z}{\bar{\sigma}}\right)|stead - state$ = Equation 8 (ANDRADE, 2009):

$$C_1 = \left[(Eq.8) + \frac{\theta}{\mu_w} - \frac{D_d}{4R\mu_w^2} + 1\right] exp^{-\frac{4R\mu_w\theta}{D_d}} \quad (55)$$

Thus, applying the boundary conditions stated previously yields:

$$C_1 = (Eq.8) - \frac{D_d}{4R\mu_w^2} + 1 \quad (56)$$

Once C1 was determined, it is possible to substitute Equation 56 into Equation 54:

$$\frac{\sigma_z}{\bar{\sigma}} = \left(-\frac{\theta}{\mu_w} + \frac{D_d}{4R\mu_w^2} - 1\right) + \left[(Eq.8) - \frac{D_d}{4R\mu_w^2} + 1\right] exp^{\frac{4R\mu_w\theta}{D_d}} \quad (57)$$

Now, considering $D_d = \frac{R_f}{2}$ and applying in Equation 57:

$$\frac{\sigma_z}{\bar{\sigma}} = \left(-\frac{\theta}{\mu_w} + \frac{R_f}{8R\mu_w^2} - 1\right) + \left[(Eq.8) - \frac{R_f}{8R\mu_w^2} + 1\right] exp^{\frac{8R\mu_w\theta}{R_f}} \quad (58)$$

Thus Equation 58 is another approach that takes into account the effect after the coring point, also designated as unsteady state, on the extrusion pressure. Moreover, evaluating Equation 58, θ should lay between 0 and 90˚. When θ is equal to 0˚ Equation 58 is equal to Equation 8, meaning that the extrusion process is in a steady state regime. Now, when θ equals to 90˚, Equation 58 tends to go to infinity.

Figure 12 and Figure 13 display, respectively, the effect of the radius of the die (R) and the exit angle (θ) on the value of Part 1 $\left(-\frac{\theta}{\mu_w} + \frac{R_f}{8R\mu_w^2} - 1\right)$ of the Equation 58. As it can noted, there is a decrease of the value of Part 1, as the radius and the angle increases. Moreover, the value of Part 1 soaks when the radius of the die increases. Therefore, it is possible to affirm that this part of the equation is more sensitive to the radius variation.

Figure 12 - Effect of the radius of the die on the value of $\left[\frac{R_f}{(8R\mu_w^2)}\right] - \left(\frac{\theta}{\mu_w}\right) - 1$

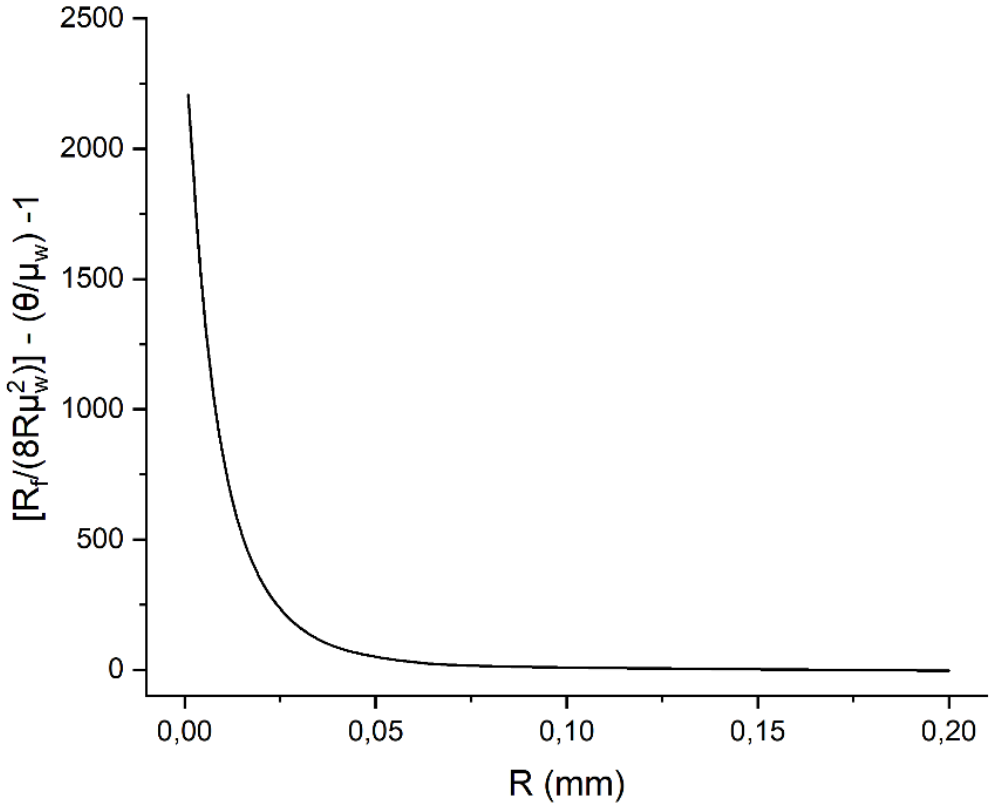

Source: Author

Figure 13 - The effect of the exit angle on the value of $\left[\frac{R_f}{(8R\mu_w^2)}\right] - \left(\frac{\theta}{\mu_w}\right) - 1$

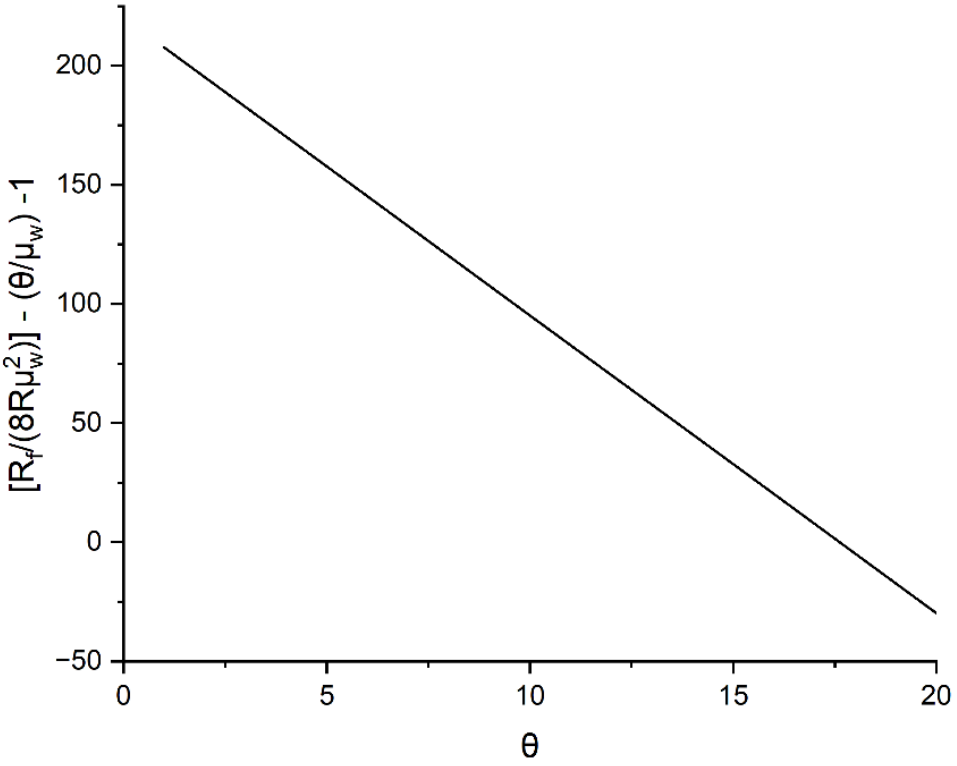

Source: Author

Moving to the analysis of the second part of Equation 58. Now we observe an opposite trend: as the radius and the angle rise, the value of the Part 2 also raises. In addition, the radius plays a more important role in the second part, when compared to the angle.

Figure 14 - Effect of the radius of the die on the value of $\left(Eq.8 - \left[\frac{R_f}{8R\pi_w^2}\right] + 1\right) exp\left(\frac{8\theta R\mu_w^2}{R_f}\right)$

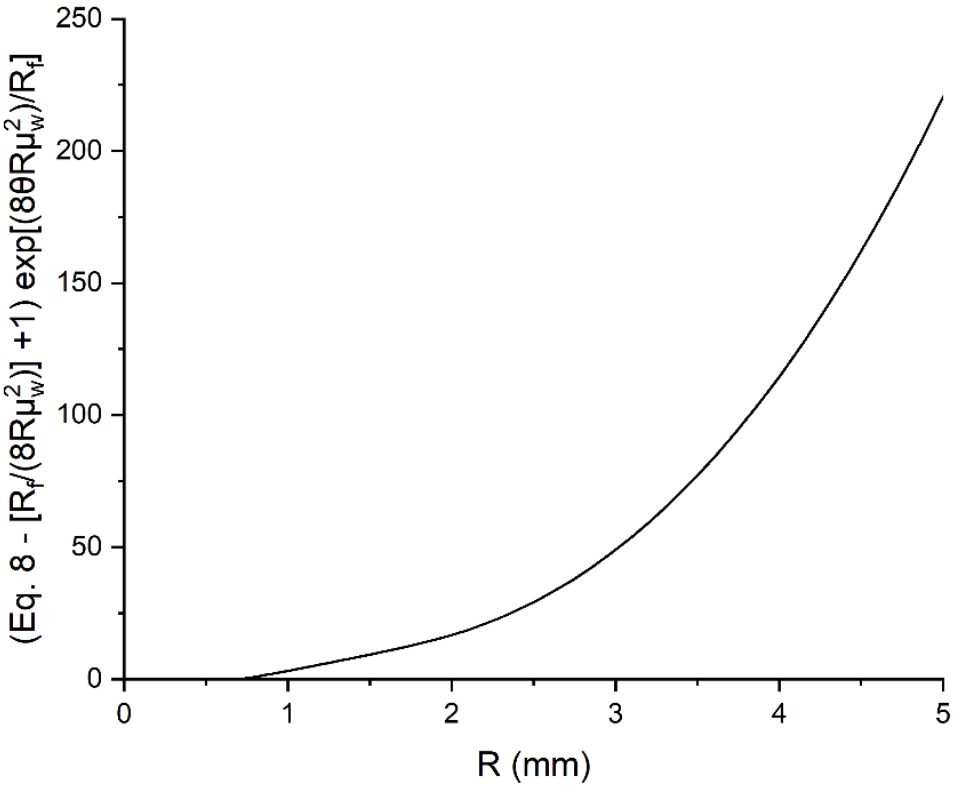

Source: Author

Figure 15 - The effect of the exit angle on the value of $\left(Eq.8 - \left[\frac{R_f}{8R\pi_w^2}\right] + 1\right) exp\left(\frac{8\theta R\mu_w^2}{R_f}\right)$

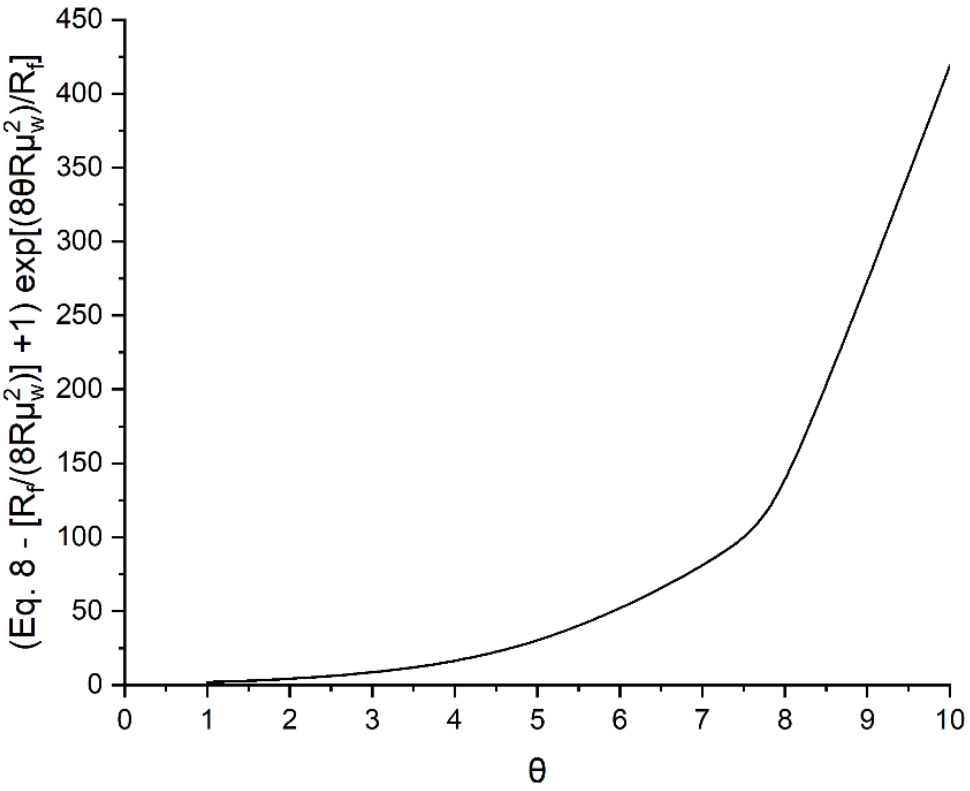

Source: Author

Now analyzing the overall influence of the radius of the die´s exit on Equation 58 (combining the results shown in Figure 12 and Figure 14), it is possible to recognize that when R approaches zero, it means that the die´s exit does not present any longer presents a round shape, instead, it has a straight edge (leading the value to infinity). Therefore, all the assumptions made to achieve Equation 58 become meaningless. In this case, it will be considered that R is not small enough of approaching a straight edge. Taking the previous consideration, it is possible to notice that as the radius of the die´s exit increases there is also a raise in the value of Equation 58. It can be explained by the fact of enlarging the radius of the die´s exit would lead to more extruded material to be in contact with the die, meaning more friction at the work-die interface (SUNIL; JOHRI; GEDAM; JAIN *et al.*, 2018). It is also known that the presence of friction within extrusion processes increases the force necessary to extrude a part.

Moving to the overall effect of the exit angle on Equation 58, one can find that the extrusion pressure increases as the exit angle rises. A higher exit angle represents more material in contact with the die´s exit, thus more friction. In this case, it is also noted that more material is in movement, particularly in the outer regions away from the center. When more material is in motion it also causes greater turbulence in the paste flow, increasing the extrusion pressure.

Still analyzing Equation 58, two parameters play a very important role in the extrusion pressure: friction coefficient (μ_w) and the percentage of cross-section reduction $\left(1 - \frac{R_f}{R_0}\right)$. Therefore, Figure 16 shows the effect of the friction coefficient on the extrusion pressure while Figure 17 displays the effect of the diameter reduction percentage on the extrusion pressure. Increasing either the friction coefficient or the percentage of diameter reduction yields a raise in the extrusion pressure throughout the entire process. Moreover, they also influence the unsteady state.

For example, for lower friction or diameter reduction percentage, the steady state was extended, and the rise of the extrusion pressure was smoother. On the other hand, for the higher friction coefficient or cross-section reduction percentage, the transition from the steady state to the unsteady state was initiated earlier and it was steeper. This trend can be explained by the fact that these conditions require a larger extrusion pressure, fomenting and intensifying the phenomenon of water migration (AZZOLINI; SGLAVO; DOWNS, 2014). This type of behavior may lead to a typical, well-known phenomenon present in other materials shaping processes (rolling, forging, direct and indirect extrusion) called the sticking region.

Summarizing, from the previous analyses, it becomes extremely evident that the pressure distribution on the unsteady state is very sensitive to the exit´s die angle, the angle of the die, the friction coefficient, and the diameter reduction percentage.

Figure 16 - The effect of the friction coefficient on the extrusion pressure

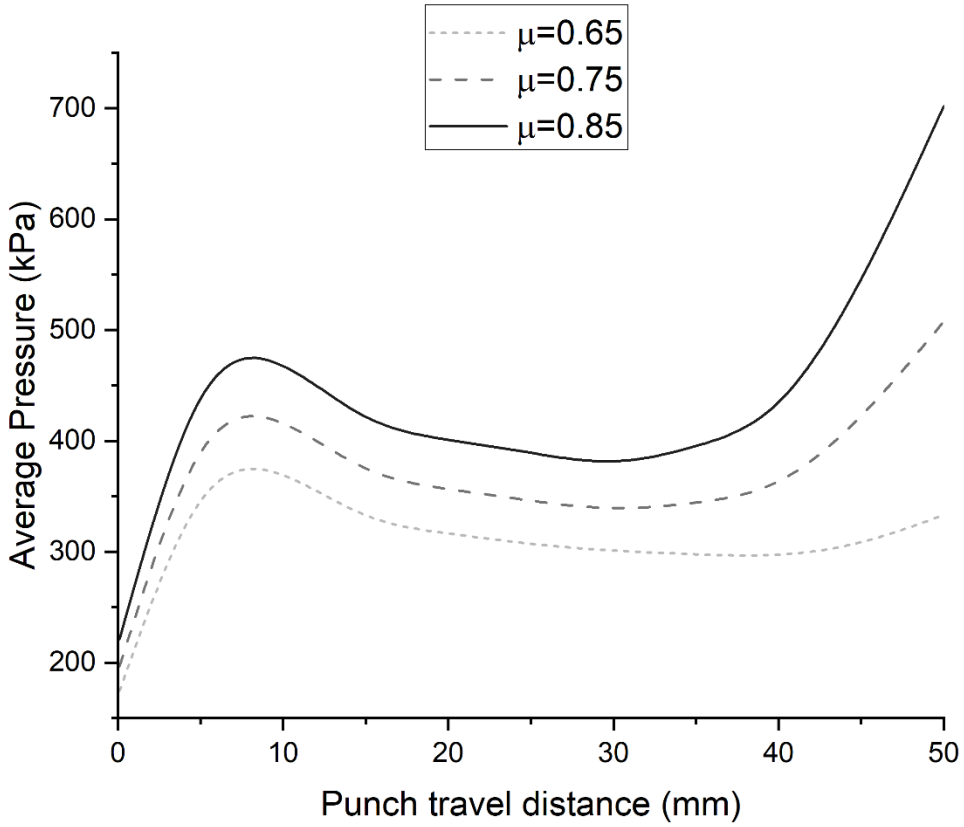

Source: Author

Figure 17 - The effect of the reduction of the diameter on the extrusion pressure

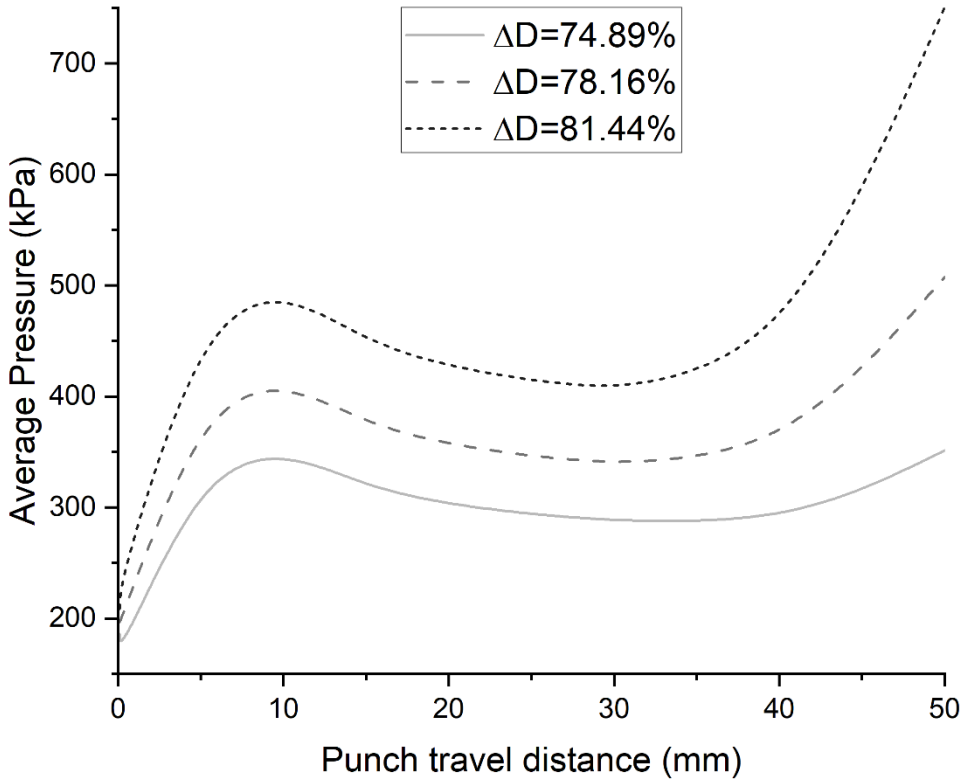

Source: Author

4.1.3 Effective compressive stress as a function of water content

Now moving to the third approach. It is found in the literature that the compressive and shear strength of the ceramic paste may vary according to the amount of water in the system (ANDRADE, 2009; BENBOW; OXLEY; BRIDGWATER, 1987; RIBEIRO; BLACKBURN; LABRINCHA, 2009; VITORINO; FREITAS; RIBEIRO; ABRANTES *et al.*, 2014; WANG; XIA; WU, 2019). For instance, Andrade (2009) found, within a certain range of humidity, a linear relation between compressive strength and water content. He observed a decrease in compressive strength when the water content increased. Yet, Wang, Xia, and Wu (2019) noticed the same trend for shear strength. Thus parameters, such as the initial bulk stress (σ_0) and the initial wall stress (τ_0), encountered in the Benbow and Bridgwater (1993) model, and the effective stress of compression ($\overline{\sigma}_{comp}$) may not be a constant value along the extrusion, especially beyond the steady state.

As it was stated previously, it is found in the literature that the compressive strength of the ceramic paste may vary according to the amount of water in the system. A published work from Andrade (2009), Ribeiro, Ferreira, and Labrincha (2005), and Hamza *et al.* (2019) show a linear trend, found in Figure 18, Figure 19, and Figure 20, respectively. All these works presented an increase in compressive strength when the water content decreased.

Figure 18 - Relation between compressive strength and water content in three different clays (A1, A2, and A3)

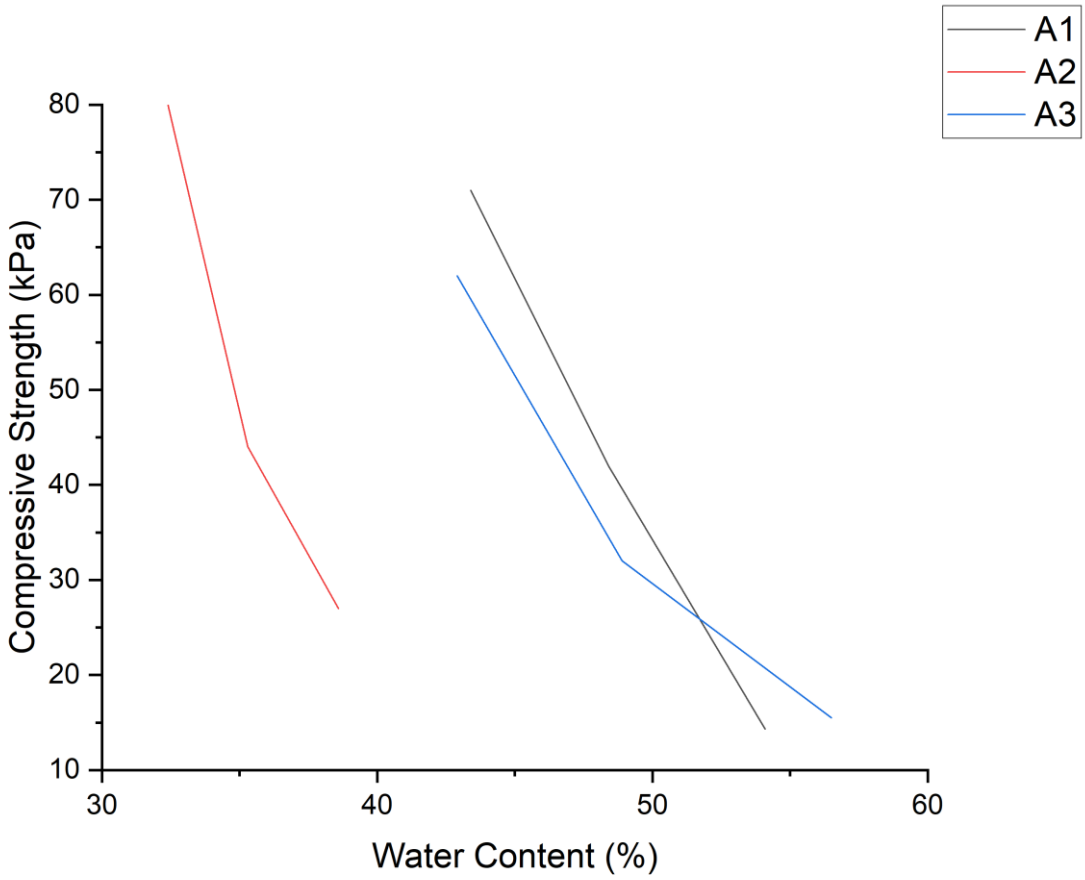

Source: Adapted from Andrade (2009)

Figure 19 - Relation between compressive strength and water content in earthenware clay

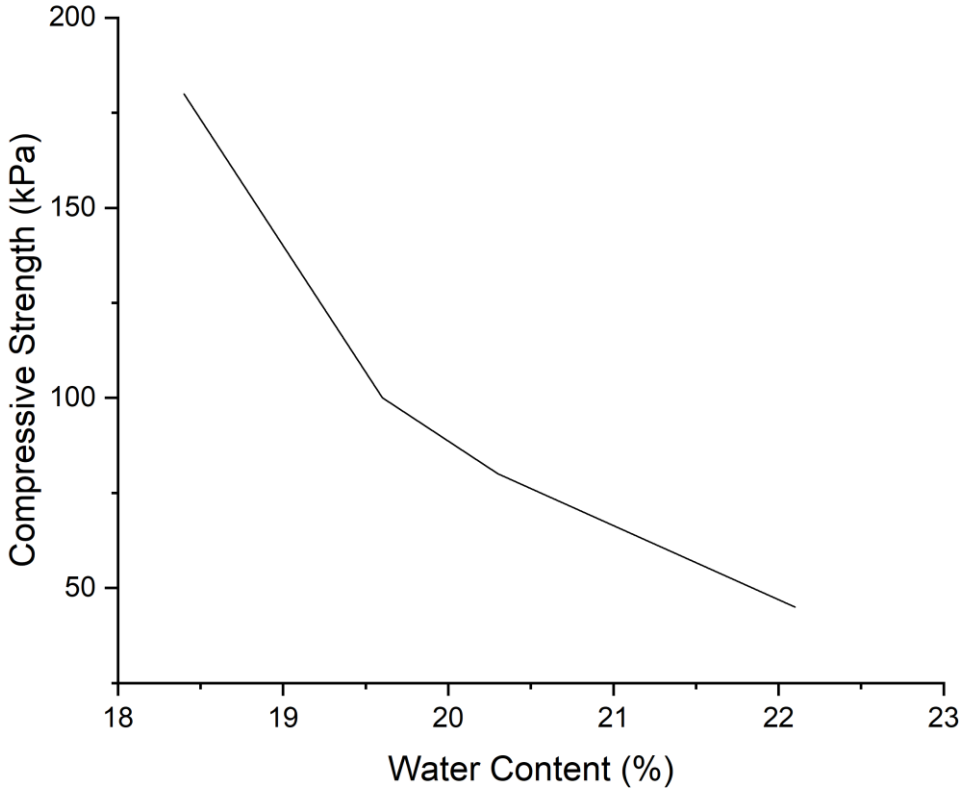

Source: Adapted from Ribeiro, Ferreira, and Labrincha (2005)

Figure 20 - Relation between compressive strength and water content in six different red clays (CC0, CC10, CC20, CC30, CFC0, CFC10, CFC20, and CFC30)

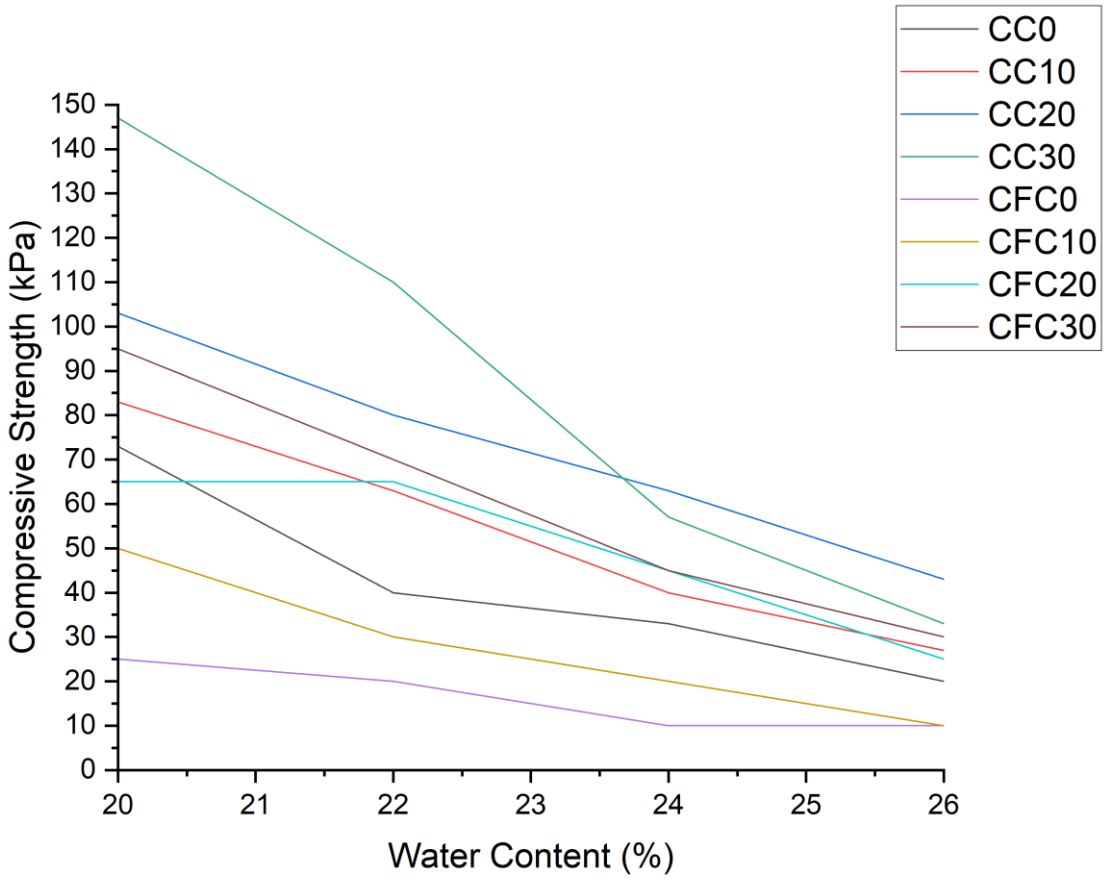

Source: Adapted from Hamza *et al.* (2019)

As can be observed in Figure 18, Figure 19, and Figure 20, it is reasonable to state that, within a certain range of water content, there is a linear relation between water content and compressive strength. Therefore, this linear tendency can be represented by the following equation:

$$\bar{\sigma}_{comp} = -aw + b \tag{59}$$

where a and b are the coefficients of the linear equation and w is the water content.

Chart 4 displays the coefficients a, and b, as well as the coefficient of determination R^2, for the published work from Andrade (2009), Ribeiro, Ferreira, and Labrincha (2005), and Hamza *et al.* (2019). As can be observed, the coefficient of determination varied from 0.8865 up to 0.9974. Moreover, half of the clays presented

values greater than 0.95, which means that the proposed assumption presents a reasonable reliability.

Chart 4 - Linear coefficients (a and b) and coefficient of determination (R^2) for different clays and published works (ANDRADE, 2009; HAMZA; KOCSERHA; GÉBER; BUZIMOV, 2019; RIBEIRO; FERREIRA; LABRINCHA, 2005)

	a	b	R^2
A1	-5.2889	299.65	0.9974
A2	-8.4707	350.48	0.9429
A3	-3.3647	202.83	0.9463
Earthenware	-3.4819	801.11	0.8865
CC0	-8.3	232.4	0.9011
CC10	-9.55	272.9	0.9888
CC20	-9.85	298.8	0.9968
CC30	-19.75	541	0.9819
CFC0	-2.75	79.5	0.8963
CFC10	-6.5	177	0.9657
CFC20	-7	211	0.8909
CFC30	-11	313	0.9878

Source: Author

Moreover, knowing the liquid limit (LL), plastic limit (PL), and the compressive strength in the plastic limit and in the liquid limit, it is suggested that within this range of water content the paste presents a linear relation, that can be represented by Equation 60:

$$A = \frac{PL + LL}{2} \tag{60}$$

It is clear that A stands for the local plastic and liquid average limit.

$$\bar{\sigma}_{comp} = w\frac{(\sigma_{PL} - \sigma_A)}{(w_{PL} - w_A)} + \left[\frac{(w_{PL}\sigma_A - w_A\sigma_{PL})}{(w_{PL} - w_A)}\right] \tag{61}$$

where σ_{PL} is the compressive strength in the plastic limit, σ_A is the compressive strength in the point A, w_{PL} is the water content in the plastic limit, and w_A is the water content in the point A.

It becomes evident, that the water content is not constant throughout the extrusion process (LIU; LIU; LEU; LANDERS *et al.*, 2013; ROUGH; BRIDGWATER; WILSON, 2000; ROUGH; WILSON; BRIDGWATER, 2002) Nevertheless, none of the previously mentioned publications related the water content and time mathematically. However, in the present work, it is proposed that the water content (w) is a function of the water content variation (dw/dt) over time as follow:

$$w = w_0 - \frac{dw}{dt}\Delta t \tag{62}$$

where w_0 stands for the initial water content, dw/dt for the water content variation over time, and Δt for a time variation. Now, combining Equation 59 and Equation 62, yields:

$$\bar{\sigma}_{x_n} = a\left(w_{x_{n-1}} - \frac{dw}{dt}\left(t_{x_n} - t_{x_{n-1}}\right)\right) + b \tag{63}$$

where $\bar{\sigma}_{x_n}$, $w_{x_{n-1}}$, t_{x_n} , and $t_{x_{n-1}}$ are, respectively, the compressive strength, water content and time at the x_n and x_{n-1} positions of the ram.

Equation 63 can also be rewritten as:

$$\bar{\sigma}_{x_n} = a\left(w_{x_{n-1}} - \frac{dw}{dt}\left(\frac{x_{x_n} - x_{x_{n-1}}}{v}\right)\right) + b \tag{64}$$

where v stands for the paste velocity in the barrel and x_{x_n} and $x_{x_{n-1}}$ for the position of the ram during extrusion.

When $x_n < x_{coring\ point}$, the water content is constant, therefore dw/dt is zero. Thus, a new mathematical model is proposed, where beyond the steady state the compressive strength no longer is constant. Combining Equation 8, Equation 61, and Equation 64 yields:

$$P_{ave} = \frac{\left[\frac{(\sigma_{PL}-\sigma_A)}{(w_{PL}-w_A)}\left(w_{x_{n-1}} - \frac{dw}{dt}\left(\frac{x_{x_n}-x_{x_{n-1}}}{v}\right)\right) + \left[\frac{(w_{PL}\sigma_A - w_A\sigma_{PL})}{(w_{PL}-w_A)}\right]\right]}{(R_f - R_0)} \frac{z}{2\mu_{cil}}\left\{1 - exp\left[\frac{2\mu_{cil}}{z}(R_f - R_0)\right]\right\}\left\{\left\{\left\{1 + \frac{(1+\mu_w \cot\theta)}{\mu_w \cot\theta}\left[\left(\frac{R_0}{R_f}\right)^{2\mu_w \cot\theta} - 1\right]\right\} exp\left\{2\mu_w \cot\theta\left[-\frac{L_c}{R_0}\tan\theta + \left(1 - \frac{R_f}{R_0}\right)\right]\right\} - 1\right\}\right. \quad (65)$$

Equation 65 describes the effect of water content variation on the extrusion pressure. It is evident that when the water content over time (dw/dt) is different than zero either the system is gaining (positive sign) or losing (negative sign) water. In the present case it is assumed that the ceramic paste is losing water (water migration) during extrusion. Hence, it has a negative signal contributing positively to the increase of the extrusion pressure. From Equation 65 it is also possible to notice that the velocity of the ram displacement plays an important role in the extrusion pressure. For instance, considering that the ceramic paste is losing water (dw/dt is negative), decreasing the ram velocity (v) will lead to a rise in the extrusion pressure. Moreover, Liu *et al.* (2013) observed this trend in their experimental results, and they stated that the steady state is enlarged when the ram velocity is increased. Additionally, they inferred this due to a lighter water loss. Reexamining Equation 65, it becomes clear that when dw/dt is equal to zero, this equation sonly stands for the steady state, which is goes back to Equation 8.

4.1.4 Dimensional analysis

In order to apply dimensional analysis to the extrusion pressure of ceramics, the following main variables were selected, and their units and dimensions are listed in Chart 5. Moreover, these variables were chosen based on three theoretical analyses discussed previously.

Chart 5 - Parameters used to estimate the extrusion pression during a direct ram extrusion process of ceramics

Parameter	Symbol	Unit	Dimension (LMT)
Pressure, stress	$P, \bar{\sigma}$	MPa	$\frac{M}{LT^2}$
Diameters, length, and height	D, D_0, L, z	mm	L
Piston velocity	v_p	mm/s	$\frac{L}{T}$
Water loss	$\frac{dm_w}{dt}$	kg/s	$\frac{M}{T}$

Source: Author

Where $v_p$is the piston velocity and $\frac{dm_w}{dt}$ is the water loss during the extrusion processes.

Taking into account the number of variables and dimensions displayed in Chart 5 and using the Buckingham π theorem, now it is possible to determine the number of dimensionless products. The Buckingham π theorem states that the number of dimensional products is equal to the number of variables and constants that describe the problem subtracted from the number of dimensions needed to express their dimensional formulae (BUCKINGHAM, 1914). Thus, it is possible to determine the number of dimensionless products using the following equation:

$$n_\pi = n_v - n_d \tag{66}$$

where n_π stands for the number of dimensional products, n_v for the number of variables, and n_d for the number of variables.

Substituting the values of n_v and n_d by 8 and 3, respectively, it is found that the number of dimensionless products is equal to 5 as it is displayed in Equation 67:

$$n_\pi = 8 - 3 = 5 \tag{67}$$

In order to achieve the exact form of the dimensionless products it is necessary to define the repeating variables. According to Buckingham, the number of repeating variables must be equal to the number of dimensions of the problem. In this case, there should be 3 repeating variables, since there are 3 distinct dimensions: L, M, and T. Moreover, the dimensions of any repeated chosen variable should not be a multiple of another repeated variable or the sum of any other repeated variables (BUCKINGHAM, 1914).

There is a straightforward way to assess if the repeated variables are feasible. It can be achieved by using a matrix where the lines represent the dimensions and the columns the variables, as shown in Chart 6. If the determinant of the matrix is different from zero, then the chosen variables can be used as the repeated variables (LEMONS, 2017). As such, the variables represented in Chart 6 were selected as the repeated variables:

Chart 6 - Matrix of coefficient containing the proposed repeating variables and their dimensions

	M	**L**	**T**
$\boldsymbol{\overline{\sigma}}$	1	-1	-2
D	0	1	0
$\boldsymbol{\frac{dm_w}{dt}}$	1	0	-1

Source: Author

Chart 6 can be rewritten as a matrix, as displayed in Equation 68. Thus, it is possible to calculate its determinant.

$$\begin{vmatrix} 1 & -1 & -2 \\ 0 & 1 & 0 \\ 1 & 0 & -1 \end{vmatrix} \quad (68)$$

The calculated determinant of Equation 68 is equal to 1. Since this value is different than 0, it means that the system has a unique solution and therefore, the selected variables can be used as the repeated variables. Thus, the remaining variables can now be iterated with the repeating variables for the sake of finding the dimensionless products, as represented in Equations 69 to 73:

$$\pi_1 = (P, \bar{\sigma}, D, \frac{dm_w}{dt}) \quad (69)$$

$$\pi_2 = (D_0, \bar{\sigma}, D, \frac{dm_w}{dt}) \quad (70)$$

$$\pi_3 = (L, \bar{\sigma}, D, \frac{dm_w}{dt}) \quad (71)$$

$$\pi_4 = (z, \bar{\sigma}, D, \frac{dm_w}{dt}) \quad (72)$$

$$\pi_5 = (v_p, \bar{\sigma}, D, \frac{dm_w}{dt}) \quad (73)$$

4.1.4.1 Determining π_1:

π_1 can be determined using a linear system. This linear system can be created by equating the dimensionless state of the dimensions of the problem to the corresponding variables elevated to the power of a new set of variables (x, y, and z). Moreover, this linear system is represented by Equation 74.

$$M^0L^0T^0 = [M^1L^{-1}T^{-2}][M^1L^{-1}T^{-2}]^x[M^0L^1T^0]^y[M^1L^0T^{-1}]^z \quad (74)$$

In order to get a better visualization of the linear system, Equation 74 can be rewritten as follows:

$$\begin{cases} M: 1 + x + z = 0 \\ L: -1 - x + y = 0 \\ T: -2 - 2x - z = 0 \end{cases} \quad (75)$$

Solving Equation 75 leads to the following values for x, y, and z: -1, 0, and 0, respectively. Now replacing the calculated values of x, y, and z in Equation 74, results in Equation 76.

$$\pi_1 = P\bar{\sigma}^{-1} \quad (76)$$

Finally, rearranging Equation 76 results in Equation 77. Furthermore, this is the first π product for the proposed theoretical extrusion model.

$$\pi_1 = \frac{P}{\bar{\sigma}} \quad (77)$$

4.1.4.2 Determining π_2:

For calculating π_2, the process used for determining π_1 was repeated. Equation 78 represents the linear system for this condition:

$$M^0L^0T^0 = [M^0L^1T^0][M^1L^{-1}T^{-2}]^x[M^0L^1T^0]^y[M^1L^0T^{-1}]^z \quad (78)$$

For the sake of getting a better visualization of the linear system, Equation 79 can be rewritten as follows:

$$\begin{cases} M: x + z = 0 \\ L: 1 - x + y = 0 \\ T: -2x - z = 0 \end{cases} \quad (79)$$

Solving Equation 79 leads to the following values for x, y: 0, -1, and 0, respectively. Now replacing the calculated values of x, y, and z in Equation 78, results in Equation 80.

$$\pi_2 = D_0 D^{-1} \tag{80}$$

Lastly, rearranging Equation 80, it derives into Equation 81. Furthermore, this is the second π product for the proposed theoretical extrusion model.

$$\pi_2 = \frac{D_0}{D} \tag{81}$$

4.1.4.3 Determining π_3:

π_3 was calculated by repeating the same process used for the previous π groups. Equation 82 represents the linear system for this condition:

$$M^0 L^0 T^0 = [M^0 L^1 T^0][M^1 L^{-1} T^{-2}]^x [M^0 L^1 T^0]^y [M^1 L^0 T^{-1}]^z \tag{82}$$

In pursuance of getting a better visualization of the linear system, Equation 82 can be rewritten as follows:

$$\begin{cases} M: x + z = 0 \\ L: 1 - x + y = 0 \\ T: -2x - z = 0 \end{cases} \tag{83}$$

Solving Equation 83 leads to the following values for x, y: 0, -1, and 0, respectively. Now replacing the calculated values of x, y, and z in Equation 82, results in Equation 84.

$$\pi_3 = L D^{-1} \tag{84}$$

Lastly, rearranging Equation 84, it derives into Equation 85. Furthermore, this is the third π product for the proposed theoretical extrusion model.

$$\pi_3 = \frac{L}{D} \tag{85}$$

4.1.4.4 Determining π_4:

In order to achieve π_4, the process used for determining the previous π groups was repeated. Equation 86 represents the linear system for this condition:

$$M^0L^0T^0 = [M^0L^1T^0][M^1L^{-1}T^{-2}]^x[M^0L^1T^0]^y[M^1L^0T^{-1}]^z \quad (86)$$

For getting a better visualization of the linear system, Equation 87 can be rewritten as follows:

$$\begin{cases} M: x + z = 0 \\ L: 1 - x + y = 0 \\ T: -2x - z = 0 \end{cases} \quad (87)$$

Solving Equation 87 leads to the following values for x, y: 0, -1, and 0, respectively. Now replacing the calculated values of x, y, and z in Equation 86, results in Equation 88.

$$\pi_4 = zD^{-1} \quad (88)$$

Lastly, rearranging Equation 88, it derives into Equation 89. Furthermore, this is the fourth π product for the proposed theoretical extrusion model.

$$\pi_4 = \frac{z}{D} \quad (89)$$

4.1.4.5 Determining π_5:

The last π group, π_5, was calculated by repeating the same process used for the previous π groups. Equation 90 represents the linear system for this condition:

$$M^0L^0T^0 = [M^0L^1T^{-1}][M^1L^{-1}T^{-2}]^x[M^0L^1T^0]^y[M^1L^0T^{-1}]^z \quad (90)$$

For the sake of getting a better visualization of the linear system, Equation 90 can be rewritten as follows:

$$\begin{cases} M: x + z = 0 \\ L: 1 - x + y = 0 \\ T: -1 - 2x - z = 0 \end{cases} \quad (91)$$

Solving Equation 91 leads to the following values for x, y, and z: -1, -2, and 1, respectively. Now replacing the calculated values of x, y, and z in Equation 90, results in Equation 92.

$$\pi_5 = v_p \bar{\sigma}^{-1} D^{-2} \left({}^{dm_w}/_{dt} \right) \quad (92)$$

Lastly, rearranging Equation 92, it derives into Equation 93. Furthermore, this is the fifth, and last, π product for the proposed theoretical extrusion model.

$$\pi_5 = \frac{v_p \left({}^{dm_w}/_{dt} \right)}{\bar{\sigma} D^2} \quad (93)$$

Once with the π groups calculated, the process to achieve the extrusion pressure using the *Dimensional Analysis* can proceed. Moreover, the fundamental equation of Buckingham π theorem, represented by Equation 94 states that (BUCKINGHAM, 1914):

$$\varphi = f(\pi_1, \pi_2, \pi_3, \pi_4, \pi_5) \quad (94)$$

As described by Buckingham each π individual group can be modified by a function with no changes to the dimension of the problem (ALMEIDA; AL-QURESHI; TUSHTEV; REZWAN, 2018; BUCKINGHAM, 1914; LANGHAAR, 1962) Therefore, some modifications will be proposed for reaching a more robust and reliable equation, as it is shown in Equation 94(a).

$$\varphi\left(exp(\pi_1), ln(\pi_2), (\pi_3)^i, \dots, \pi_{m-n}\right) = 0 \quad (94a)$$

4.1.4.6 Modification of π_2:

As mentioned previously, Benbow and Bridgwater (1993) proposed a model, broadly used and cited in the literature, where they conjectured the ceramic paste as a mixture of perfect plastic and viscous flow in the die entry region (first term in Equation 95) and as a rigid plug flow, as stated by Horrobin and Nedderman (1998) (velocity of the fluid is considered constant along the cross-section) in the die land region (second term in Equation 95).

$$P = 2(\sigma_0 + \alpha {v_d}^m) ln\left(\frac{D_0}{D}\right) + (\tau_0 + \beta {v_d}^n)\frac{4L}{D} \quad (95)$$

where P stands for extrusion pressure; σ_0 for yield stress extrapolated to zero velocity; α for velocity factor of bulk yield stress; v_d for mean extrudate velocity in the die land; D_0 for the diameter of the barrel; D for the diameter of the die land; τ_0 for the initial wall shear stress of paste; β for velocity factor of wall shear stress; L for the length of the die land; m for the paste parameter determining the dependence of the bulk paste yield stress on velocity; and n for the paste parameter determining the dependence of wall shear stress on velocity.

Now analyzing Equation 95 and the π groups encountered in the fundamental equation of Buckingham π theorem (Equation 94a), the group $\pi_2$will be modified into π_2^* by a function that will not lead to any changes to the dimension of the problem, as follows:

$$\pi_2^* = \ln\frac{D_0}{D} \quad (96)$$

This equation also resembles the true strain encountered in the extrusion process.

4.1.4.7 Modification of π_4:

Now recalling Equation 8, part 2, proposed by Andrade (2009), and comparing it to π_4 the following modifications are suggested for μ_4^*, in such a way that the dimension of π_4 will have no change:

$$\pi_4^* = exp(\pi_4^{-1}\mu_{cil}) \tag{97}$$

Finally, rearranging Equation 97 leads to:

$$\pi_4^* = \exp\left(\frac{D\mu_{cil}}{z}\right) \tag{98}$$

4.1.4.8 Modification of π_1, π_3, and π_5:

The following modifications are proposed for of π_1 and π_3, respectively, assuring that the functions π_1^* and π_3^* will not have any changes in their dimensions. Starting with π_1^*:

$$\pi_1^* = \pi_1^2 \tag{99}$$

Rewriting Equation 99, yields Equation 100:

$$\pi_1^* = \left(\frac{P}{\bar{\sigma}}\right)^2 \tag{100}$$

Now moving to π_3^*. Equation 101 is proposed:

$$\pi_3^* = \mu_w \pi_3^2 \tag{101}$$

Rearranging Equation 101 leads to:

$$\pi_3^* = \mu_w \left(\frac{L}{D}\right)^2 \tag{102}$$

Considering all the modifications in the π groups mentioned and listed previously; therefore, Equation 103 is proposed from Equation 94(a):

$$\varphi = f(\pi_1^2, \ln(\pi_2), \mu_w \pi_3^2, exp(\pi_4^{-1}\mu_{cil}), \pi_5) \tag{103}$$

By applying properties of multivariable functions to equation 103, it yields to Equation 104:

$$\pi_1^* = \pi_2^* \pi_3^* \pi_4^* \pi_5 \tag{104}$$

All these modifications were chosen in order to make the solution viable and more representative, keeping it dimensionless. Now substituting the modified π groups encountered before in Equation 104, then it is possible to achieve Equation 105:

$$\left(\frac{P}{\bar{\sigma}}\right)^2 = \ln\frac{D_0}{D}\mu_w\left(\frac{L}{D}\right)^2 exp\left(\frac{D\mu}{z}\right)\frac{v_p\left(dm_w/dt\right)}{\bar{\sigma}D^2} \tag{105}$$

Manipulating the terms in Equation 105 gives Equation 106:

$$P = \left[ln\left(\frac{D_0}{D}\right)\right]^{1/2} \exp\left(\frac{D\mu}{z}\right)\left(\frac{L}{D^2}\right)\left(v_p\mu_w\bar{\sigma}\left(\frac{dm_w}{dt}\right)\right)^{1/2} \tag{106}$$

Hence Equation 106 is another approach that takes into account the effect of the coring point on the extrusion pressure. Moreover, this analysis considered the main variables described in the three previous theoretical analyses. However, it led to a shorter and more straightforward equation. Moreover, additional analysis related to uncertainty would be suitable for this model.

Analyzing Equation 106, three parameters play a very important role in the extrusion pressure, namely, extrusion velocity or velocity of the piston (v_p), friction coefficient (μ_w), and the percentage of cross-section reduction $\left(1 - \frac{R_f}{R_0}\right)$.

Figure 21 depicts the variation of the extrusion pressure for different extrusion velocities. For this proposed model, the velocity of the piston has a power law influence on the value of the extrusion pressure. Moreover, analyzing the model proposed by Benbow and Bridgwater (1993), it is possible to observe that the velocity of the piston also presents a power law impact on the extrusion pressure. For instance, in their mathematical model, the velocity is a parameter by a power factor of m and n. Typical values encountered in the literature for m and n range from 0.10 up to 0.87 (GUILHERME; RIBEIRO; LABRINCHA, 2009; NATH DAS; MADHUSOODANA; OKADA, 2002; RAUPP-PEREIRA; RIBEIRO; SEGADÃES; LABRINCHA, 2007; RIBEIRO; BLACKBURN; FERREIRA; LABRINCHA, 2006; RIBEIRO; LABRINCHA, 2007). In the proposed model, the velocity is by a power factor of 0.5, which is a value within the range found in the literature.

Figure 21 - The effect of the piston velocity on the extrusion pressure during the direct extrusion

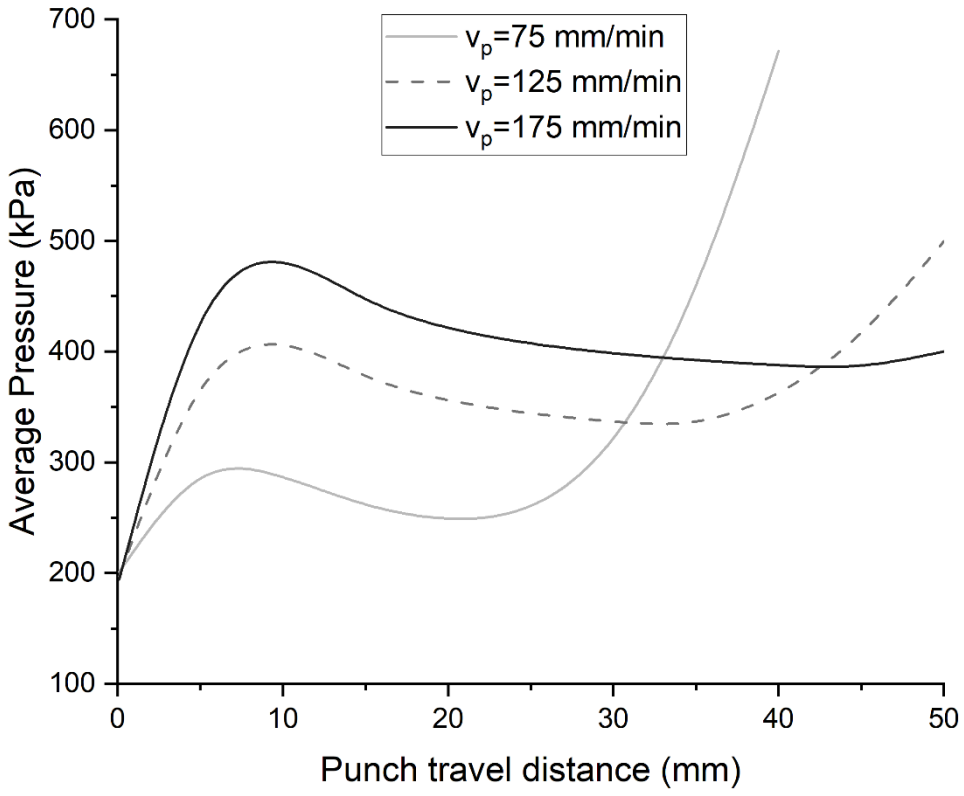

Source: Author

Analyzing the effect of the piston velocity on the extrusion pressure, it is possible to observe that increasing the piston velocity yielded a delay in the transition from the steady to the unsteady state, in other words, the point of coring is withheld. Yekta *et al.* (2007) published a work where the authors defended the following hypothesis: "*It should be noted that if there is drainage phenomenon susceptibility in the paste, phase separations will take place in it and there will be a tendency for a more fluent liquid phase to move ahead of the solid particles. In this case, local loss of liquid increases and the remaining paste becomes more rigid, leading to increase the resistance to flow. It seems that in high velocity extrusion with constant paste content, the extrusion time is less enough to prevent separation of water from solids*." Therefore, this statement seems to be a reasonable explanation for the behavior encountered in Figure 21.

Regarding the phenomenon of water migration cited by Yekta *et al.* (2007), Azzolini *et al.* (2014) published a study where they plotted extrusion curves for different content of solid loadings. Their results showed that increasing the solid content percentage (i.e. decreasing the water content), led to an abrupt rise in the extrusion pressure, corroborating the hypothesis proposed by Yekta *et al.* (2007).

Now, analyzing Figure 22 and Figure 23, it is possible to notice a similar trend showed in both figures. For instance, increasing either the friction coefficient or the percentage of diameter reduction yields a raise in the extrusion pressure throughout the entire process. Moreover, they also influence the unsteady state. For example, for lower friction or diameter reduction percentage, the steady state was extended, and the rise of the extrusion pressure was smoother.

Figure 22 - The effect of the friction coefficient on the extrusion pressure during the direct extrusion

.

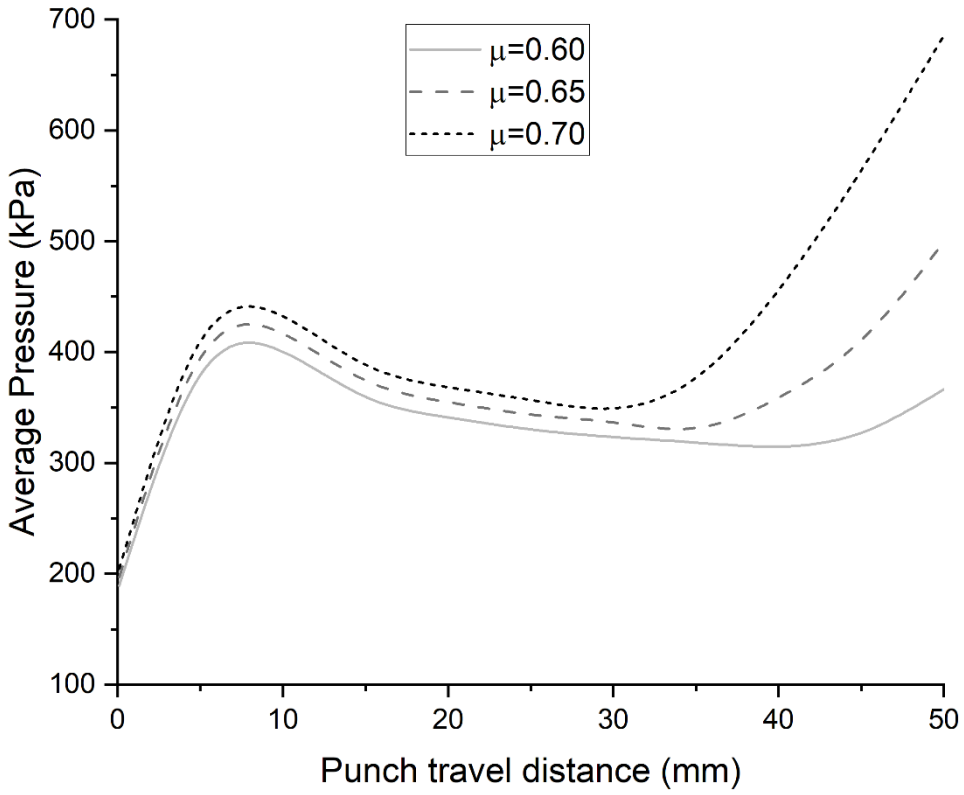

Source: Author

Figure 23 - The effect of the cross-section reduction on the extrusion pressure during the direct extrusion

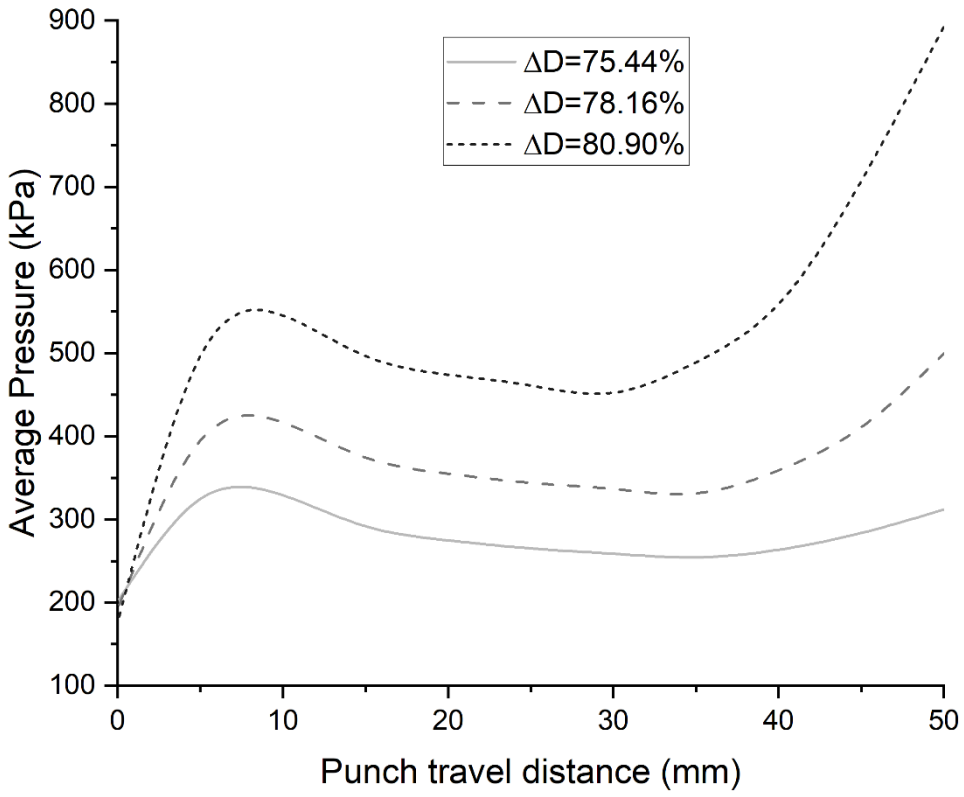

Source: Author

On the other hand, for higher friction coefficient or cross-section reduction percentage, the transition from the steady state to the unsteady state was initiated earlier and it was steeper. This trend can be explained by the fact that these

conditions require a larger extrusion pressure, fomenting and intensifying the phenomenon of water migration (AZZOLINI; SGLAVO; DOWNS, 2014).

It becomes evident that this equation is simpler when compared to the three other models. In addition, in this case, the aid of complex and robust calculations and computational simulations are not necessary. Nevertheless, unlike the three other approaches, this one does not present and differentiate within the equation the two stages (steady and unsteady state) that occurs during the extrusion process.

4.2 GENERAL RESULTS AND DISCUSSION

For the sake of comparison, validation and assessment of the four new proposed equations, a previously published work from Andrade (2009) was used and reproduced. Chart 7 recaps and all the mentioned equations, while Figure 24 displays the variation of the applied extrusion pressure as a function of the position of the ram. Three phases can be recognized in Figure 24 as already reported by Andrade (2009): a coining phase, marked by compression of the ceramic paste; a steady state phase, where the pressure is stabilized and the extrusion continues steadily; and an unsteady state phase, beyond the coring point, showing an evident rise in the extrusion pressure. As it can be observed, for Andrade's curve, Equation 8, (black line) it is possible to notice only two phases during the extrusion process: the coining and the steady state phase, once in his mathematical modeling, he did not take into account the implications beyond the coring point.

Chart 7 - Matrix containing proposed model by Andrade (2009) and the four developed theoretical models (Eq. 11, Eq, 58, Eq. 65, and Eq. 106)

Eq.8	$\frac{P_{ave}}{\bar{\sigma}_{comp}} = \frac{1}{(R_f - R_0)} \frac{z}{2\mu_{cil}} \Bigg\{ 1 - exp\left[\frac{2\mu_{cil}}{z}(R_f - R_0)\right] \Bigg\} \Bigg\{ \Bigg\{ \Bigg\{ 1 + \frac{(1+\mu_w \cot\alpha)}{\mu_w \cot\alpha} \left[\left(\frac{R_0}{R_f}\right)^{2\mu_w \cot\alpha} - 1 \right] \Bigg\} exp\left\{ 2\mu_w \cot\alpha \left[-\frac{L_c}{R_0} \tan\alpha + \left(1 - \frac{R_f}{R_0}\right) \right] \right\} - 1 \Bigg\}$
Eq. 11	$\frac{P_{ave}}{\bar{\sigma}_{comp}} = \frac{1}{(R_f - R_0)} \frac{z}{2\mu_{x_{n-1}} 2^{x_n/x_{n-1}}} \Bigg\{ 1 - exp\left[\frac{2\mu_{x_{n-1}} 2^{x_n/x_{n-1}}}{z}(R_f - R_0)\right] \Bigg\} \Bigg\{ \Bigg\{ 1 + \frac{(1+\mu_w \cot\alpha)}{\mu_w \cot\alpha} \left[\left(\frac{R_0}{R_f}\right)^{2\mu_w \cot\alpha} - 1 \right] \Bigg\} exp\left\{ 2\mu_w \cot\alpha \left[-\frac{L_c}{R_0} \tan\alpha + \left(1 - \frac{R_f}{R_0}\right) \right] \right\} - 1 \Bigg\}$
Eq. 58	$\frac{\sigma_z}{\bar{\sigma}} = \left(-\frac{\theta}{\mu_w} + \frac{R_f}{8R\mu_w^2} - 1 \right) + \left[(Eq.8) - \frac{R_f}{8R\mu_w^2} + 1 \right] exp^{\frac{8R\mu_w\theta}{R_f}}$
Eq. 65	$P_{ave} = \frac{\left[\frac{(\sigma_{PL} - \sigma_A)}{(w_{PL} - w_A)} \left(w_{x_{n-1}} - \frac{dw}{dt}\left(\frac{x_{x_n} - x_{x_{n-1}}}{v}\right) \right) + \left[\frac{(w_{PL}\sigma_A - w_A\sigma_{PL})}{(w_{PL} - w_A)} \right] \right]}{(R_f - R_0)} \frac{z}{2\mu_{cil}} \Bigg\{ 1 - exp\left[\frac{2\mu_{cil}}{z}(R_f - R_0)\right] \Bigg\} \Bigg\{ \Bigg\{ \Bigg\{ 1 + \frac{(1+\mu_w \cot\theta)}{\mu_w \cot\theta} \left[\left(\frac{R_0}{R_f}\right)^{2\mu_w \cot\theta} - 1 \right] \Bigg\} exp\left\{ 2\mu_w \cot\theta \left[-\frac{L_c}{R_0} \tan\theta + \left(1 - \frac{R_f}{R_0}\right) \right] \right\} - 1 \Bigg\}$
Eq. 106	$P = \left[ln\left(\frac{D_0}{D}\right) \right]^{1/2} \exp\left(\frac{D\mu}{z}\right)\left(\frac{L}{D^2}\right)\left(v_p \mu_w \bar{\sigma} \left(\frac{dm_w}{dt}\right) \right)^{1/2}$

Source: Author

Figure 24 - Comparison among experimental work (black squares), Andrade (2009)'s theory (solid black line - Equation 8), and proposed equations: Friction's equation (dashed black line – Equation 11) (TAJIRI; PIERI; AL-QURESHI, 2019), spring-back's approach (short dashed-dotted black line - Equation 58), water loss's approach (dashed-dotted black line – Equation 65), and dimensional analysis´s approach (dotted black line – Equation 106)

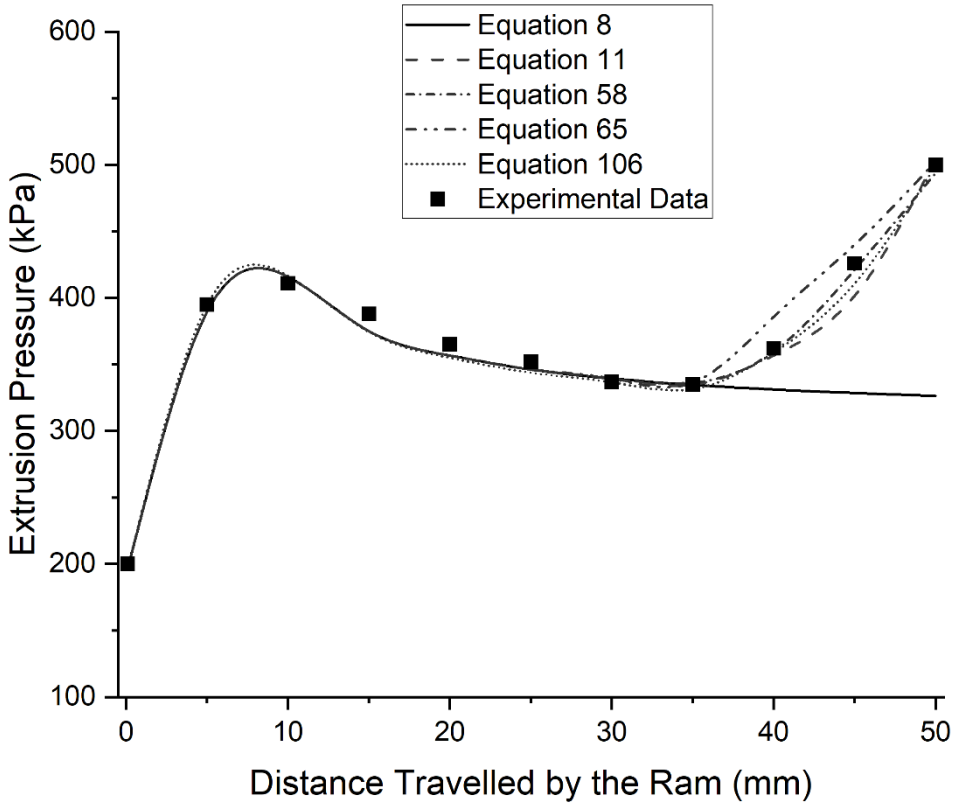

Source: Author

In addition, Figure 24 displays a satisfactory correlation between the experimental curve points (represented by black squares) and the new proposed equations: Equation 11, represented by a dashed black line; Equation 58, displayed with a short dashed dotted black line; Equation 65, expressed with a dashed dotted black line; and Equation 106, represented by dotted black line. Even though the equations are substantial and complex, they can be easily determined and calculated with the aid of computers.

Table 1 highlights the importance of considering the effect of the coring point on the extrusion pressure. For sake of comparison, when this phenomenon is neglected a difference in extrusion pressure can deviate more than fifty percent from

the real value. This difference of pressure can compromise the quality of the extruded parts and even worse, it can damage the equipment.

Table 1 - Extrusion pressure comparison among experimental, Andrade (2009)'s theory and the four theoretical analyses proposed in the present work

Punch travel (mm)	Exp. (kPa)	Δ Equation 8/Exp. (%)	Δ Equation 11/Exp. (%)	Δ Equation 58/Exp. (%)	Δ Equation 65/Exp. (%)	Δ Equation 106/Exp. (%)
0	200	-1.3	-1.6	-1.6	-1.6	-1.4
5	395	-1.0	-1.4	-1.4	-1.4	-0.1
10	411	1.5	1.2	1.2	1.2	1.4
15	388	-3.1	-3.4	-3.4	-3.4	-3.5
20	365	-2.0	-2.3	-2.3	-2.3	-2.8
25	352	-1.3	-1.7	-1.7	-1.7	-2.3
30	337	1.1	0.7	0.7	0.7	-0.1
35	335	0.2	-0.1	0.4	0.4	-1.1
40	362	-8.9	-1.5	6.6	-0.7	-0.8
45	426	-29.2	-6.1	3.3	-1.1	-3.6
50	500	-52.7	0.85	0.5	-1.3	-0.1

Source: Author

Now focusing on the four proposed theoretical analyses, displayed with higher amplification in Figure 25, it is noticeable that among the four proposed equations, Equation 65 seemed to be the most conservative approach since it yielded the highest extrusion pressure. On the other hand, Equation 11 delivered the lowest extrusion pressure. Likewise, even though, the friction variation equation (Equation 11) shows a good fit with the experimental curve, as it has already been stated, it is more likely that the compressive strength presents a higher impact on the extrusion pressure when compared to the friction coefficient (ANDRADE, 2009; HAMZA; KOCSERHA; GÉBER; BUZIMOV, 2019; RIBEIRO; FERREIRA; LABRINCHA, 2005). Equation 58 presented the closest results when compared with the experimental points; nevertheless, it is more difficult to acknowledge all the variables within the

equation with precision. Finally, the dimensional analysis approach, Equation 106, showed promising results, with a straightforward equation.

Figure 25 - Amplified visualization of comparison among experimental work (black squares), Andrade (2009)'s theory (solid black line - Equation 8), and proposed equations: Friction's equation (dashed black line – Equation 11) (TAJIRI; PIERI; AL-QURESHI, 2019), spring-back's approach (short dashed-dotted black line - Equation 58), water loss's approach (dashed-dotted black line – Equation 65), and dimensional analysis´s approach (dotted black line – Equation 106)

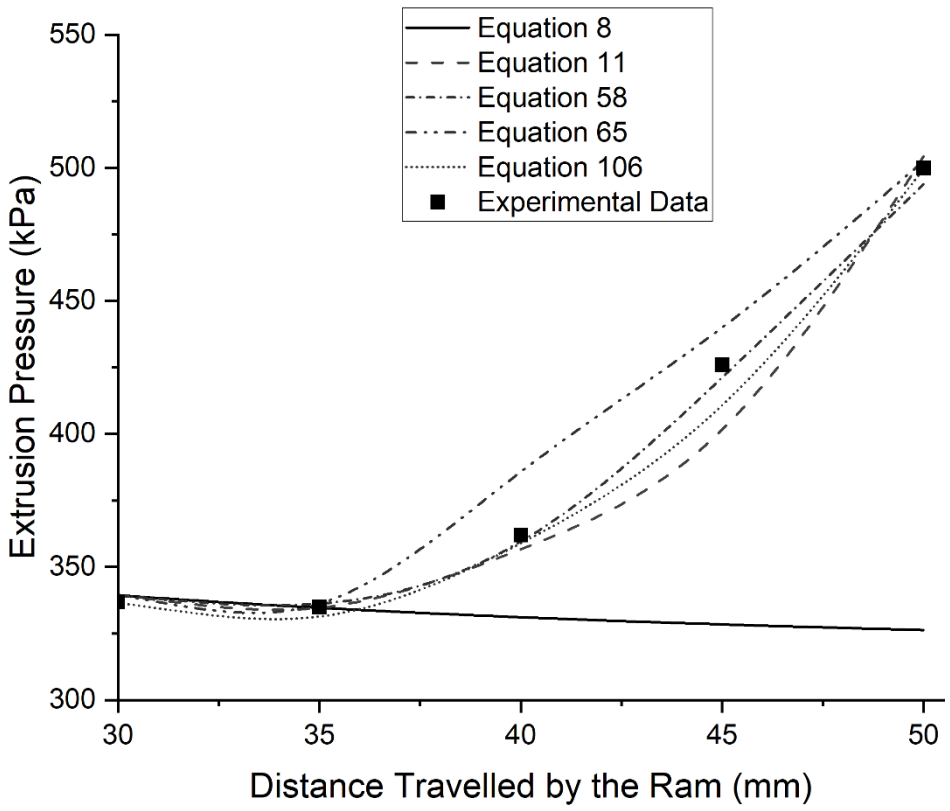

Source: Author

In conclusion, these theories will help the designer of the product to conceive projects avoiding defects due to material and pressure gradients, guaranteeing the integrity of its projected properties. For instance, in order to minimize the effect of the water (solvent) migration on the product´s quality and on the extrusion pressure, with the aim of moisture sensors and an accomplished tool to the barrel, it would be possible to track the water content in the ceramic paste and water (liquid) could be added to the paste when necessary.

5 CONCLUSIONS

In the present thesis, a brief literature review on: basic concepts about ceramic extrusion; ceramic plasticity; compression test as a means to evaluate the ceramic paste plasticity; dimensional analysis; and to recapitulate an equation of the extrusion process considering friction and angular variation, was made.

Therefore, as a final consideration, one can observe that:

- Extrusion is a widely employed processing technique used from the traditional industry up to the advanced ceramic industry.

- Plasticity plays a very important role in ceramic extrusion, in addition, there are, at least, five different ways to assess the plasticity of ceramic paste, cited in the literature.

- Compression test seems to be a suitable technique to evaluate ceramic paste plasticity.

- Dimensional analysis is a powerful tool which allows modeling physical dimensions into simple and straightforward equations.

- There is an evident lack of studies and publications in the literature regarding mathematical modeling and extrusion pressure beyond the steady state.

Therefore, it was possible to develop four mathematical equations for the extrusion of ceramic paste to analyze the pressure increase beyond the steady state phase. Regarding the proposed theoretical analyses, one equation (Equation 11) proposed a coefficient of friction as a function of density of the extruded ceramic material. Another approach (Equation 58) incorporated the effect of the spring-back phenomenon on the extrusion pressure. The third model (Equation 65) introduced the mathematical relation between effective stress of compression and water content of material. Finally, the last mathematical model (Equation 106) employed the main

variables encountered in other three approaches and came up with a new theoretical analysis using the dimensional analysis technique.

From the results of the proposed mathematical theories, it was possible to observe that the radius of the die´s exit, exit angle, friction coefficient, and diameter reduction percentage, piston velocity and water migration influence considerably the profile of the extrusion pressure. Increasing these variables led to a raise in the extrusion pressure and, in some cases, to an anticipation of the coring point.

In conclusion, it became evident that variables such as friction coefficient, piston velocity, humidity of the ceramic paste, diameter reduction percentage, and others, not only play an important role during the steady state regime, in direct extrusion of ceramics, but also, they are crucial, after the coring point, in the unsteady state. Three robust models are introduced (Equations 11, 58, and 65), which can easily be determined using either computational simulations or complex calculations. Moreover, these three approaches can be effortlessly identified and divided into two parts: steady and unsteady state. On the other hand, the model derived using the dimensional analysis technique yielded a very straightforward equation. However, in this model it was not possible to identify and divide the equation into the parts, that were mentioned before. Even within all the limitations in the present thesis, still, it furnishes the tool designer or engineer with important pieces of information that detail the entire process of direct extrusion, including the unsteady state. These theories, eventually, will help to produce an optimized tooling that might be used in the process.

6 FUTURE WORK

As a suggestion for future work the following is proposed: construction of an adapted ram extruder with a split barrel, as illustrated in Figure 26. Moreover, this apparatus is proposed in order to assess the behavior of the material beyond the steady state. Moreover, it will be possible to evaluate the relation among the extrusion pressure and the material chemical and physical properties such as the density and the water content along the extrusion process. With this split cylinder it will be also viable to investigate possible variations of the paste properties along the cylinder.

It is also suggested for future work a meticulous study in the rheology of the ceramic pastes in order to assess the influence of the agglomerates (and also the zeta potential of the paste) on the extrusion pressure. It would be also of great value to refine the proposed equation using dimensional analysis, introducing new variables that might be important during the direct ram extrusion. None the least, It would be also of great importance to analyze the micro mechanical behavior, such as the movement of the grains and the internal friction.

Figure 26 - Adapted ram extruder with a split cylinder

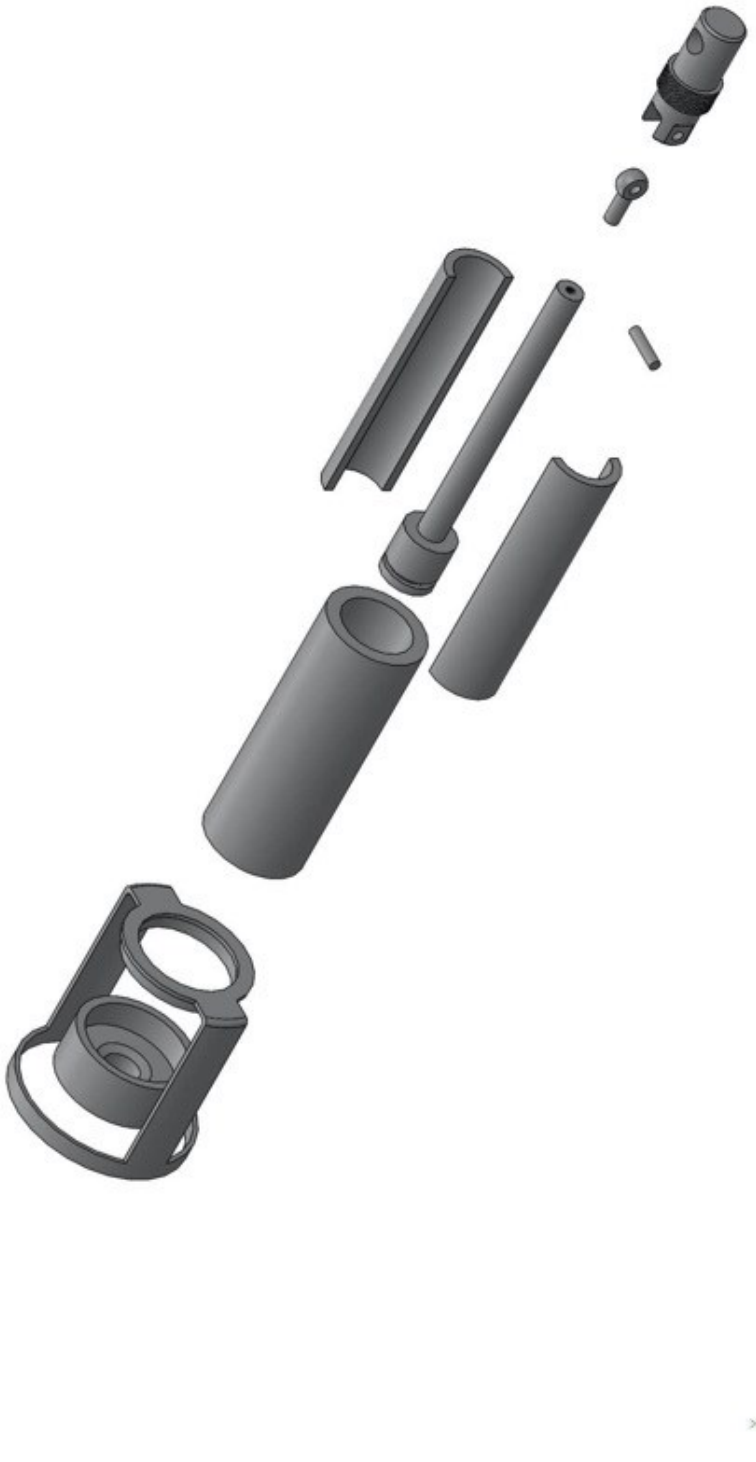

Source: Author

7 REFERENCES

AL-QURESHI, H. Spring-back of sheet metal when using compressible tools. **Sheet Metal Industries**, 51, p. 695-698, 707, 1974.

AL-QURESHI, Hazim. Elastic-plastic analysis of tube bending. **International Journal of Machine Tools and Manufacture**, 39, p. 87-104, 1999.

AL-QURESHI, H.; RUSSO, A. Spring-back and residual stresses in bending of thin-walled aluminium tubes. **Materials & Design**, 23, p. 217–222, 04/01 2002.

ALFANI, R.; GRIZZUTI, N.; GUERRINI, G. L.; LEZZI, G. The use of the capillary rheometer for the rheological evaluation of extrudable cement-based materials. **Rheologica Acta**, 46, p. 703-709, 2007.

ALMEIDA, R. S.; AL-QURESHI, H. A.; TUSHTEV, K.; REZWAN, K. On the dimensional analysis for the creep rate prediction of ceramic fibers. **Ceramics International**, 44, n. 13, p. 15924-15928, 2018.

ALTINKAYNAK, A. **Three dimensional finite element simulation of polymer melting and flow in a single-screw extruder : optimization of screw channel geometry**. Michigan Technological University, 2010.

ANDRADE, F. A. **Modelamento Matemático do Comportamento Plástico do Sistema Argila-água no Processo de Extrusão**. Orientador: AL-QURESHI, H. A. 2009. (Mestrado) - Programa de Pós-Graduação em Ciência e Engenharia de Materiais, Universidade Federal de Santa Catarina, 2009.

ANDRADE, F. A.; AL-QURESHI, H. A.; HOTZA, D. Measuring the plasticity of clays: A review. **Applied Clay Science**, 51, n. 1, p. 1-7, 2011.

ANDRADE, F. A.; AL-QURESHI, H. A.; HOTZA, D. Modeling of Clay Paste Extrusion through a Rectangular Die. **International Review of Chemical Engineering**, v. 2, n. 4, p. 478-483, 2010.

AVITZUR, B. Steady and unsteady state extrusion. **Journal of Engineering for Industry**, 175, n. 89, 1967.

AVITZUR, B.; FUEYO, J.; THOMPSON, J. Analysis of Plastic Flow Through Inclined Planes in Plane Strain. **Journal of Engineering for Industry**, 89, n. 2, p. 361-375, 1967.

AZZOLINI, A.; SGLAVO, V. M.; DOWNS, J. A. Novel method for the identification of the maximum solid loading suitable for optimal extrusion of ceramic pastes. **Journal of Advanced Ceramics**, 3, n. 1, p. 7-16, 2014.

BARENBLATT, G. I. **Dimensional analysis**. CRC Press, 1987. 288124226X.

BARENBLATT, G. I.; ISAAKOVICH, B. G. **Scaling, self-similarity, and intermediate asymptotics: dimensional analysis and intermediate asymptotics**. Cambridge University Press, 1996. v. 14). 0521435226.

BENBOW, J.; BRIDGWATER, J. **Paste flow and extrusion**. Oxford: Clarendon Press, 1993. 0198563388 : ¹37.50.

BENBOW, J. J.; OXLEY, E. W.; BRIDGWATER, J. The extrusion mechanics of pastes—the influence of paste formulation on extrusion parameters. **Chemical Engineering Science**, 42, n. 9, p. 2151-2162, 1987.

BHAIRY, S.; HABADE, B.; GUPTA, S.; GHODKE, V. *et al.* Pellets and Pelletization as Multiparticulate Drug Delivery Systems (MPDDS): A Conventional and Novel Approach. **International Journal of Institutional Pharmacy and Life Sciences**, 5, p. 79-126, 2015.

BRIDGMAN, P. W. **Dimensional analysis**. Yale university press, 1922.

BUCKINGHAM, E. On Physically Similar Systems; Illustrations of the Use of Dimensional Equations. **Physical Review**, 4, n. 4, p. 345-376, 1914.

BURBIDGE, A. S.; BRIDGWATER, J. The single screw extrusion of pastes. **Chemical Engineering Science**, 50, n. 16, p. 2531-2543, 1995.

CARLEY, J.; STRUB, R. Basic concepts of extrusion. **Industrial & Engineering Chemistry**, 45, n. 5, p. 970-973, 1953.

CHEN, Z.; LI, Z.; LI, J.; LIU, C. *et al.* 3D printing of ceramics: A review. **Journal of the European Ceramic Society**, 39, n. 4, p. 661-687, 2019.

CHENG, Y.-T.; CHENG, C.-M. Scaling, dimensional analysis, and indentation measurements. **Materials Science and Engineering: R: Reports**, 44, n. 4, p. 91-149, 2004.

CHEVALIER, L.; HAMMOND, E.; POITOU, A. Extrusion of TiO2 ceramic powder paste. **Journal of materials processing technology**, 72, n. 2, p. 243-248, 1997.

CHONGTHAIRUNGRUANG, B.; UTHAISANGSUK, V.; SURANUNTCHAI, S.; JIRATHEARANAT, S. Springback prediction in sheet metal forming of high strength steels. **Materials & Design**, 50, p. 253-266, 2013.

DE WIT, C. T.; ARENS, P. L. Moisture content and density of some clay minerals and some remarks on the hydration pattern of clay. *In*: Transactions of the International Congress of Soil Science, 1950, Amsterdam.

DODEJA, L. C.; JOHNSON, W. The cold extrusion of circular rods through square multiple hole dies. **Journal of the Mechanics and Physics of Solids**, 5, n. 4, p. 281-295, 1957.

DONDI, M. Caracterização Tecnológica dos Materiais Argilosos: Métodos Experimentais e Interpretação dos Dados. **Revista Cerâmica Industrial**, 11, n. 3, p. 36-40, 2006.

FLORES, O.; MENDES, L.; OLIVEIRA, A.; FREDEL, M. *et al.* Modelo Matemático Aplicado à Avaliação da Plasticidade de Argilas. In: **50º Congresso Brasileiro de Cerâmica**. 2006.

GIBBINGS, J. C. **Dimensional analysis**. Springer Science & Business Media, 2011. 1849963177.

GRAY, A. **Modern Differential Geometry of Curves and Surfaces with Mathematica**. CRC Press, Inc., 1996. 0849371643.

GUILHERME, P.; RIBEIRO, M. J.; LABRINCHA, J. A. Behaviour of different industrial ceramic pastes in extrusion process. **Advances in Applied Ceramics**, 108, n. 6, p. 347-351, 2009.

HALL, S. E.; REGIS, J. E.; RENTERIA, A.; CHAVEZ, L. A. *et al.* Paste extrusion 3D printing and characterization of lead zirconate titanate piezoelectric ceramics. **Ceramics International**, 47, n. 15, p. 22042-22048, 2021.

HAMZA, A.; KOCSERHA, I.; GÉBER, R.; BUZIMOV, A. Plasticity of Red Mud and Clay Mixtures. **IOP Conference Series: Materials Science and Engineering**, 613, p. 012051, 2019.

HARPER, J. M. **Extrusion of foods**. CRC press, 2019. 1000694356.

HOFFMAN, O.; SACHS, G. **Introduction to the Theory of Plasticity for Engineers**. McGraw-Hill, 1953.

HOFFMANNER, A. L.; COMMITTEE, M. S. O. A. S. A. F. **Metal forming: interrelation between theory and practice: proceedings of a symposium on the relation between theory and practice of metal forming, held in Cleveland, Ohio, in October, 1970**. Plenum Press, 1971.

HORROBIN, D. J.; NEDDERMAN, R. M. Die entry pressure drops in paste extrusion. **Chemical Engineering Science**, 53, n. 18, p. 3215-3225, 1998.

HU, F.; MIKOLAJCZYK, T.; PIMENOV, D. Y.; GUPTA, M. K. Extrusion-Based 3D Printing of Ceramic Pastes: Mathematical Modeling and In Situ Shaping Retention Approach. **Materials**, v.14, n. 5, 2021. DOI: 10.3390/ma14051137.

HÄNDLE, F. **Extrusion in ceramics**. Berlin ; New York: Springer, 2007. 9783540271000 (hardcover : alk. paper).

JANNEY, M. A. Plastic forming of ceramics: extrusion and injection moulding. *In*: TERPSTRA, R. A.;PEX, P. P. A. C.*, et al* (Ed.). **Ceramic Processing**. Dordrecht: Springer Netherlands, p. 174-211, 1995.

JIANG, G. P.; YANG, J. F.; GAO, J. Q. Effect of starch on extrusion behaviour of ceramic pastes. **Materials Research Innovations**, 13, n. 2, p. 119-123, 2009/06/01 2009.

JOHNSON, W. Experiments in plane-strain extrusion. **Journal of the Mechanics and Physics of Solids**, 4, n. 4, p. 269-282, 1956.

JOHNSON, W. An elementary consideration of some extrusion defects. **Applied Scientific Research, Section A**, 8, n. 1, p. 52-60, 1959.

JOHNSON, W.; KUDŌ, H. **The mechanics of metal extrusion**. Manchester University Press, 1962.

KOCSERHA, I.; KRISTÁLY, F. Effects of Extruder Head's Geometry on the Properties of Extruded Ceramic Products. **Materials Science Forum**, 659, 09/01 2010.

LAFLEUR, P. G.; VERGNES, B. **Polymer extrusion**. John Wiley & Sons, 2014. 1118827171.

LANGHAAR, H. L. **Dimensional analysis and theory of models**. 1962.

LEMONS, D. S. **A Student's Guide to Dimensional Analysis**. Cambridge: Cambridge University Press, 2017. (Student's Guides. 9781107161153).

LIU, H.; LEU, M. C. Liquid Phase Migration in Extrusion of Aqueous Alumina Paste for Freeze-Form Extrusion Fabrication. **International Journal of Modern Physics B**, 23, n. 06n07, p. 1861-1866, 2009.

LIU, H.; LIU, J.; LEU, M. C.; LANDERS, R. *et al.* Factors influencing paste extrusion pressure and liquid content of extrudate in freeze-form extrusion fabrication. **The International Journal of Advanced Manufacturing Technology**, 67, n. 1, p. 899-906, 2013.

MACEDO, R. S.; MENEZES, R.; NEVES, G.; FERREIRA, H. Estudo de argilas usadas em cerâmica vermelha. **Cerâmica**, v. 54, p. 411-417, 2008.

MEASURES, I. B. O. W. A.; TAYLOR, B. N.; THOMPSON, A. **The international system of units (SI)**. US Department of Commerce, Technology Administration, National Institute, 2001.

NATH DAS, R.; MADHUSOODANA, C. D.; OKADA, K. Rheological studies on cordierite honeycomb extrusion. **Journal of the European Ceramic Society**, 22, n. 16, p. 2893-2900, 2002.

ORDOÑEZ, E.; GALLEGO, J. M.; COLORADO, H. A. 3D printing via the direct ink writing technique of ceramic pastes from typical formulations used in traditional ceramics industry. **Applied Clay Science**, 182, p. 105285, 2019.

POTENTE, H.; HANHART, W.; RESKI, T. Design and processing optimization of extruder screws. **Polymer Engineering & Science**, 34, n. 11, p. 937-945, 1994. https://doi.org/10.1002/pen.760341111.

RAUPP-PEREIRA, F.; RIBEIRO, M. J.; SEGADÃES, A. M.; LABRINCHA, J. A. Extrusion and property characterisation of waste-based ceramic formulations. **Journal of the European Ceramic Society**, 27, n. 5, p. 2333-2340, 2007.

REED, J. S. **Principles of Ceramics Processing**. Wiley, 1995. 9780471597216.

RIBEIRO, M.; BLACKBURN, S.; FERREIRA, J.; LABRINCHA, J. A. **Extrusion of alumina and cordierite-based tubes containing Al-rich anodising sludge**. p. 817-823, 2006.

RIBEIRO, M.; FERREIRA, A.; LABRINCHA, J. A. Aspectos Fundamentais Sobre a Extrusão de Massas de Cerâmicas Vermelhas. **Ceramica Industrial**, 8, 2003.

RIBEIRO, M.; LABRINCHA, J. Rod Extrusion of Cordierite-Based Paste Containing Aluminum-Rich Anodizing Sludge. **American Ceramic Society Bulletin**, 86, n. 9, 2007.

RIBEIRO, M. J.; BLACKBURN, S.; LABRINCHA, J. A. Single screw extrusion of mullite-based tubes containing Al-rich anodising sludge. **Ceramics International**, 35, n. 3, p. 1095-1101, 2009.

RIBEIRO, M. J.; FERREIRA, J. M.; LABRINCHA, J. A. Plastic behaviour of different ceramic pastes processed by extrusion. **Ceramics International**, 31, n. 4, p. 515-519, 2005.

ROMANCZUK-RUSZUK, E.; SZTORCH, B.; PAKUŁA, D.; GABRIEL, E. *et al.* 3D Printing Ceramics—Materials for Direct Extrusion Process. **Ceramics**, v.6, n. 1, p. 364-385, 2023. DOI: 10.3390/ceramics6010022.

ROUGH, S. L.; BRIDGWATER, J.; WILSON, D. I. Effects of liquid phase migration on extrusion of microcrystalline cellulose pastes. **International Journal of Pharmaceutics**, 204, n. 1, p. 117-126, 2000.

ROUGH, S. L.; WILSON, D. I.; BRIDGWATER, J. A Model Describing Liquid Phase Migration Within an Extruding Microcrystalline Cellulose Paste. **Chemical Engineering Research and Design**, 80, n. 7, p. 701-714, 2002.

RUSCITTI, A.; TAPIA, C.; RENDTORFF, N. M. A review on additive manufacturing of ceramic materials based on extrusion processes of clay pastes. **Cerâmica**, 66, 2020.

RUSSELL, B.; WILSON, I.; LASENBY, J.; BLACKBURN, S. On-line monitoring of pastes undergoing extrusion. In: **Proceedings of the 4th World Congress on Particle Technology**, p. 21-25, 2002.

SIMONI, R. **Teoria Local das Curvas**. Orientador: DORIA, P. D. C. M. 2005. 86 f. (Bachelor) - Centro de Ciências Físicas e Matemática, Universidade Federal de Santa Catarina, Florianópolis.

STURGESS, C. E. N.; DEAN, T. A. Breakthrough pressures in lubricated extrusion. **Journal of Mechanical Working Technology**, 3, n. 2, p. 119-135, 1979.

SUNIL, K.; JOHRI, I.; GEDAM, C.; JAIN, P. *et al.* **Effects of Cold Extrusion on Material Properties**. 2018.

TAJIRI, H.; PIERI, E.; AL-QURESHI, H. Modified Modeling of Clay Paste Extrusion through a Circular Die: Beyond the Steady-State. **International Journal of Metallurgy and Metal Physics**, 4, p. 1-9, 2019.

TRANCANELLI, D. Grandezas físicas e análise dimensional: da mecânica à gravidade quântica. **Revista Brasileira de Ensino de Física**, 38, 2016.

VITORINO, N.; FREITAS, C.; RIBEIRO, M. J.; ABRANTES, J. C. C. *et al.* Extrusion of ceramic emulsions: Plastic behavior. **Applied Clay Science**, 101, p. 315-319, 2014.

W. NELSON, F.; P. BARRINGTON, G.; J. STRAUB, R.; D. BRUHN, H. Design Parameters for Rotary Extrusion Macerators. **Transactions of the ASAE**, 26, n. 4, p. 1011-1015, 1983.

WANG, Y.; XIA, X.; WU, Y. Experimental Study on Shear Properties of Interface between Clay and Cement Paste. **IOP Conference Series: Earth and Environmental Science**, 267, p. 052049, 2019.

YEKTA, B.; MAHABAD, N.; EBADZADEH, T. Rheological Study on Cordierite Paste During Extrusion. **Advances in Applied Ceramics**, 106, p. 161-164, 2007.

YU, J.; ZHANG, Z.; WANG, Q.; HAO, H. *et al.* Rotary extrusion as a novel severe plastic deformation method for cylindrical tubes. **Materials Letters**, 215, p. 195-199, 2018.

8 APPENDIX

Published papers:

TAJIRI, H.; PIERI, E.; AL-QURESHI, H. Modified Modeling of Clay Paste Extrusion through a Circular Die: Beyond the Steady-State. **International Journal of Metallurgy and Metal Physics**, 4, p. 1-9, 01/21 2019.

TAJIRI, H.A.; HOTZA, D.; DE PIERI, E. R.; AL-QURESHI, H. Analysis of the spring-back and water effect on the coring point during direct extrusion. **Journal of the Brazilian Society of Mechanical Sciences and Engineering**, 45, n. 4, p. 1-11, 2023.

Conference:

The 7th Asia Conference on Mechanical and Materials Engineering (ACMME). Paper title: Modeling Beyond the Coring Point of Viscous Ceramic Extrusion through a Circular Die. Oral Presentation. June 14-17 2019.

Research Article: Open Access

VIBGYOR ePress

International Journal of
Metallurgy and Metal Physics

Modified Modeling of Clay Paste Extrusion through a Circular Die: Beyond the Steady-State

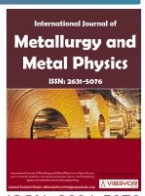

ISSN: 2631-5076

Henrique A Tajiri[1*], Edson R de Pieri[2] and Hazim A Al-Qureshi[3]

[1]*Department of Mechanical Engineering, CTC, Federal University of Santa Catarina, Florianopolis, Brazil*

[2]*Department of Automation and Systems, CTC, Federal University of Santa Catarina, Florianopolis, Brazil*

[3]*Graduate Program in Mechanical Science and Engineering, CTJ, Federal University of Santa Catarina, Joinville, Brazil*

Abstract

The aim of this study is to develop a mathematical modeling of direct paste extrusion through a circular die going beyond the steady-state, where the coring point becomes evident. The proposed study considers a previous mathematical modeling of clay paste extrusion which did not consider the behavior beyond the steady-state. Therefore, it is proposed that the coefficient of friction is no longer constant after the steady-state. Moreover, beyond the coring point, two types of behavior can be noticed, an acceleration of the extrusion pressure decrease rate or an increase of the extrusion pressure. The latter behavior harms the ceramic industry since it can lead to die damage, lubrication problems, product defects and raise the production cost. This increase in the extrusion pressure, during the unsteady-state, can be regarded to the water loss and densification of the ceramic paste. Four types of clay were used in the present work and cylindrical specimens were extruded. Four cylindrical samples were prepared for the compression test to determine the effective compressive stress and friction coefficient between the clay and the punch. These two determined parameters were further used in the mathematical modeling of the extrusion process. The effective compressive stress varied from 0.07 up to 0.11 MPa. A friction coefficient of 0.134 was found from the compression test. In addition, after the coring point, extrusion pressures 50% greater than the steady-state were recorded. In conclusion, the mathematical modeling for the compression test and for the extrusion process demonstrated good correlation with the experimental points.

Keywords

Clay extrusion modeling, Coring point, Density, Plasticity

Abbreviations and Greek Letters

A_0: Initial Area; A_f: Final Area; D_0: Initial Diameter; H: Height; Lc: Critical Length (Coring point); F: Instantaneous Axial Force; P_{ave}: Average Extrusion Pressure; R_0: Initial Radius; R_f: Final Radius; z: Punch Travel; α: Semicone Angle of the Die; $\overline{\varepsilon}$: Effective Strain; μ_{comp}: Coefficient of Friction Between Punch and Clay Paste; μ_w: Coefficient of Friction Between Wall and Clay Paste; σ_{ave}: Average Extrusion Pressure; σ_r: Radial Stress; σ_z: Axial Stress; $\overline{\sigma}$: Effective Stress; $\overline{\sigma}_{comp}$: Effective Stress of Compression

***Corresponding author:** *Henrique A Tajiri, Department of Mechanical Engineering, CTC, Federal University of Santa Catarina, Florianopolis, Brazil, Tel: +55-48-988085257*

Accepted: January 19, 2019; **Published:** January 21, 2019

ISSN 2631-5076

Tajiri et al. Int J Metall Met Phys 2019, 4:027

Citation: Tajiri HA, de Pieri ER, Al-Qureshi HA (2019) Modified Modeling of Clay Paste Extrusion through a Circular Die: Beyond the Steady-State. Int J Metall Met Phys 4:027

Introduction

There are few areas in technology in which development has met many application fields as extrusion. Initially, it was employed only for simple ceramic materials. Nevertheless, nowadays extrusion is employed in different areas such as ceramic, metallurgy, polymers industry, chemical or even food industry. For instance, Benbow, et al. mentioned some application of extruded parts such as earthenware pipes, thermocouple tubes, catalyst monoliths, and animal feeds [1].

Currently, many studies are being conducted in this area focusing on producing advanced ceramics by extrusion. Examples such as ceramic honeycombs, high-Al2O3 ceramics for insulation, and aerospace components were pointed out by Händle [2]. Besides that, tests which forecast the behavior of clay during extrusion, as well as mathematical modelling of some properties, specially plasticity, make the results difficult due to many parameters that are involved in the process. In the literature, there is no consensus regarding which method should be used to evaluate the plasticity to be chosen [3,4]. For instance, the Pferfferkorn's plasticity index, Atterberg's plasticity index, indentation, stress/strain curves, and rheological analysis are methods cited which aim to evaluate the plasticity of a ceramic [5].

Energy saving, flux regularity, and adequate extrusion pressure are factors which depends on the type of extruder used and plasticity of the clay paste [6]. The type of extruders can be classified according to the method which produces pressure to be applied to a paste. For example, if the pressure is generated by the forcing of two rolling surfaces, it is called rotary extrusion; if the pressure is produced by the use of rotating screws or augers, it is named screw's extruder; and, finally, if the pressure is achieved by casting the paste inside a cylinder pressed with a ram, it is termed ram extruder [1]. So far, the extrusion of ceramic paste has been studied and understood in a limited way [7]. Moreover, seldom are there studies in the literature which explore the behavior of the extruded clay beyond the unsteady-state. The reason for that is the fact that, historically, the extrusion of ceramic pastes was restricted to the manufacture of products of low cost such as the red ceramic industry which did not require a strict dimensional and quality control [8].

Reed JS defined plasticity in ceramics as a particular mode of mechanical behavior when a plastic material features a permanent deformation without fracture under shear stress greater than the yield strength of the material [3]. Moreover, in the literature, another issue is found concerning ceramic extrusion: There is no consensus among researchers regarding which method should be used to evaluate the plasticity to be chosen. For instance, Andrade, et al. listed 5 main methods to evaluate the plasticity of a ceramic paste: Pferfferkorn's plasticity index, Atterberg's plasticity index, indentation, stress/strain curves, and rheological analysis as methods used to evaluate the plasticity of a ceramic paste [5]. Even though there are diverse proposed methods to assess the plasticity of the paste, Dondi stated that they may not deliver equivalent results [4].

In metallurgy, Johnson [9,10], studying the plane-strain extrusion of aluminum and lead, observed that the extrusion load decreased as the extrusion punch moved forward. However, the travel punch reached a point, before the unsteady-sate, which he named "coring point", also recognized by Avitzur [11] and Hoffmanner [12]. At this point, graphically, he perceived that there was a noticeable acceleration of the extrusion load decrease rate [9,13]. The phenomenon of the pressure rises near the end of both extrusion processes (direct and indirect extrusion) where the defect of a pipe or hole forms in the billet. This Johnson [9] coined as "coring point", that is the point at which the piston, or the end of the cylinder, upstream from the die, enters the plastic zone in front of the die. Therefore, a disturbance is initiated which causes termination of the steady phase of the flow pattern. Other authors [14] observed a different behavior for the coring point as stated by Johnson [9,13]. Instead of a decrease of the extrusion load, an increase of this load was detected, so the point of coring lay at the minimum extrusion load pressure [14]. For the extrusion of ceramics, this shift from the steady-state to the unsteady-state is also present [1,15], but very little is discussed or explored about it.

Based on a mathematical model for extrusion of clay published by Andrade [16], a modification of the model to predict the effect of the unsteady-state on the extrusion pressure is proposed in this work. This focus on studying beyond the coring point is important, since this point is reached, an unsteady-state of the material behavior and high

Citation: Tajiri HA, de Pieri ER, Al-Qureshi HA (2019) Modified Modeling of Clay Paste Extrusion through a Circular Die: Beyond the Steady-State. Int J Metall Met Phys 4:027

pressures are achieved. This significant increase in the extrusion pressure, in industry, gives a greater possibility of dealing with damage of the die and lubrication problems leading to products with defect and increasing costs.

Theoretical analysis

Equation in the compression process: For the sake of defining some parameters of the extrusion process, Flores, et al. proposed a mathematical modeling [17]. They considered the hypothesis that the cylindrical clay body, under compression stress, presents an axial and symmetrical deformation. Moreover, they stated that as the compression force is applied, the height of the specimen decreased while its instantaneous radius increased. Using the equations from Levy-Mises for the plastic zone [18] and the equation from von Mises for the effective stress, they proposed the following mathematical modeling (Eq. 1) [16,17]:

$$F = -2\pi\bar{\sigma}\left[-\frac{h}{2\mu}\left(r_f+\frac{h}{2\mu}\right)+\frac{h^2}{4\mu^2}\exp\left(\frac{2\mu r_f}{h}\right)\right] \quad (1)$$

Where F is the instantaneous axial force, $\bar{\sigma}$ the flow stress, h the final height of the sample, μ the friction coefficient between the surface of the compression machine and the clay, and r_f the final radius of the specimen.

Eq. 1 is used to assess the plasticity of the clay during the axial compression test. Additionally,

Figure 1: Sectioned clay paste sample showing strain lines representing the stress distribution [19].

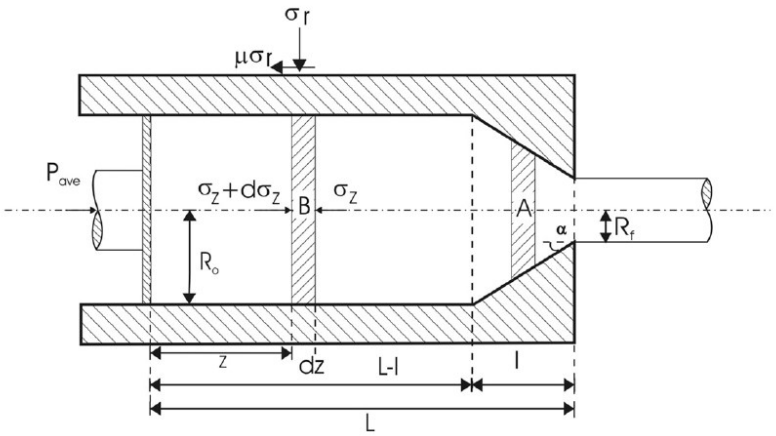

Figure 2: Diagrammatic sketch of extrusion of clay paste through a circular die with angular variation [16].

Citation: Tajiri HA, de Pieri ER, Al-Qureshi HA (2019) Modified Modeling of Clay Paste Extrusion through a Circular Die: Beyond the Steady-State. Int J Metall Met Phys 4:027

using Eq. 1 it is possible to determine the effective stress ($\bar{\sigma}$) and the friction coefficient (μ) between the clay and the punch by an iterative method. The flow stress was measured using different uniaxial compressive loadings as shown in Figure 1. It can be easily seen that barreling has occured, and this is due to the friction between the ends of the specimen and the deforming tools/punch. As a result, the coefficient of friction was included as one of the mathematical parameters to analyze the forces that act on a cylindrical clay compact and was also assumed to be constant according to Andrade, et al. [19].

Equation in the extrusion process considering the friction and the angular variation: The extrusion molding process consists of compelling a paste through a die with a desired final cross section. Moreover, it shortens its cross-sectional area from initial (A_0) to final (A_f) and expands its length. In the proposed model, it is assumed a steady-state during the extrusion process. Therefore, the ideal average extrusion pressure (considering no friction during the process $\mu_{comp} = \mu_w = 0$) for uniform deformation can be expressed as (Eq. 2):

$$\sigma_{ave}\Big|_{\mu=0} = 1.5\int_0^{\bar{\varepsilon}} \bar{\sigma}\, d\bar{\varepsilon} \quad (2)$$

Where σ_{ave} is the average extrusion pressure, μ is the coefficient of friction between the cylinder wall and the clay paste, 1.5 is the shear factor which is used to compensate the energy loss, mainly due to the friction and redundant work that are not included in equation, $\bar{\sigma}$ is the flow stress and $\bar{\varepsilon}$ is the flow strain.

In Eq. 2, it is possible to observe that it does not consider the friction in the cylinder wall; so, Eq. 3 is proposed, which takes into account the cylinder wall friction in the extrusion direction (Figure 2).

$$d\sigma_z = \frac{4\mu_w \sigma_r}{D_0} dz \quad (3)$$

Where σ_z is the axial stress, μ_w the coefficient of friction between the wall and the clay paste, σ_r the radial stress, z the punch travel and D_0 the initial diameter.

Observing, Figure 2, one can note that the diameter of the cylinder is constant, until reaching the conical part of the extruder (L-l). Moreover, considering the Levy-Mises relationships [20], which states that $\sigma_r = \sigma_z$, Eq. 4 is reached:

$$\ln \sigma_z = \frac{4\mu_w z}{D_0} + C \quad (4)$$

Taking into account the boundary condition where σ_{ave} ($\mu_w = 0$) at $z = L_c$, considering that the total pressure can be written as $(\sigma_z)_{total} = (\sigma_z)_{\mu \neq 0} + (\sigma_z)_{\mu = 0}$, and the funneling effect [19], Eq. 5 and Eq. 6 can be derived:

$$p_{total} = (\sigma_z)_{total} = \left\{1+\exp\left[\frac{4\mu_w}{D_0}(z - L_c)\right]\right\} 1.5\int_0^{\bar{\varepsilon}} \bar{\sigma}\, d\bar{\varepsilon} \quad (5)$$

$$\bar{\sigma} = \sigma_z = -\overline{\sigma_{comp}} \exp\left[\frac{2\mu}{h}\left(R_f - R_0\right)\right] \quad (6)$$

Where $\overline{\sigma_{comp}}$ stands for the effective stress of compression, R_f the final radius and R_o the initial radius.

Combining Eq. 5 and Eq. 6, yields Eq. 7:

$$p_{total} = 0.75\frac{\overline{\sigma_{comp}}\, z}{\left(R_f - R_0\right)\mu_{comp}}\left\{1+\exp\left[\frac{2\mu_w}{R_0}(z - L_c)\right]\right\}\left\{1-\exp\left[\frac{2\mu_{comp}}{z}\left(R_f - R_0\right)\right]\right\} \quad (7)$$

Eq. 7 does not consider a circular die with angular variation, it is only the expression for total extrusion pressure, when the semicone angle of the die (α) is equal to 90°. However, taking into account the angular variation of the die and making the pressure balance in the A and B region of the die, as can be seen in Figure 2, the average extrusion pressure can be determined, Eq. 8:

$$P_{ave} = \frac{\overline{\sigma_{comp}}\, z}{\left(R_f - R_0\right) 2\mu_{comp}}\left\{1-\exp\left[\frac{2\mu_{comp}}{z}\left(R_f - R_0\right)\right]\right\} \left\{\left\{1+\frac{\left(1+\mu_w \cot\alpha\right)}{\mu_w \cot\alpha}\left[\left(\frac{R_0}{R_f}\right)^{2\mu_w \cot\alpha} - 1\right]\right\} \exp\left\{2\mu_w \cot\alpha\left[-\frac{L_c}{R_0}\tan\alpha + \left(1-\frac{R_0}{R_f}\right)\right]\right\} - 1\right\} \quad (8)$$

Beyond the steady-state: After the point of coring, there are many significant changes in the mechanical and physical properties of the ceramic paste. Moreover, the punch proceeds to move forward, to the end of the matrix, so some operational parameters may change. As a result, the friction changes along the punch and the cylinder wall. In addition, it is assumed that the composition pressure is not anymore at a steady-state as in the previous stage. It becomes non-steady and it varies according to the punch movement. This action causes loss of water content and densification of the clay, and also changes the viscosity of the clay paste. It is well known that friction dominates the flow of the clay paste throughout the die. Hence it influences greatly the density along the extruded part after the coring point.

It is very difficult to derive these variations of the parameters mathematically. However, the initial

Table 1: Chemical composition in weight percentage of the AC12 clay obtained by XRF.

Oxide	SiO_2	Al_2O_3	Fe_2O_3	CaO	Na_2O	K_2O	MnO	TiO_2	MgO	P_2O_5	*L.F.
Wt.%	69.41	18.51	2.20	0.05	0.08	2.91	< 0.01	0.73	0.82	0.14	5.15

*L.F. stands for loss on fire (1000 °C).

trial is to assess the varieties of the experimental entries, considering also the Arrhenius relation. In this work it is suggested that the relationship among ram displacement, coefficient of friction, and density variation is given by the following equation (Eq. 9):

$$\mu_{x_n} = \mu_{x_{n-1}} \left[\frac{\rho_{x_n}}{\rho_{x_{n-1}}} \right]^{x_n / x_{n-1}} \quad (9)$$

Where μ_{x_n}, $\mu_{x_{n-1}}$ are the coefficient of friction at the x_n and x_{n-1} positions of the ram. Similarly, the densities are the position ρ_{x_n} and $\rho_{x_{n-1}}$, respectively.

De Wit, et al. demonstrated in a conference held in Amsterdam that the density of some clay minerals, can have their densities doubled depending on the moisture content on the material [21]. In fact, the plot of ρ_{x_n} against $\rho_{x_{n-1}}$ can be considered linear and $\rho_{x_{n-1}}$ have their approximate relationship, expressed in Eq. 10:

$$\rho_{x_n} = 2\rho_{x_{n-1}} \quad (10)$$

The above equation makes the solution of Eq. 9 easier and enhance the extrusion pressure, given in Eq. 8 at any ram position, which would predict the final extrusion pressure as expressed in Eq. 11:

$$P_{ext} \frac{\overline{\sigma_{comp}}}{(R - R_f)_2 / 2} \left\{ 1 - \exp\left[\frac{2 / 2}{(R_f - R)} \right] \right\} \left\{ \left\{ 1 + \frac{(1 \ \mu \ \cot \alpha)}{\mu_w \cot \alpha} \left[\left(\frac{R_0}{R_f} \right)^{2\mu \cot \alpha} - 1 \right] \right\} \exp\left\{ 2\mu \ \cot \alpha \left[-\frac{L}{R} \tan \alpha + \left(1 - \frac{R_0}{R_f} \right) \right] \right\} - 1 \right\} \quad (11)$$

Material and Methods

The materials and methods were based on Andrade and Flores previous works [16,17]. The material used was a clay AC12 supplied by Colorminas. The chemical composition of the clay is shown in Table 1.

The as received AC12 clay was disaggregated using a dry ball milling for 20 min, followed by a sieving process through a mesh of 420 µm. One kg of the disaggregated and sieved material was collected. Moreover, in order to quantify the humidity percentage in the clay, approximately 10 g of the sieved clay were placed in an oven at 110 ± 5 °C for 24 h for calcination. From the results

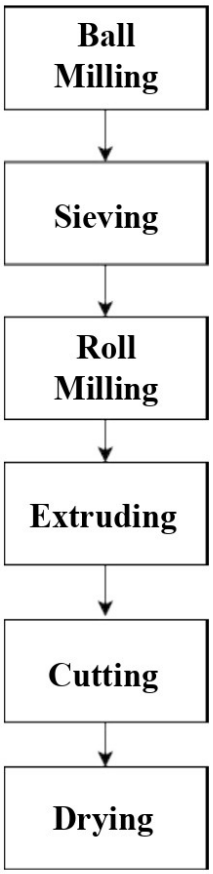

Figure 3: Experimental flowchart of the ceramic samples.

obtained by the calcination of the clay, samples with a moisture content of 55.2% were prepared and homogenized via mechanical mixing and left in a sealed plastic container for 24 h. The whole experimental procedures to produce the cylindrical specimen is shown in Figure 3. The moisture content of 55.2% was chosen since this moisture content lies between the Atterberg's plastic and liquid limits. Samples with moisture content near the liquid limit do not present enough green strength, and some manometers may not have

enough accuracy to measure its pressure. On the other hand, specimens near the plastic limit present higher extrusion pressure, being not so interesting in industry.

In order to obtain the specimens for the compression test, cylindrical samples were prepared manually in PVC molds with diameter and height of 17.0 and 23.0, respectively. Then, four specimens were used for the uniaxial compression test, using a TA-XT2i (Stable Micro System) machine, with velocity of 0.1 mm/min and cell of 25 kgf. Finally, the samples had their average diameter measured by means of digital photographs and use of an image processing software, ImageTool. With the compression test results, it was possible to determine the effective compressive stress and the friction coefficient between the clay paste and the punch.

For the extrusion process, the disaggregated and sieved clay was roll milled using a Gelenski LIG-05 machine, for better disaggregation of the granules and better homogenization of the clay paste. Finally, the paste was extruded using a Gelenski MVIG-05 machine. In order to measure the extrusion pressure a manometer was installed between the barrel and the interchangeable die. The manometer had capacity to measure up to 20 kgf/cm^2 with a graduated scale of 0.1 kgf/cm^2.

Results and Discussion

Prior to verify the proposed mathematical modeling expressed in Eq. 10, it is important to find the effective stress of the clay. As mentioned before, it can be determined when the clay is subjected to uniaxial compression stress. In addition, in order to evaluate and validate the mathematical modeling proposed for the uniaxial compression test (Eq. 1), a published work from Guilherme, et al. [22] was chosen and the mathematical model was applied. The load-radial curves for different materials and humidity percentages are shown in Figure 4.

As it can be seen in Figure 4, at first, there is a small elastic strain with a subsequent relatively high plastic strain. In addition, it is possible to observe a good correlation between the experimental points and the theoretical curves. Using Eq. 1, and applying the iterative process, it was possible to determine the effective stress of compression and the coefficient of friction between the punch and the clay paste. Furthermore, the calculated effective compressive flow stress for Terracotta, Porcelain and Earthenware were respectively, 0.08, 0.11, and 0.07 MPa. When compared to the paste bulk yield values published by Guilherme, et al. [22] for these materials, these values are in the same range of magnitude. Moving to the friction coefficient values, applying the iterative process for Eq. 1, all the materials presented the same friction coefficient, 0.134. Contrasting with the calculated values of static friction from Guilherme, et al. [22], a greater difference was found for Porcelain (μ = 0.387), while for Terracotta (μ = 0.134) and Earthenware (μ = 0.147), it was observed no or little difference.

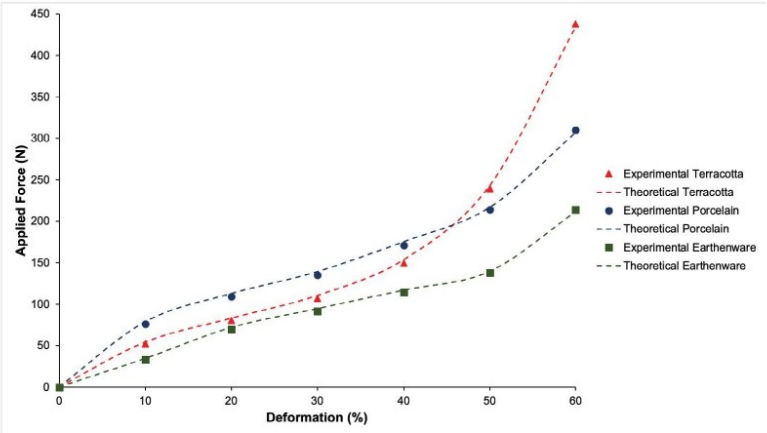

Figure 4: Experimental points and theoretical curves (dashed curves) from compression test. Terracotta with 25% of humidity, Porcelain with 31% of humidity, and Earthenware with 25.3% of humidity.

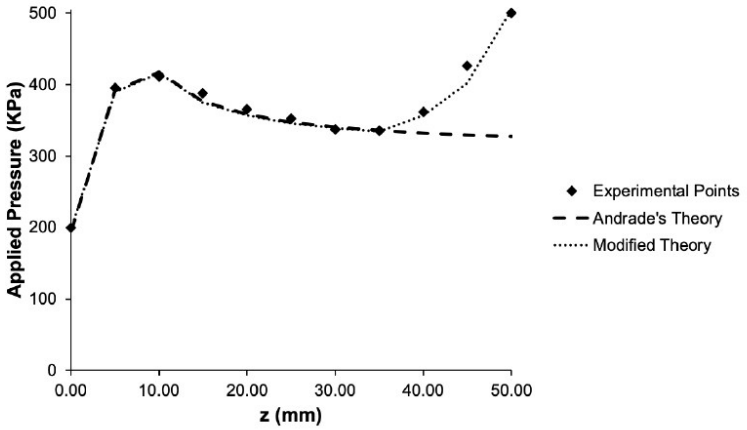

Figure 5: Comparison among experimental (diamond marks), Andrade (dashed line) [16] and Modified theoretical (round dot line) extrusion pressure varying the punch travel distance.

Table 2: Extrusion pressure comparison among experimental, Andrade's theoretical [16] and Modified Andrade's theoretical extrusion pressure for AC12 clay through a circular die, considering an angular variation.

Punch travel (mm)	Experimental extrusion pressure (kPa)	Andrade theoretical extrusion pressure (kPa)	Difference between Andrade and experimental pressure (%)	Modified theoretical extrusion pressure (kPa)	Difference between modified and experimental pressure (%)
0.10	200.0	197.5	-1.26	196.8	-1.63
5.00	395.0	391.0	-1.03	389.5	-1.40
10.00	411.0	417.3	1.51	415.8	1.15
15.00	388.0	376.4	-3.07	375.1	-3.45
20.00	365.0	357.9	-1.97	356.6	-2.34
25.00	352.0	347.4	-1.32	346.1	-1.69
30.00	337.0	340.6	1.06	339.4	0.70
35.00	335.0	335.9	0.25	334.6	-0.11
40.00	362.0	332.4	-8.92	356.6	-1.50
45.00	426.0	329.7	-29.22	401.6	-6.08
50.00	500.0	327.5	-52.66	504.3	0.85

For the extrusion curve, it was used a previously published work from Andrade [16] and reproduced for evaluating and validating a modified theory. Figure 5 displays the variation of the applied extrusion pressure as a function of the distance travelled by the piston. Three phases can be recognized in Figure 5: A coining phase, marked by compression of the ceramic paste; a steady-state phase, where the pressure is stabilized and the extrusion continues steadily; and an unsteady-state phase, also called as coring point, showing an evident increase in the extrusion pressure. As it can be noted, for Andrade's curve it is possible to notice only two phases the coining and the steady-state phase, once in his mathematical modeling [16], he did not consider implications of the coring point.

Figure 5 shows a good correlation between the experimental points and the modified theory throughout the entire curve. Even though, Andrade's theory shows a good fit up to the unsteady-state phase, it fails to neglect the coring point. Moreover, for this case, the coring point lays after 35 mm of ram displacement.

Table 2 highlights the differences in percentage between the experimental points and both theories (Andrade and Modified). One trend can be noticed for Andrade's theory, subsequently

to the coring point, as the piston moves forward, the extrusion pressure difference increases in a nonlinear fashion. In addition, pressure difference up to 53% can be reached. On the other hand, for the Modified theoretical curve, pressure difference greater than 7% was not observed.

Conclusion

In this work it was possible to apply mathematical modeling successfully. The theoretical curves showed good agreement with the experimental data for both compression tests and extrusion processes. Moreover, it was possible to develop a mathematical model for the extrusion of clay paste to analyze the pressure beyond the steady-state phase. The coefficient of friction in the unsteady-state regime was no longer constant, since the ceramic past became drier and denser. It is interesting to predict the coring point, since after reaching that point, high pressures can be achieved. The expression for the variation of the coefficient of friction was proposed in the unsteady-state zone. This is fundamental for predicting the total extrusion pressures. The good correlation shown by the proposed theory makes it a potential tool for the assessment of clay material with optimized properties. Additionally, with this theory it will be possible to manufacture extrusion equipment accurately.

Acknowledgements

The authors wish to thank the Departments of Mechanical and Chemical Engineering, in UFSC for the use of the facilities and CNPq for partially financing the project and grants for the authors.

Competing Interests

Authors have declared that no competing interests exist.

References

1. Benbow J, Bridgwater J (1993) Paste flow and extrusion. Oxford: Clarendon Press.
2. Händle F (2007) Extrusion in ceramics. Berlin, New York: Springer.
3. Reed JS (1995) Principles of ceramics processing. (2nd edn), Wiley & Sons, Chichester, New York.
4. Dondi M (2006) Caracterização tecnológica dos materiais argilosos: Métodos experimentais e interpretação dos dados. Revista Cerâmica Industrial 11: 36-40.
5. Andrade FA, Al-Qureshi HA, Hotza D (2011) Measuring the plasticity of clays: A review. Applied Clay Science 51: 1-7.
6. Ribeiro MJ, Ferreira JM, Labrincha JA (2005) Plastic behaviour of different ceramic pastes processed by extrusion. Ceramics International 31: 515-519.
7. Burbidge AS, Bridgwater J (1995) The single screw extrusion of pastes. Chemical Engineering Science 50: 2531-2543.
8. Macedo RS, Menezes RR, Neves GA, Ferreira HC (2008) Estudo de argilas usadas em cerâmica vermelha. Cerâmica 54: 411-417.
9. Johnson W (1956) Experiments in plane-strain extrusion. Journal of the Mechanics and Physics of Solids 4: 269-282.
10. Johnson W (1959) An elementary consideration of some extrusion defects. Applied Scientific Research, Section A 8: 52-60.
11. Avitzur B (1967) Steady and unsteady state extrusion. J Engng Ind, 175.
12. Hoffmanner AL (1970) Metal forming interrelation between theory and practice: Proceedings of a symposium on the relation between theory and practice of metal forming, held in Cleveland. Plenum Press.
13. Dodeja LC, Johnson W (1957) The cold extrusion of circular rods through square multiple hole dies. Journal of the Mechanics and Physics of Solids 5: 281-295.
14. Sturgess CEN, Dean TA (1979) Breakthrough pressures in lubricated extrusion. Journal of Mechanical Working Technology 3: 119-135.
15. Janney MA (1995) Plastic forming of ceramics: Extrusion and injection moulding, in Ceramic Processing. Springer Netherlands: Dordrecht, 174-211.
16. Andrade FA (2009) Modelamento Matemático do Comportamento Plástico do Sistema Argila-água no Processo de Extrusão, in Programa de Pós-Graduação em Ciência e Engenharia de Materiais. Universidade Federal de Santa Catarina.
17. Flores OJU, Mendes L, Novaes de Oliveira AP, Fredel MC, Al-Qureshi HA, et al. (2006) Modelo matemático aplicado à avaliação da plasticidade de argilas.
18. Avitzur B, Fueyo J, Thompson J (1967) Analysis of plastic flow through inclined planes in plane strain. Journal of Engineering for Industry 89: 361-375.
19. Andrade FA, Al-Qureshi HA, Hotza D (2013) Modeling

of clay paste extrusion through a rectangular die. International Journal of Advanced Materials and Technologies, 1.

20. Hoffman O, Sachs G (1953) Introduction to the theory of plasticity for engineers. McGraw-Hill.
21. De Wit CT, Arens PL (1950) Moisture content and density of some clay minerals and some remarks on the hydration pattern of clay. Transactions of the International Congress of Soil Science, 2.
22. Guilherme P, Ribeiro MJ, Labrincha JA (2009) Behaviour of different industrial ceramic pastes in extrusion process. Advances in Applied Ceramics 108: 347-351.

ISSN 2631-5076

Citation: Tajiri HA, de Pieri ER, Al-Qureshi HA (2019) Modified Modeling of Clay Paste Extrusion through a Circular Die: Beyond the Steady-State. Int J Metall Met Phys 4:027

Journal of the Brazilian Society of Mechanical Sciences and Engineering (2023) 45:225
https://doi.org/10.1007/s40430-023-04135-8

TECHNICAL PAPER

Analysis of the spring-back and water effect on the coring point during direct extrusion

Henrique A. Tajiri[1] · Dachamir Hotza[2] · Edson Roberto De Pieri[3] · Hazim A. Al-Qureshi[4]

Received: 13 September 2022 / Accepted: 6 March 2023 / Published online: 29 March 2023

Abstract
The present work proposes to come up with theoretical analyses and equations describing the extrusion pressures for direct ceramic paste extrusion through a circular die considering the coring point. For example, in a ceramic paste, the coring point is evidenced by a significant rise in the extrusion pressure beyond the steady state. This increase in the extrusion pressure may be linked to a change in the paste behavior during the unsteady state. Furthermore, regarding the feedstock properties' variations, it may be accounted to water loss, densification of the clay paste, and shift of the friction coefficient. In practice, when the coring point is forecast during extrusion, die damages, lubrication problems, product defects, and a raise in the production cost can be minimized and even avoided. This work proposes two theoretical analyses and equations considering the effect of the coring point on the extrusion pressure. For instance, one analysis considers the effect of the spring-back phenomenon on the pressure, while the second considers the influence of water loss (water migration) during extrusion. The two proposed approaches demonstrated a satisfactory correlation with an experimental curve. In addition, the water loss approach seemed to be more conservative when compared to the spring-back phenomenon. In conclusion, the theoretical analyses seemed to be very useful to aid the construction of new equations. Thus, it was possible to fill a gap in the direct extrusion of ceramic, where publications about the unsteady state regime and equations which acknowledge it are very rare.

Keywords Coring point · Direct extrusion of ceramics · Spring-back · Water loss · Friction

1 Introduction

Extrusion plays an important role in material processing. Händle [1] states that extrusion is a shaping technique widely employed to produce constant cross-sectional area products. In ceramics, this process is used either in the traditional clay-based industry as well as in the advanced ceramic industry. For instance, clay bricks and roof-tiles are classic examples of traditional ceramics cited by Kocserha and Kristály [2], while Händle [1] mentioned high-alumina insulators and zirconia aerospace components as examples of advanced ceramics. In addition, Nath Das et al. [3] highlighted the cordierite honeycomb catalyst production in the advanced ceramic industry. Also, in the past few years, extrusion has been cited as being pivotal in additive manufacturing [4–9]. Importantly, extrusion is employed not only in the ceramic industry, but also widely found in the metallic, polymeric, and food industry.

The extrusion process consists of pushing material through an orifice, known as a die. Therefore, pressure is required in the process. In ceramic extrusion, the type of

Technical Editor: Izabel Fernanda Machado.

✉ Henrique A. Tajiri
henriquetajiri@hotmail.com

[1] Department of Mechanical Engineering (EMC), Technology Center (CTC), Federal University of Santa Catarina (UFSC), Florianopolis, SC 88040-900, Brazil

[2] Department of Chemical Engineering and Food Engineering (EQA), Technology Center (CTC), Federal University of Santa Catarina (UFSC), Florianopolis, SC 88040-900, Brazil

[3] Department of Automation and Systems (DAS), Technology Center (CTC), Federal University of Santa Catarina (UFSC), Florianopolis, SC 88040-900, Brazil

[4] Graduate Program in Materials Science and Engineering (PGMAT), Technology Center (CTC), Federal University of Santa Catarina (UFSC), Florianopolis, SC 88040-900, Brazil

extruders can be classified according to the mechanism in which pressure is produced and further, it is transferred to the paste. There are three more frequent ways in which pressure can be generated. For example, Benbow and Bridgwater [10] identified three different types of extrusion. For instance, if the pressure is achieved by forcing two rolling surfaces, it is known as a rotary extruder; if the pressure is produced by means of rotating screws or augers, it is termed a screw extruder; and if the pressure is generated by casting the paste inside a cylinder pressed with a ram or piston, it is named as a ram or direct extruder.

According to Vitorino et al. [11], in ceramic extrusion, the plasticity of the paste contributes significantly throughout the process. Reed [12] defined plasticity in ceramics as a particular mode of mechanical behavior when a plastic material features a permanent deformation without fracture under shear stress greater than the yield strength of the material. Furthermore, an issue is found in the literature regarding ceramic extrusion: the researchers do not have a universal consensus concerning which method should be used to evaluate the plasticity of the paste. For example, Andrade et al. [13] review the main methods to assess the ceramic paste's plasticity: rheological analysis; Pfefferkorn's plasticity index; Atterberg's plasticity index; stress/strain curves; and indentation. Dondi [14] suggests that there are a variety of methods to evaluate the plasticity of the ceramic paste; nevertheless, they may not yield similar outcomes.

In terms of the extrusion pressure and extrusion ram displacement, as shown in

Figure 1, Benbow and Bridgwater [10] identified and divided the extrusion curve into three parts. Initially, the ram extrusion is marked by a steep extrusion pressure raise, while the ram flattens the paste. Afterward, the paste reaches a steady state, where it is noticeable a modest and gradual decrease in the extrusion pressure until it approaches a minimum. Finally, a sharp increase in the extrusion pressure occurs, entering an unsteady state. This point, which is a shift from a steady to an unsteady state, more common and reported in metals, is also known as the coring point [15, 16].

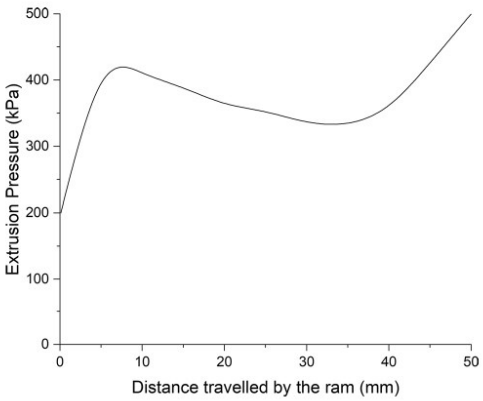

Fig. 1 Extrusion pressure of an alumina paste as a function of the ram's displacement. Adapted from Benbow and Bridgwater [10]

Still, Burbidge and Bridgwater [17] affirmed that ceramic extrusion has been understood and explored in a restricted way when compared to polymeric extrusion. Moreover, there are scarce works that investigate the behavior of the extruded paste beyond the steady state. The reason for that is that, historically, the extrusion of ceramic pastes was restrained to the production of goods of low cost, such as the clay-based industry, which according to Macedo et al. [18] did not demand a meticulous dimensional and quality control. Besides that, tests trying to predict the behavior of the ceramic paste during extrusion, as well as mathematical modeling of some properties, especially plasticity, are difficult due to many parameters involved in the process.

In metal processing, Johnson [16, 19], investigating the plane-strain extrusion of aluminum and lead, noticed a decline in the extrusion load while the ram moved forward. Nevertheless, the punch approached a position before reaching the unsteady state, which Johnson coined as the "coring point." Later on, it was also identified and reported by Avitzur [20] and Hoffmanner et al. [21]. Graphically, at this specific point, Johnson [16] and Dodeja and Johnson [15] identified a remarkable acceleration of the extrusion pressure decrease rate. Moreover, Johnson [16] named as "coring point" the point at which the piston, or the end of the cylinder, upstream from the die, enters the plastic zone in front of the die. In metals, the phenomenon of pressure increase, close to the end of the extrusion process (encountered either in direct and also in indirect extrusion), can generate defects such as pipe or hole formation in the billet. Therefore, a disturbance is initiated, which leads to the end of the steady phase of the flow pattern.

Other authors, such as Sturgess and Dean [22], observed a different behavior for the coring point as stated by Johnson [16] and by Dodeja and Johnson [15]. Rather than a decline in the extrusion load, a raise in this load was observed. Therefore, Sturgess and Dean [22] suggested that the coring point is located at the minimum extrusion load pressure in the steady state regime. This phenomenon is also found in the extrusion of ceramic pastes as early displayed by Janney [23] and Benbow and Bridgwater [10]; however, it is still not well explained or studied.

Mathematical modeling applied to extrusion is appealing. It is a powerful tool that helps to optimize the extrusion process and get a better understanding of the variables within the process. According to Reed [12], a ceramic plastic body or paste comprises a liquid and a solid phase, within the

plastic and the liquid limits. A divergence emerges when dealing with the mathematical modeling of ceramics submitted to extrusion. For example, Horrobin and Nedderman [24] proposed a model assuming the ceramic paste as a plastic-elastic formulation; on the other hand, Benbow and Bridgwater [10] proposed a model, broadly used and cited in the literature, where they conjectured the ceramic paste as a mixture of perfect plastic and viscous flow in the die entry region (first term in Eq. 1) and as a rigid plug flow, as stated by Horrobin and Nedderman [24] (velocity of the fluid is considered constant along the cross section) in the die land region (second term in Eq. 1):

$$P = 2\left(\sigma_0 + \alpha v_d^m\right)\ln\left(\frac{D_0}{D}\right) + \left(\tau_0 + \beta v_d^n\right)\frac{4L}{D} \tag{1}$$

where P stands for extrusion pressure; σ_0 for yield stress extrapolated to zero velocity; α for velocity factor of bulk yield stress; v_d for mean extrudate velocity in the die land; D_0 for the diameter of the barrel; D for the diameter of the die land; τ_0 for the initial wall shear stress of paste; β for velocity factor of wall shear stress; L for the length of the die land; m for the paste parameter determining the dependence of the bulk paste yield stress on velocity; and n for the paste parameter determining the dependence of wall shear stress on velocity.

According to Benbow and Bridgwater's [10] extrusion model, the extrusion pressure depends on flow properties, extrusion rate, and physical and geometrical details of the extruder. Moreover, as can be seen in Eq. 1, ten variables are involved. Vitorino et al. [25] aggrouped these variables into four groups: known geometrical parameters (D_0, D, and L), processing parameters (v_d), unknown physical parameters (α, β, σ_0, and τ_0), and mathematical fitting (n and m). Even though this model is widely cited and used in the literature, the calculated overall pressure drop is only valid in the steady state.

Andrade [26] in an attempt to model the pressure behavior during extrusion, the author used the free-body equilibrium approach. Therefore, he considered the ceramic paste as an ideal plastic solid (Eq. 2). Thus, the paste behavior has been modeled using different flow assumptions. Furthermore, there is no consensus among the researchers concerning which approach presents a more accurate description of the ceramic paste behavior during the extrusion process:

$$\frac{P_{\text{ave}}}{\overline{\sigma}_{\text{comp}}} = (\text{PartA})(\text{PartB})(\text{PartC})(\text{PartD}) \tag{2}$$

$$\text{PartA} = \frac{1}{\left(R_f - R_0\right)}\frac{z}{2\mu_{\text{cil}}}$$

$$\text{PartB} = 1 - \exp\left[\frac{2\mu_{\text{cil}}}{z}\left(R_f - R_0\right)\right]$$

$$\text{PartC} = 1 + \frac{\left(1 + \mu_w \cot\theta\right)}{\mu_w \cot\theta}\left[\left(\frac{R_0}{R_f}\right)^{2\mu_w \cot\theta} - 1\right]$$

$$\text{PartD} = \exp\left\{2\mu_w \cot\theta\left[-\frac{L_c}{R_0}\tan\theta + \left(1 - \frac{R_f}{R_0}\right)\right]\right\} - 1$$

where P_{ave} is the average pressure during extrusion; $\overline{\sigma}_{\text{comp}}$ is the effective stress of compression; z is the distance traveled by the piston; R_f is the die land radius; R_0 is the barrel radius; μ_{cil} is the coefficient of friction between punch and clay paste; μ_w is the coefficient of friction between wall and clay paste; and θ is the semicone angle of the die. The effective stress of compression can be estimated using Flores et al. [27] mathematical modeling using stress-deformation curves.

Benbow and Bridgwater's [10] extrusion model and Andrade's [26] equation failed to forecast the unsteady state behavior and its consequences. However, Tajiri et al. [28], in one attempt to overcome this gap, suggested a modified mathematical modeling, represented in Eq. 3, where the authors took into account Andrade's equation [26] and modified it. Moreover, they also assumed that the friction coefficient is no longer constant along the extrusion process. They related this friction coefficient variation with the fact that there should be a loss of water content (water migration), which is a known phenomenon already noticed and described by researchers such as Benbow and Bridgwater [10], Khan et al. [29], Wilson and Rough [30], Yekta et al. [31], and Patel et. al [32]. In addition, Tajiri et al. [28] suggested that this water loss would lead to further densification of the paste, causing also changes in the flow behavior of the ceramic paste, which have already been noticed and published by Händle [1], Mason et al. [33], and Tajiri et al. [28]:

$$\frac{P_{\text{ave}}}{\overline{\sigma}_{\text{comp}}} = (\text{Part1})(\text{Part2})(\text{Part3})(\text{Part4}) \tag{3}$$

$$\text{Part1} = \frac{1}{\left(R_f - R_0\right)}\frac{z}{2\mu_{x_{n-1}} 2^{x_n/x_{n-1}}}$$

$$\text{Part2} = 1 - \exp\left[\frac{2\mu_{x_{n-1}} 2^{x_n/x_{n-1}}}{z}\left(R_f - R_0\right)\right]$$

$$\text{Part3} = \left\{ 1 + \frac{\left(1 + \mu_w \cot\theta\right)}{\mu_w \cot\theta} \left[\left(\frac{R_0}{R_f} \right)^{2\mu_w \cot\theta} - 1 \right] \right\}$$

$$\text{Part4} = \exp\left\{ 2\mu_w \cot\theta \left[-\frac{L_c}{R_0} \tan\theta + \left(1 - \frac{R_f}{R_0} \right) \right] \right\} - 1$$

where μ_{x_n} and $\mu_{x_{n-1}}$ are the coefficient of friction at the x_n and x_{n-1} positions of the ram, respectively. Tajiri et al. [28] also stated that:

As shown through experimental results by some researchers such as Benbow and Bridgwater [10], Liu et al. [34], Rough et al. [35], and others [36–38], the extrusion pressure does not remain constant throughout the entire extrusion process, and there is a lack of studies and thorough investigation in this topic. Moreover, it is possible to observe a significant rise in the extrusion pressure, highlighting the shift from a steady state to a non-steady state behavior. It is also important to bear in mind that when the transition from the steady state to the non-steady state is neglected, it can lead to vulnerable issues ranging from the compromised quality of the final product to the damage of the extrusion equipment.

Tajiri et al. [28] proposed an equation that considered mathematically this phenomenon in the extrusion pressure profile. However, there might be other variables, other than the friction coefficient, that might impact the extrusion pressure during the unsteady state. In order to fill this gap in the scientific and industrial realm and build the theory proposed by Tajiri et al. [28], novel theoretical analyses will be performed and two equations will be introduced. The first approach associates the unsteady state with the spring-back phenomenon during extrusion, while the second approach correlates the increase in the extrusion pressure with the water content change of the ceramic paste over time.

2 Theoretical analysis beyond the coring point

As stated previously, two theoretical analyses will be proposed and discussed further. These analyses bring to discussion new variables which were not included in Tajiri et al. [28] work, but might be relevant after the coring point.

2.1 Spring-back phenomenon

As mentioned before, the point of coring can be marked by a sudden increase in the extrusion pressure [15, 16]. Moreover, another theoretical explanation for it could be reached by analyzing the effect of the elastic recovery of the material after being extruded.

This novel proposed theory considers the influence of the material spring-back. The spring-back phenomenon is widely referred to and studied mainly in metal forming [39–41]. According to Chongthairungruang et al. [42], the spring-back phenomenon can be inferred as a physical phenomenon associated with elastic strain recovery after reloading deformation loads. In addition, the authors state it is a mechanism that is governed basically by stress [42].

In summary, when the material is extruded, it is under compressive stresses due to the barrel and die constraints. After the material exits the die, there is no longer any constraint in the radial direction and the material is free for elastic recovery. Furthermore, the greater the compressive stress, the greater the strain of the material. Regarding the strain of the material, it is deeply linked to Poisson's ratio. The Poisson's ratio is the negative of the ratio of transverse strain to axial or lateral strain. In this case, $\upsilon = -\varepsilon_R / \varepsilon_z$, where ν is the Poisson's ratio and ε_R and ε_z are the strains in the radial and axial direction (z direction). Therefore, when the material is relieved from the radial stress (after exiting the die's outlet) and it causes a counter axial stress, opposite to the extrusion direction, rising the extrusion pressure. The combination of the radial stress release and the effect of the counter axial stress causes the spring-back phenomenon.

So far, in the literature, regarding the direct extrusion of ceramics, it is not possible to find any published work that considers this phenomenon and expresses it mathematically. Thus, it becomes evident that all the previous responses that the material undergoes during extrusion, in special the spring-back phenomenon is the main objective of this approach; however, once again, it is worth mentioning that this kind of behavior has, yet not been published previously. Hence, the proposed spring-back phenomenon can be incorporated into the extrusion equation as follows.

In Fig. 2a, it is clearly shown, on the exit side of the die, that the material recovers elastically after being processed. For further analyses, the circled area on the die (Fig. 2a) is amplified to show the acting stresses in that section (Fig. 2b). Now, considering a simple element in equilibrium, represented by the shaded area displayed in Fig. 2a, the balance of forces can be calculated ($\sum F_z = 0$), which leads to the following equation:

$$\left(\sigma_z + d\sigma_z\right)\frac{\pi D_d^2}{4} - \sigma_z \pi \frac{\left(D_d + dD\right)^2}{4} - \mu_w \sigma_R \cos\theta \frac{dz}{\cos\theta} \pi D_d + \sigma_R \sin\theta \frac{dz}{\cos\theta} \pi D_d = 0 \tag{4}$$

where σ_z is the axial stress, μ_w is the coefficient of friction between the wall and the clay paste, σ_R is the radial stress, z is the punch travel, D_d is the diameter of the die, and D is the diameter of the extrudate within the shaded area (Fig. 2a). The above equation can be simplified:

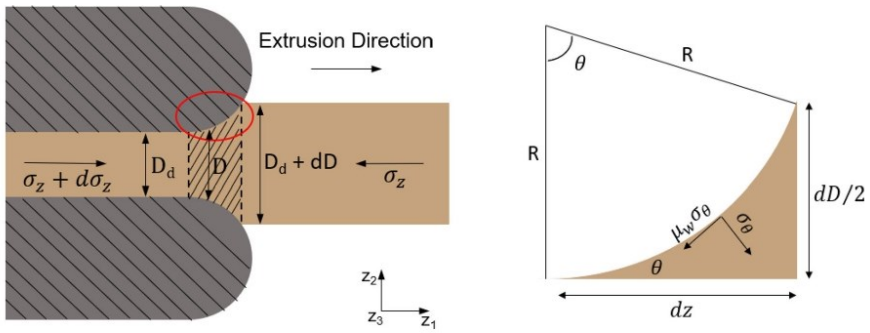

a) Spring-back phenomenon occurring at the die's exit b) Zoom at the area surrounded by the red circle.

Fig. 2 Illustration of the spring-back phenomenon during the extrusion of the ceramic paste after the coring point

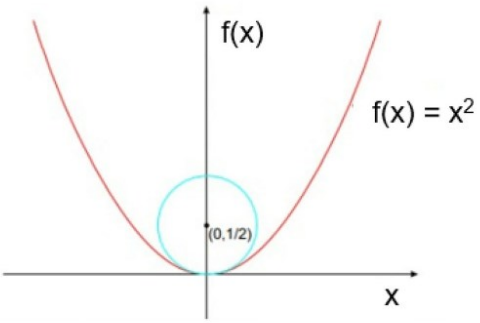

Fig. 3 Example of an osculating circle of a parable. Adapted from [44]

Considering the equation above (Eq. 4), it becomes fundamental to find a way, to eliminate D in Eq. 4. Simply, the equation itself is difficult to solve in a simplified way. For this reason, the present work simplifies the calculations by replacing the circle of radius R, exhibited in Fig. 2b, with a second order curve, using the principles of an osculating circle. In addition, the osculating circle of a curve can be defined as the circle which presents the same tangent and the same curvature at a point [43]. An example of the osculating circle of the parable is displayed in Fig. 3.

Still related to the osculating circle, it is known that it can be mathematically described as follows:

$$\kappa(x) = \frac{|f''(x)|}{\left(1 + (f'(x))^2\right)^{3/2}} \text{ and } \rho(x) = \frac{1}{\kappa(x)}$$

where $\kappa(x)$ is the curvature of the curve; $f'(x)$ and $f''(x)$ are, respectively, the first and second derivative of the equation of the curve; and $\rho(x)$ is the radius of the curve. Thus, as stated previously, for the sake of eliminating D, the osculating circle concept was adopted, and a second-order equation was used to simplify the calculus.

After some mathematical manipulations and calculations, defining and setting some boundary conditions and integrating Eq. 4 using the method of integrating factor, finally, it was possible to achieve Eq. 5, as it is described as follows:

$$\frac{\sigma_z}{\overline{\sigma}} = \left(-\frac{\theta}{\mu_w} + \frac{R_f}{8R\mu_w^2} - 1\right) + \left[\left(\frac{P_{ave}}{\overline{\sigma}_{comp}}\right) - \frac{R_f}{8R\mu_w^2} + 1\right] \exp^{\frac{8R\mu_w\theta}{R_f}} \quad (5)$$

where θ is the exit angle, R is the radius of the die's exit, and $\left(\frac{P_{ave}}{\overline{\sigma}_{comp}}\right)$ corresponds to the steady state regime (Eq. 2).

Thus, Eq. 5 shows another approach that takes into account the effect of the coring point on the extrusion pressure. Moreover, evaluating Eq. 5, θ should lay between 0 and 90°. If θ is equal to 0° Eq. 5 then equal to Eq. 2 (Andrade [26]), meaning that the extrusion process is in a steady state regime. Now, when θ equals 90°, Eq. 5 tends to go to infinity.

2.2 Effective stress of compression as a function of water content

Now moving to the second approach, it is found in the literature that the compressive and shear strength of the ceramic paste may vary according to the amount of water in the system [11, 26, 45–47]. For instance, Andrade [26] found

a linear relation between compressive strength and water content within a certain range of humidity. He observed a decrease in compressive strength when the water content increased. Yet et. al [45] noticed the same trend for the shear strength. Thus, parameters, such as the initial bulk stress (σ_0) and the initial wall stress (τ_0), encountered in the Benbow and Bridgwater [10] model, and the effective stress of compression ($\overline{\sigma}_{comp}$) may not be a constant value along the extrusion, especially beyond the steady state.

As it was stated previously, it is found in the literature that the compressive strength of the ceramic paste may vary according to the amount of water in the system. Published works from Andrade [26], Ribeiro et al. [48], and Hamza et al. [49] show a linear trend, as found in Fig. 4. All these works presented an increase in compressive strength when the water content decreased.

As can be observed in Fig. 4, it is reasonable to state that, within a certain range of water content, there is a linear relationship between water content and compressive strength. Therefore, this linear tendency can be represented by the following equation:

$$\overline{\sigma}_{comp} = -aw + b \tag{6}$$

where a and b are the coefficients of the linear equation, and w is the water content.

Moreover, knowing the liquid limit (LL), plastic limit (PL), and the compressive strength in the plastic limit and in point A (Eq. 7), where within this range of water content, the paste presents a linear relation, Eq. 7 can be drawn:

$$A = \frac{\mathrm{PL} + \mathrm{LL}}{2} \tag{7}$$

It is clear that A stands for the plastic and liquid average limit:

$$\overline{\sigma}_{comp} = w\frac{(\sigma_{PL} - \sigma_A)}{(w_{PL} - w_A)} + \left[\frac{(w_{PL}\sigma_A - w_A\sigma_{PL})}{(w_{PL} - w_A)}\right] \tag{8}$$

where σ_{PL} is the compressive strength in the plastic limit, σ_A is the compressive strength in point A, w_{PL} is the water content in the plastic limit, and w_A is the water content in point A.

It becomes clear that the water content is not constant throughout the extrusion process [34, 35, 50]. None of the previously mentioned publications related the water content and time mathematically. However, in the present work, it is proposed that the water content (w) is a function of the water content variation (dw/dt) over time as follows:

$$w = w_0 - \frac{dw}{dt}\Delta t \tag{9}$$

where w_0 stands for the initial water content, dw/dt for the water content variation over time, and Δt for a time variation. Now, combining Eq. 6 and Eq. 9, yields:

$$\overline{\sigma}_{x_n} = a\left(w_{x_{n-1}} - \frac{dw}{dt}\left(t_{x_n} - t_{x_{n-1}}\right)\right) + b \tag{10}$$

where $\overline{\sigma}_{x_n}$, $w_{x_{n-1}}$, t_{x_n}, and $t_{x_{n-1}}$ are, respectively, the compressive strength, water content, and time at the x_n and x_{n-1} positions of the ram.

Equation 10 can also be rewritten as follows:

$$\overline{\sigma}_{x_n} = a\left(w_{x_{n-1}} - \frac{dw}{dt}\left(\frac{x_{x_n} - x_{x_{n-1}}}{v}\right)\right) + b \tag{11}$$

where v stands for the paste velocity in the barrel and x_{x_n} and $x_{x_{n-1}}$ for the position of the ram during extrusion.

When $x_n < x_{coring\ point}$, the water content is constant; therefore, dw/dt is zero. Thus, a new mathematical model is proposed, where beyond the steady state the compressive strength no longer is constant. Combining Eq. 3, Eq. 8 and Eq. 11 yields:

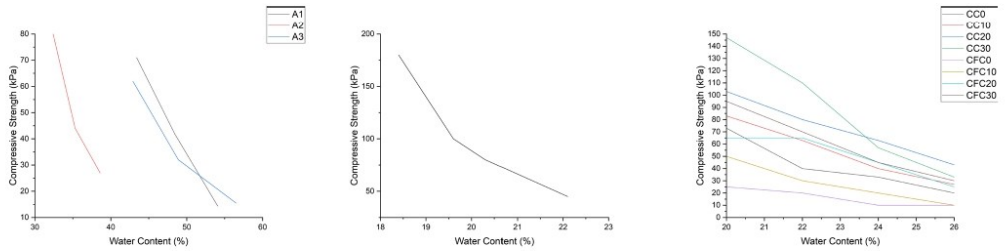

a) Adapted from Ribeiro et al. [48] b) Adapted from Andrade [26] c) Adapted from Hamza et al. [49]

Fig. 4 Relationship between compressive strength and water content

$$P_{ave} = \frac{\left[\frac{(\sigma_{PL}-\sigma_A)}{(w_{PL}-w_A)}\left(w_{x_{n-1}} - \frac{dw}{dt}\left(\frac{x_n - x_{n-1}}{v}\right)\right) + \left[\frac{(w_{PL}\sigma_A - w_A\sigma_{PL})}{(w_{PL}-w_A)}\right]\right]}{(R_f - R_0)} \frac{z}{2\mu_{comp}}$$
$$\left\{1 - \exp\left[\frac{2\mu_{comp}}{z}(R_f - R_0)\right]\right\}$$
$$\left\{\left\{1 + \frac{(1+\mu_w \cot\theta)}{\mu_w \cot\theta}\left[\left(\frac{R_0}{R_f}\right)^{2\mu_w \cot\theta} - 1\right]\right\}\right.$$
$$\left.\exp\left\{2\mu_w \cot\theta\left[-\frac{L_c}{R_0}\tan\theta + \left(1 - \frac{R_f}{R_0}\right)\right]\right\} - 1\right\} \quad (12)$$

Equation 12 describes the effect of water content variation on the extrusion pressure. When the water content over time (dw/dt) is different than zero, either the system is gaining (positive sign) or losing (negative sign) water. In the present case, it is assumed that the ceramic paste is losing water (water migration) during extrusion. Hence, it has a negative signal contributing positively to the increased extrusion pressure. From Eq. 12, it is also possible to notice that the velocity of the ram displacement plays an important role in the extrusion pressure. For instance, considering that the ceramic paste is losing water (d*w*/d*t* is negative), decreasing the ram velocity (v) will lead to a rise in the extrusion pressure. Moreover, Liu et al. [42] observed this trend in their experimental results, stating that the steady state is enlarged when the ram velocity is increased. Additionally, they inferred this due to lighter loss of water.

3 Results and discussion

Figure 5 displays the effect of the radius of the die's exit (R) and the exit angle (θ) on the value of Part 1 $\left(-\frac{\theta}{\mu_w} + \frac{R_f}{8R\mu_w^2} - 1\right)$ of Eq. 5. As it can noted, there is a decrease in the value of Part 1, as the radius and the angle increases. Moreover, the value of Part 1 soaks when the radius of the die increases. Therefore, it is possible to affirm that this part of the equation is more sensitive to the radius variation.

Moving to the analysis of the second part of Eq. 5, as shown in Fig. 6. Now, we observe an opposite trend: as the radius and the angle rise, the value of Part 2 also raises. In addition, the radius plays a more important role in the second part, when compared to the angle.

Now analyzing the overall influence of the radius of the die's exit in Eq. 5 (combining the results shown in Fig. 5 and Fig. 6), it is possible to recognize that when R approaches zero, it means that the die's exit no longer presents a round shape, instead, it has a straight edge (leading the value to

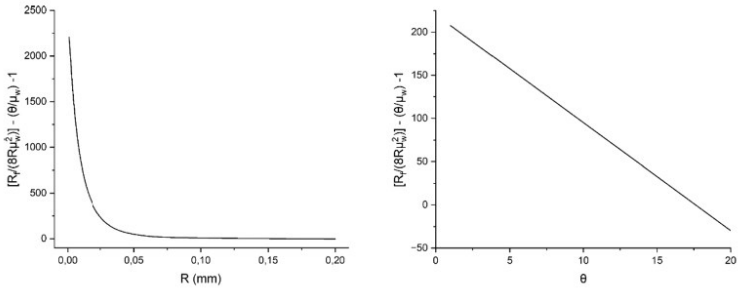

a) Effect of the radius die´s exit b) The effect of the exit angle

Fig. 5 Effect of the radius of the die's exit (**a**) and the exit angle (**b**) on the value of $\left(-\frac{\theta}{\mu_w} + \frac{R_f}{8R\mu_w^2} - 1\right)$

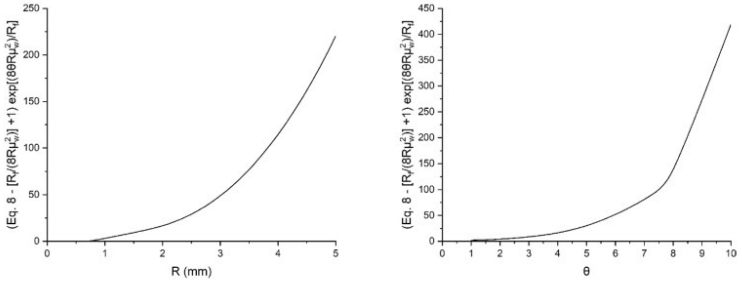

a) Effect of the radius die´s exit b) The effect of the exit angle

Fig. 6 Effect of the radius of the die's exit (**a**) and the exit angle (**b**) on the value of $\left[(Eq.8) - \frac{R_f}{8R\mu_w^2} + 1\right]\exp^{\frac{8R\mu_w\theta}{R_f}}$

infinity). Therefore, all the assumptions made to achieve Eq. 5 become meaningless. In this case, it will be considered that R is not small enough of approaching a straight edge. Taking the previous consideration, it is possible to notice that as the radius of the die's exit increases, there is also a raise in the value of Eq. 5. It can be explained by the fact of enlarging the radius of the die's exit would lead to more extruded material to be in contact with the die, meaning more friction at the work–die interface [51]. It is also known that the presence of friction within extrusion processes increases the force necessary to extrude a part.

Moving to the overall effect of the exit angle in Eq. 5, one can find that the extrusion pressure increases as the exit angle rises. A higher exit angle represents more material in contact with the die's exit, thus more friction. In this case, it is also noted that more material is in movement, particularly in the outer regions away from the center. When more material is in motion, it also causes greater turbulence in the paste flow, increasing the extrusion pressure.

Still analyzing Eq. 5, two parameters play a very important role in the extrusion pressure: friction coefficient (μ_w) and the percentage of cross section reduction $\left(1-\frac{R_f}{R_0}\right)$. Therefore, Fig. 7 shows the effect of the friction coefficient (Fig. 7a) and the diameter reduction percentage (Fig. 7b) on the extrusion pressure. Increasing either the friction coefficient or the percentage of diameter reduction yields a raise in the extrusion pressure throughout the entire process. Moreover, they also influence the unsteady state. For example, for lower friction or diameter reduction percentage, the steady state was extended, and the rise of the extrusion pressure was smoother. On the other hand, for the higher friction coefficient or cross section reduction percentage, the transition from the steady state to the unsteady state was initiated earlier and it was steeper. This trend can be explained by the fact that these conditions require a larger extrusion pressure, fomenting and intensifying the phenomenon of water migration [37]. This type of behavior may lead to a typical, well-known phenomenon present in other materials shaping processes (rolling, forging, direct, and indirect extrusion) called the sticking region.

For comparison, validation, and assessment of the two new proposed equations, previously published works from Andrade (2009) and Tajiri et al. [28] were used and reproduced. Figure 8 displays the variation of the applied extrusion pressure as a function of the position of the ram. Three phases are recognized in Fig. 8 as already reported by Andrade [26]: a coining phase, marked by compression of the ceramic paste; a steady state phase, where the pressure is stabilized and the extrusion continues steadily; and an unsteady state phase, beyond the coring point, showing an evident rise in the extrusion pressure. As it can be observed, for Andrade's curve, Eq. 3, (black line) it is possible to notice only two phases during the extrusion process: the coining and the steady state phase, once in his mathematical modeling, he did not consider the implications beyond the coring point.

Figure 8 displays a satisfactory correlation between the experimental curve points (represented by black squares) and the new proposed equations: Eq. 5, displayed with a short dashed-dotted gray line; and Eq. 12, expressed with a dashed-dotted light gray line. Even though the equations are substantial and complex, they can be easily determined and calculated with the aid of computers.

Among the results in Fig. 8, Eq. 12 seemed to be the most conservative approach since it yielded the highest extrusion pressure. On the other hand, in Eq. 3, the equation published by Tajiri et al. [28] delivered the lowest extrusion pressure. Even though the friction variation equation (Eq. 3) shows a good fit with the experimental curve, as it has already been stated, it is more likely that the compressive strength presents a higher impact on the extrusion pressure when compared to the friction coefficient [26, 48, 49]. Equation 5 presented the closest results compared with the experimental points; nevertheless, it is

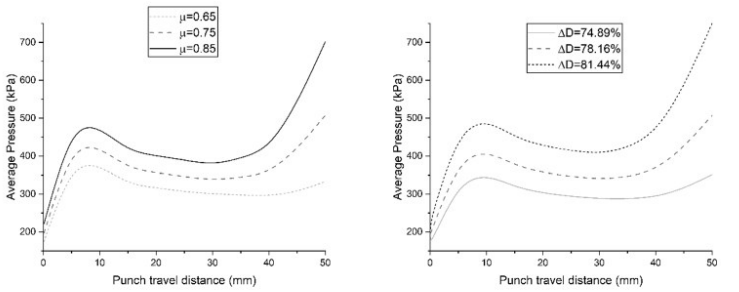

Fig. 7 Effect of the radius of the die (a) and the exit angle (b) on the extrusion pressure

a) Effect of the friction coefficient

b) The effect of the reduction of the diameter

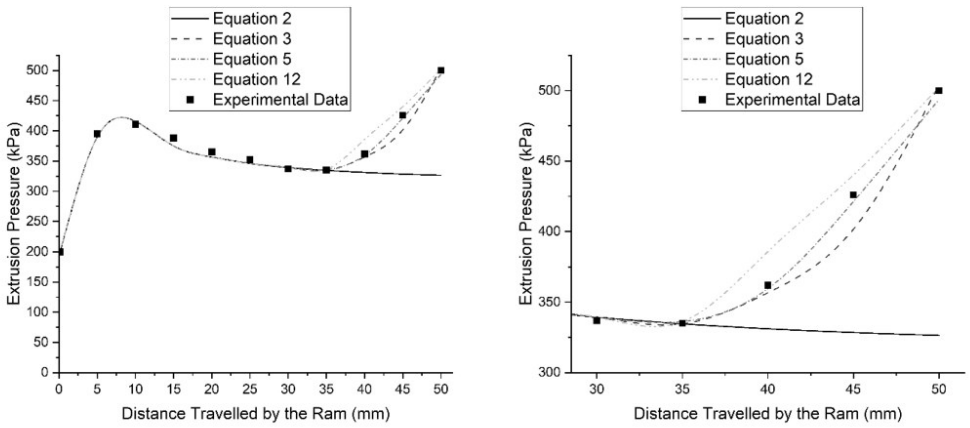

a) Complete curve.

b) Amplified curve within the unsteady state regime.

Fig. 8 Comparison among experimental work (black squares), Andrade's theory (solid black line—Eq. 2) [26], Tajiri et al.'s equation (dashed dark gray line—Eq. 3) [28], and proposed equations: spring-back's approach (short dashed-dotted gray line Eq. 5) and water loss's approach (dashed-dotted light gray line—Eq. 12)

more difficult to accurately acknowledge all the variables within the equation.

Also, these theories will help the product designer to conceive projects avoiding defects due to material and pressure gradients, guaranteeing the integrity of the projected properties. For instance, to minimize the effect of the water (solvent) migration on the product's quality and the extrusion pressure, with the aim of moisture sensors and an accomplished tool to the barrel, it would be possible to track the water content in the ceramic paste and water (solvent) could be added to the paste when necessary.

4 Conclusions

In the present work, it was possible to acknowledge that there is an evident gap in the literature regarding mathematical analysis and extrusion pressure beyond the steady state. Therefore, it was possible to develop two mathematical equations for the extrusion of ceramic paste to analyze the pressure increase beyond the steady state phase. One equation (Eq. 5) came up with the effect of the spring-back phenomenon on the extrusion pressure, and the other mathematical model (Eq. 12) introduced the mathematical relation between the effective stress of compression and the water content of the material. It was also observed that the radius of the die's exit, exit angle, friction coefficient, and diameter reduction percentage influence considerably the profile of the extrusion pressure. Increasing this variable led to a raise in the extrusion pressure and, in some cases, to an anticipation of the coring point. In conclusion, all the newly proposed equations showed a good agreement with the experimental data, and new variables within the extrusion process were introduced and mathematically related to a published equation (Eq. 3), and they supported the equation proposed by Tajiri et al. [28]. The theoretical analyses seemed to be very useful in aiding the construction of new equations. Thus, it was possible to fill a gap in the direct extrusion of ceramic, where publications about the unsteady state regime and equations which acknowledge it has not been explored previously.

Acknowledgements The authors wish to thank the Departments of Mechanical and Chemical Engineering, at the Federal University of Santa Catarina and CNPq, for partially financing the project, for granting the authors, and for fomenting the participation of the authors in international conferences. The authors also thank Fernando Y. Miyata for all the help and suggestions in this work. The first author thanks CAPES for fully granting him.

Declarations

Conflict Interests The Authors have declared that no competing interests exist.

References

1. Händle F (2007) Extrusion in ceramics. Springer, Berlin; New York
2. Kocserha I, Kristály F (2010) Effects of extruder head's geometry on the properties of extruded ceramic products. Mater Sci Forum 659:495
3. Nath Das R, Madhusoodana CD, Okada K (2002) Rheological studies on cordierite honeycomb extrusion. J Eur Ceram Soc 22(16):2893–2900
4. Chen Z et al (2019) 3D printing of ceramics: a review. J Eur Ceram Soc 39(4):661–687
5. Hall SE et al (2021) Paste extrusion 3D printing and characterization of lead zirconate titanate piezoelectric ceramics. Ceram Int 47(15):22042–22048
6. Hu F et al (2021) Extrusion-based 3D printing of ceramic pastes: mathematical modeling and in situ shaping retention Approach. Materials. https://doi.org/10.3390/ma14051137
7. Romanczuk-Ruszuk E et al (2023) 3D Printing ceramics - materials for direct extrusion process. Ceramics 6:364–385. https://doi.org/10.3390/ceramics6010022
8. Ordoñez E, Gallego JM, Colorado HA (2019) 3D printing via the direct ink writing technique of ceramic pastes from typical formulations used in traditional ceramics industry. Appl Clay Sci 182:105285
9. Ruscitti A, Tapia C, Rendtorff NM (2020) A review on additive manufacturing of ceramic materials based on extrusion processes of clay pastes. Cerâmica 66:354
10. Benbow J, Bridgwater J (1993) Paste flow and extrusion. Clarendon Press, Oxford
11. Vitorino N et al (2014) Extrusion of ceramic emulsions: plastic behavior. Appl Clay Sci 101:315–319
12. Reed JS (1995) Principles of ceramics processing. Wiley
13. Andrade FA, Al-Qureshi HA, Hotza D (2011) Measuring the plasticity of clays: a review. Appl Clay Sci 51(1):1–7
14. Dondi M (2006) Caracterização tecnológica dos materiais argilosos: métodos experimentais e interpretação dos dados. Revis Cerâm Ind 11(3):36–40
15. Dodeja LC, Johnson W (1957) The cold extrusion of circular rods through square multiple hole dies. J Mech Phys Solids 5(4):281–295
16. Johnson W (1956) Experiments in plane-strain extrusion. J Mech Phys Solids 4(4):269–282
17. Burbidge AS, Bridgwater J (1995) The single screw extrusion of pastes. Chem Eng Sci 50(16):2531–2543
18. Macedo RS et al (2008) Estudo de argilas usadas em cerâmica vermelha. Cerâmica 54:411
19. Johnson W (1959) An elementary consideration of some extrusion defects. Appl Sci Res Sect A 8(1):52–60
20. Avitzur B (1967) Steady and unsteady state extrusion. J Engng Ind 175 (89)
21. Hoffmanner, A.L. and M.S.o.A.S.a.F. Committee, *Metal forming: interrelation between theory and practice: proceedings of a symposium on the relation between theory and practice of metal forming, held in Cleveland, Ohio, in October, 1970*. 1971: Plenum Press.
22. Sturgess CEN, Dean TA (1979) Breakthrough pressures in lubricated extrusion. J Mech Work Technol 3(2):119–135
23. Janney MA (1994) Plastic forming of ceramics: extrusion and injection moulding. In: Terpstra RA, Pex PPAC, de Vries AH (eds) Ceramic Processing. Springer, Netherlands, Dordrecht, pp 174–211
24. Horrobin DJ, Nedderman RM (1998) Die entry pressure drops in paste extrusion. Chem Eng Sci 53(18):3215–3225
25. Vitorino N et al (2015) Porous hollow tubes processed by extrusion of ceramic emulsions. Appl Clay Sci 105–106:60–65
26. Andrade FA (2009) Modelamento matemático do comportamento plástico do sistema argila-água no processo de extrusão, in Programa de Pós-Graduação em Ciência e Engenharia de Materiais. Universidade Federal de Santa Catarina
27. Flores O, et al., (2006) Modelo matemático aplicado à avaliação da plasticidade de argilas
28. Tajiri H, Pieri E, Al-Qureshi H (2019) Modified modeling of clay paste extrusion through a circular die: Beyond the Steady-State. Int J Metall Metal Phys 4:1–9
29. Khan AU, Briscoe BJ, Luckham PF (2001) Evaluation of slip in capillary extrusion of ceramic pastes. J Eur Ceram Soc 21(4):483–491
30. Wilson DI, Rough SL (2006) Exploiting the curious characteristics of dense solid–liquid pastes. Chem Eng Sci 61(13):4147–4154
31. Yekta B, Mahabad N, Ebadzadeh T (2007) Rheological study on cordierite paste during extrusion. Adv Appl Ceram 106:161–164
32. Patel M, Blackburn S, Wilson I (2017) Modelling of paste ram extrusion subject to liquid phase migration and wall friction. Chem Eng Sci 172:487
33. Mason MS et al (2009) Aqueous-based extrusion of high solids loading ceramic pastes: process modeling and control. J Mater Process Technol 209(6):2946–2957
34. Liu H et al (2013) Factors influencing paste extrusion pressure and liquid content of extrudate in freeze-form extrusion fabrication. Int J Adv Manuf Technol 67(1):899–906
35. Rough SL, Wilson DI, Bridgwater J (2002) A Model describing liquid phase migration within an extruding microcrystalline cellulose paste. Chem Eng Res Des 80(7):701–714
36. Jiang GP, Yang JF, Gao JQ (2009) Effect of starch on extrusion behaviour of ceramic pastes. Mater Res Innov 13(2):119–123
37. Azzolini A, Sglavo VM, Downs JA (2014) Novel method for the identification of the maximum solid loading suitable for optimal extrusion of ceramic pastes. J Adv Ceram 3(1):7–16
38. Liu H, Leu MC (2009) Liquid phase migration in extrusion of aqueous alumina paste for freeze-form extrusion fabrication. Int J Modern Phys B 23(06n07):1861–1866
39. Al-Qureshi H (1974) Spring-back of sheet metal when using compressible tools. Sheet Metal Ind 51:695–698
40. Al-Qureshi H (1999) Elastic-plastic analysis of tube bending. Int J Mach Tools Manuf 39:87–104
41. Al-Qureshi H, Russo A (2002) Spring-back and residual stresses in bending of thin-walled aluminium tubes. Mater Des 23:217–222
42. Chongthairungruang B et al (2013) Springback prediction in sheet metal forming of high strength steels. Mater Des 50:253–266
43. Gray A (1996) Modern differential geometry of curves and surfaces with mathematica. CRC Press, Inc.
44. Simoni R (2005) Teoria local das curvas, in Centro de Ciências Físicas e Matemática. Universidade Federal de Santa Catarina, Florianópolis, p 86
45. Wang Y, Xia X, Wu Y (2019) Experimental study on shear properties of interface between clay and cement paste. IOP Conf Seri Earth Environ Sci 267:052049
46. Ribeiro MJ, Blackburn S, Labrincha JA (2009) Single screw extrusion of mullite-based tubes containing Al-rich anodising sludge. Ceram Int 35(3):1095–1101
47. Benbow JJ, Oxley EW, Bridgwater J (1987) The extrusion mechanics of pastes: the influence of paste formulation on extrusion parameters. Chem Eng Sci 42(9):2151–2162

48. Ribeiro MJ, Ferreira JM, Labrincha JA (2005) Plastic behaviour of different ceramic pastes processed by extrusion. Ceram Int 31(4):515–519
49. Hamza A et al (2019) Plasticity of red mud and clay mixtures. IOP Conf Ser Mater Sci Eng 613:012051
50. Rough SL, Bridgwater J, Wilson DI (2000) Effects of liquid phase migration on extrusion of microcrystalline cellulose pastes. Int J Pharm 204(1):117–126
51. Sunil K et al. (2018) Effects of cold extrusion on material properties